THE INFLUENCE OF WATER SPRAYS ON THE PROPAGATION OF LAMINAR FLAMES IN H_2S-AIR MIXTURES

BY

© YA'ACOV KINCLER

A THESIS SUBMITTED TO THE FACULTY OF GRADUATE STUDIES AND RESEARCH IN PARTIAL FULFILLMENT OF THE REQUIREMENT FOR THE DEGREE OF

MASTER OF ENGINEERING

March, 1980

DEPARTMENT OF MECHANICAL ENGINEERING

MCGILL UNIVERSITY

MONTREAL, QUEBEC, CANADA

To my beloved parents for
their encouragement and support.
To my dear wife, Dida, for her
patience, understanding and help.

RESUME

L'addition d'eau (ou de vapeur d'eau) à un mélange de gaz inflammable peut avoir à la fois des effets thermophysiques et chimiques sur le processus de combustion.

Des études théoriques et experimentales ont été entreprises, afin de déterminer l'influence de l'eau atomisée sur la combustion de mélanges H_2S-air. Les vitesses de propagation des flammes ont été mesurées en laboratoire, pour de nombreux rapports H_2S-air (7% - 20%), et différents jets d'eau, utilisant la méthode du tube cylindrique. Les jets d'eau ont été rendus inertes, étant imprégnés de H_2S.

L'analyse théorique des effets thermophysiques a été effectuée en regroupant les équations de combustion, mécanique des fluides, thermodynamique et d'eau atomisée, résultant en un modèle simple prédisant les vitesses de propagation des flammes. Cette analyse constitue une extension des études de Johnson & Nachbar, par l'addition des effets de jets d'eau atomisée au mélange gazeux H_2S-air. Une analyse numérique a été effectuée, dans les cas de mélanges stoichiométriques H_2S-air, de jets d'eau de différentes densités et degré d'atomisation. Les vitesses de propagation sont calculées par intégration des equations caractéristiques.

Enfin, les résultats tant théoriques qu'expérimentaux démontrent que la présence de particules d'eau retarde la vitesse de propagation des flammes dans les mélanges H_2S-air.

ABSTRACT

The addition of water (or water vapor) to a combustible gas mixture can have both, thermophysical and chemical kinetic effects on the combustion process.

An experimental and theoretical investigation was undertaken to determine the influence of water sprays on the combustion of H_2S-air mixtures. Burning velocities were measured experimentally, using the cylindrical tube method, over a wide range of mixture compositions (7% - 20% in air) and for various inert water sprays. The water sprays were rendered inert by being presaturated with H_2S.

A theoretical analysis of the thermophysical effects of the water droplets on the flame propagation was performed by coupling together the combustion, fluid dynamic, thermodynamic and spray equations to provide a simple model for the prediction of the burning velocity. The earlier work of Johnson and Nachbar is extended to incorporate the water spray in the gaseous H_2S-air mixture. The numerical analysis is applied to the stoichiometric H_2S-air mixture for different water spray densities and droplet size distributions. The resulting burning velocity is then calculated by integrating the eigenvalue equations.

Both, the experimental and numerical results showed that the presence of water spray decreases the burning velocity of the H_2S-air flames.

ACKNOWLEDGEMENTS

The author wishes to express his gratitude to his research director, Professor J.H.S. Lee, for initiating the topic of this thesis and to Drs. Ingar Moen and Christiane Guirao for their helpful advice throughout the course of this study. Dr. Ingar Moen's suggestions for the improvement of the text are sincerely appreciated.

Special thanks are due to the undergraduate laboratory technicians for their assistance in making the experiments possible and to Ms. Assunta Cerrone for her patience and rapidity in typing this thesis.

This research was supported by Atomic Energy Canada Ltd.

TABLE OF CONTENTS

LIST OF TABLES

LIST OF FIGURES

NOMENCLATURE

Symbol	Description
A_{fl}	flame surface area
A_t	cross sectional area of the flammability tube
a	$\equiv G/J$
	or
	$\equiv \min\left(\frac{a_K}{\nu'_K}\right)$
a_I	inert species coefficient in the gas phase reaction
a_K	coefficient of reactant or product species K in the reaction
B	frequency factor coefficient for k
C_l	defined by Eqn. (2-75c), see also Eqn. (2-75a)
$\bar{C}_p$	mean isobaric specific heat
D	mass diffusion coefficient
$\bar{d}_0$	initial droplet median volume diameter
E	activation energy for K
F	force per unit mass exerted on a droplet by the surrounding gas
$\%F_v$	fraction of water spray evaporated
f	probability function for spray particles
G	initial mass fraction of consumable reactant species defined equivalently as "dilution factor" by Eqn. (I-6)
H	the droplet size distribution function defined by Eqn. (III-1)

Symbol	Description
h	specific enthalpy of the mixture
h_I	specific enthalpy of the inert species
h_K	specific enthalpy of the reactant or product species K
h_K^0	standard heat of formation of species K
h_{fg}	latent heat of vaporization
J	defined by Eqn. (2-75d), see also Eqn. (2-75a)
$\bar{K}$	"scale factor", a constant of the particular mixture defined by Eqn. (II-11)
$\bar{K}^*$	$\equiv \frac{\bar{K}}{1/r_f}$; defined by Eqn. (2-43) B_f
k	specific reaction rate coefficient
or	
	exponent in the evaporation rate equation, Eqn. (2-61)
M_K	chemical symbol for reactant or product species K
M.R.	magnification ratio
MVD	median volume diameter
$\dot{m}$	total mass flux
$\dot{m}_K$	mass flux of reactant or product species K
$\dot{m}_I$	mass flux of inert species I
n	total number of reactant and product species
or	
	number of droplets per unit volume of the mixture
p	static pressure

Symbol	Description
q_-	total heat released in the reaction per gram of reaction products formed under standard conditions
R	$\equiv \frac{dr}{dt}$; rate of change of droplet radius
or	universal gas constant
or	radius of flammability tube
r	droplet radius
or	number of reactant species
r_f	overall forward reaction order
rpm	revolutions per minute
s	number of reactant species consumed completely in the reaction
or	separation distance between two successive flame fronts
or	surface tension of a water droplet
T	temperature
T_b	boiling temperature
T_f	free stream temperature
T_i	ignition temperature
$T_{\infty,a}$	ideal adiabatic flame temperature
$T_{\infty,e}$	empirical adiabatic flame temperature
$\tilde{T}$	non-dimensional temperature defined by Eqns. (2-20) and (2-75a)
T^*	$\equiv \frac{q}{c_p}$
t	time

Symbol	Description
U_K	diffusion velocity of species K
u	flow velocity of the gas mixture
or	$\equiv \tilde{T}(\zeta)$; a transformation defined by Eqn. (II-13)
u_0	burning velocity
u_0^c	computed burning velocity
u_0^e	experimentally measured burning velocity
u_{sp}	spatial or observed flame velocity
u_u	flow velocity of the unburned gas mixture
V_{eff}	effective spray volume
V_u	volume of remaining portion of unburned gas
$\bar{v}$	mean flow velocity of water droplets
$v(u)$	$\equiv \tilde{T}'(\zeta)$
W_K	molecular weight of species K
W_I	molecular weight of all inert species I
$\bar{W}$	average molecular weight of gaseous mixture
W_{total}	total molecular weight of overall mixture
$\dot{w}$	chemical source function
X_K	mole fraction of species K
X_I	mole fraction of all inert species I
X	space coordinate
Y_K	mass fraction of species K
Y_I	mass fraction of all inert species I

Symbol	Description
Y_K^*	reference mass fraction of species K defined by Eqn. (I-1)
Y	a function defined implicitly by Eqns. (I-7) and explicitly by Eqn. (I-8)
Y*	a function defined by Eqn. (2-81)
Z	mixture gaseous mass fraction
Z*	hot boundary value of Z in parametric study
α	thermal diffusivity
or	
	temperature dependence of mass diffusion coefficient (Eqn. (II-4))
β	temperature dependence of pre-exponential factor in K
γ'_K, γ''_K	empirically determined reaction order with respect to species K
δ	flame reaction zone thickness
ζ	nondimensional space coordinate defined by Eqn. (2-25)
η	number of open slits in the stroboscopic disc
or	
	variable of integration in Eqn. (II-18)
Λ	eigenvalue of laminar flame problem
λ	thermal conductivity
μ	dynamic viscosity
or	
	function defined by Eqn. (2-28)
μ_f	dimensionless specific reaction rate function defined by Eqn. (II-10)
ν	kinematic viscosity
or	$\equiv \sum_{K=1}^{S} \nu'_K$

Symbol	Description
ν'_K, ν''_K	stoichiometric coefficients for the gas phase reaction
ρ	density
ρ_{s_0}	initial spray density
ϕ	equivalence ratio
ϕ	function defined by Eqns. (2-45)
X	evaporation coefficient defined by Eqn. (2-62)
Ψ	dimensionless chemical source function defined by Eqn. (2-37)

Subscripts

$( )_f$	term related to forward reaction
$( )_b$	term related to backward reaction
$( )_0$	initial (cold boundary) conditions in unburned gas mixture
$( )_\infty$	final (hot boundary) conditions in burned gas mixture
$( )_u$	unburned gas
$( )_g$	gas phase
$( )_\ell$	liquid phase
$( )_v$	vapor phase

Superscripts

$( )^c$	computed
$( )^e$	experimental

Superscripts	Description
$(\bar{})$	mean or effective
$(\dot{})$	first derivative with respect to time
$(\,)^{+}$	upper bound
$(\,)^{-}$	lower bound

CHAPTER I

GENERAL INTRODUCTION

The addition of water (or water vapor) to a combustible gas mixture can have both physical and chemical kinetic effects on the combustion process, the magnitudes of which will depend on how water is introduced to the combustion environment and at what concentration.

Water is the most abundant, often the only available suppressant for a fully developed deflagration and since the earliest times has been used as such.

When dealing with the complex problem of flame inhibition in pre-mixed flames, it is generally accepted that there are two classes of inhibitors [1]. The first consists of inert gases such as nitrogen or the noble gases whose effect is primarily one of dilution. The addition of these to a flammable fuel air mixture increases the heat capacity contribution of the inert constituents in the mixture and leads to lower adiabatic flame temperature for the diluted mixture. The second class is comprised of inhibiting agents such as powdered metal salts (Na_2CO_3) and halogenated hydrocarbons such as CF_3Br (halon 1301), CF_2ClBr (halon 1211) and $C_2F_4Br_2$ (halon 2402). These chemical inhibitors act by interfering with the normal chemical reaction paths in flames. In a series

of reports Biordi et al. [2,3] studied the reaction rates and mechanisms in a methane flame inhibited with CF_3Br in an attempt to develop a detailed understanding at the molecular level, of the mechanisms by which flame retardants operate. Generally, chemical flame inhibitors are identified on the basis of their relative reduction of burning velocity.

Water combines both, the physical and chemical effects of flame inhibition. For large scale fires and explosions it is the most widely used agent either by itself or together with other constituents. Liebman et al. [4], for example, showed that finely dispersed water can be effective even in quenching full scale mine explosions involving coal dust as long as adequate dispersion is insured. Later in another paper, Liebman et al. [5] showed that water atomized by pressurized nitrogen was efficient in stopping also fully developed gas explosions in mines, but it had little effect against the explosion during its incipient stage. Hybrid combinations of currently known extinguishants, however, were successful against incipient explosions. One of the hybrids developed consists of halon 1301 combined with water, and results of tests indicated that the halon aids in dispersing its constituents and also converts the water into fine drops.

Dryer, F.L. [6] gives an historical review, with an extensive reference list, on the applications of water addition to practical combustion systems. The fundamental effects of

water on the combustion properties such as chemical inhibition (e.g. due to hydrogen abstraction from hydrocarbons by hydroxyl radicals), decreasing the system temperature and lowering the rate of flame propagation, are discussed in his paper. According to Dryer [6], very little information about the effect of water vapor addition on flame burning velocity exists, with the exception of carbon monoxide and hydrogen flames. An increase in absolute humidity drastically accelerates "dry" stoichiometric carbon-monoxide flames. However, laminar hydrogen-air flames are inhibited by water vapor addition, but only by about 1/3 of the amount predicted from inert dilution.

Sapko et al. [7] in their report describe the results of laboratory scale experiments in which methane-air ignitions were quenched or rendered inert by fine water sprays or by a combination of sprays and steam. The inerting results for pre-mixed methane-air-water mixtures indicated that water droplets of less than 10 μm are as effective as the vapor. Water requirements for inerting such mixtures were much smaller than those for quenching the sustained flame propagation by the application of water sprays.

The main aim of this research was to investigate the inhibitive effects of inert water sprays on the propagation of laminar flames in hydrogen sulfide-air mixtures.

Very little information is available about the combustion

of hydrogen sulfide-air mixtures and even less is known about the kinetics of the chemical reactions associated with this combustion process. Hydrogen sulfide is used in large quantities as an agent in the production of heavy water and it was important to investigate the possibility of using water spray curtains for flame suppression in the case of an accidental release of this flammable gas.

This investigation deals with inerting the combustible mixtures rather than quenching them. Quenching a propagating flame requires massive amounts of water sprays in comparison with that required for inerting and by the time the flame is quenched, some damage could already have occurred or transition from a deflagration to detonation could take place nullifying the effect of the water sprays. If possible, inerting the mixture to the point in which an incipient ignition would be prevented from developing into a self propagating flame is therefore a preferable method of flame suppression.

For this thesis the emphasis was on studying the physical and thermodynamic influence of water droplets within the reaction zone of the hydrogen sulfide-air flame in light of the dilution capacity and the fraction of available combustion energy consumed by the water droplets heating and vaporizing.

The study included experimental observations using an apparatus designed and built especially for this purpose, a theoretical analysis based on the classical laminar flame

theory, and explicit computer calculations to simulate some of the experiments.

The laboratory scale experiments carried out in this research were similar to the inerting experiments performed by Sapko et al. [7]. Initially, methane-air flames without and with water sprays were investigated in order to test the experimental apparatus and confirm the reliability of the method used. A similar but modified apparatus was designed and built for the hydrogen sulfide-air experiments.

These experiments were designed to study the effect of water spray addition on the burning velocity of the flame. The flame, while propogating upwards in a cylindrical Plexiglas tube, was photographed in a stroboscopic sequence. Its burning velocity was then determined from the picture taken. The burning velocity is the velocity of the flame front relative to the fresh gas immediately ahead of it in a direction normal to the flame front. It is a fundamental property of the mixture and is directly related to the overall reaction rate, thermodynamic and transport properties of the combustible mixture.

After performing experiments in dry hydrogen sulfide-air mixtures over a wide range of compositions (7% - 20% H_2S in air), water sprays were added and experiments were performed over the same composition range.

The water spray parameters were also varied so that their

influence on the propagating flame could be determined. The water spray variables were the droplet size distribution and the water spray density (or effective spray volume participating in the process). These two variables could be easily controlled experimentally and their effect on the burning velocity measured and analyzed.

The theoretical analysis was done in the context of an adiabatic, laminar, one-dimensional flame, fixed in a coordinate system normal to the surface with a forward, one-step chemical reaction and involving an arbitrary number of species. In this frame of reference cold gases flow from negative infinity into the stationary flame surface and hot gases move away from the flame surface to reach an equilibrium flame temperature at positive infinity (Fig. 1). The mathematical statement of this problem on the entire real line is defined as the classical laminar flame problem.

The theoretical analysis is based on first principles. The laws of conservation of mass, momentum and energy, together with the species diffusion and species mass conservation equations, are combined to give the governing flame equations. To generalize the analysis, the equations and definitions are presented in non-dimensionalized forms. The equations are first derived for a fuel-oxidizer laminar flame. The same equations are then modified to include the influence of water sprays by considering the water as an inert species added

to the mixture initially in liquid phase and then transformed partially or wholly to vapor phase within the reaction zone. The combustion problem can then be reduced to a first order boundary value problem which, with the temperatures at the ignition and hot boundaries given, has two boundary conditions in the form of non-dimensional temperature gradient defined for the ignition and final equilibrium planes (Fig. 2). This set of equations leads to an eigenvalue problem.

The formulation of the eigenvalue problem and the casting of the equations in a form suitable for numerical computations is done using the Johnson and Nachbar [8,9] method of determining upper and lower bounds for the burning rate eigenvalue. According to Williams [10, Chpt. 5], this method is the most accurate technique known for the solution of simple laminar flame problems.

Due to the complexity of the flame equations and the difficulty in bringing them to the appropriate closed form suitable for numerical computations, a simplified model was developed here. The numerical analysis was performed using this model for stoichiometric hydrogen sulfide-air mixtures (12% H_2S in air), for which the burning velocity is approximately maximum. The computations were done for the whole range of the variable spray parameters, i.e. for various droplet sizes and spray densities as dictated by the experiments, and the results were then tested by performing a parametric study.

The results of this investigation augment the currently available data on laminar flame propagation in combustible gas plus water spray mixtures.

After introducing the background and objectives of this thesis, a simplified analytical model of the problem is presented in Chapter II. First, the governing equations and boundary conditions of the combustion problem, without involving water sprays, are derived and non-dimensionalized. Then, the governing differential equation and corresponding boundary conditions are derived, and expressions for the upper and lower bounds of the eigenvalue are determined. Following this there is a discussion of the application of the theory to the stoichiometric H_2S-air mixture. The chapter is concluded with an analysis of laminar flame propagation in a gas plus water spray combustible mixture. In that analysis a simplified analytical model is developed to account for the presence of water droplets in the H_2S-air mixture.

In Chapter III, the cylindrical tube method for the measurement of burning velocities is discussed with reference to related works.

In Chapter IV the experimental apparatus and procedures are described in detail.

Chapter V is devoted to the presentation and discussion of the experimental and numerical results of this work.

In the last chapter of the thesis, Chapter VI, the main

conclusions are set out and some projections are suggested.

There are four appendices in this thesis after the Tables and Figures: the first three deal with definitions and mathematical derivations needed to support the analytical developments in Chapter II. In Appendix IV, sample computer program listings with the results printout are presented.

CHAPTER II

THEORETICAL ANALYSIS

2.1 INTRODUCTION AND BACKGROUND

The laminar flame problem is one of the earliest combustion problems to require for its solution the simultaneous consideration of both fluid dynamics and chemical kinetics.

The problem of determining the propagation velocity of a deflagration wave was first studied by Mallard and Le Chatelier [11] (see also Glassman, I. [12, Chpt. 4, p. 66]) who proposed that it is the conduction of heat back through layers of unburned gas that is the controlling mechanism in flame propagation. This was the basis for the so-called thermal theories where the back diffusion of particles such as molecules and free radicals was not considered to affect the reaction mechanism. By using simplified models of the deflagration wave, Mallard's student, Taffanel [13] and later but independently, Danielle [14], appear to have been the first investigators to demonstrate the important result that the burning velocity is proportional to the square root of the product of reaction rate and the thermal diffusivity ($\alpha = \lambda/\rho C_p$) at constant pressure.

Subsequent studies involve the utilization of more comprehensive theories (e.g. the consideration of particle

diffusion), refinements in accuracy, and inclusion of the effects of chain reactions and other physical phenomena. Among the important theoretical studies of laminar flame propagation, the work of Zeldovich, Frank-Kamenetsky and Semenov [15] should be noted. They include the diffusion of molecules as well as heat but not of free radicals or atoms. These authors used the concept of an ignition temperature close to the adiabatic flame temperature and thus it was eliminated from the final equation making it more useful. Following the work of Boy and Corner [16], numerical solutions to the complete flame equation were obtained by Hirschfelder et al. [17,18]. Von Karman et al. [19,20] succeeded in obtaining approximate analytical solutions to a number of laminar flame problems. In later reviews of progress in the analysis of steady flame propagation, Penner and Williams [21] or Williams in his book [10, Chpt. 5] and also Hirschfelder and Curtis [22] have devoted major attention to the calculation of the burning velocity and temperature profile in one dimensional, laminar flow of pre-mixed combustible gases.

With the essential assumptions of a one-step reaction and Lewis number equal to one ($Le = \alpha/D = \lambda/C_p\rho D = 1$), it has been shown that this problem can be reduced to the determination of the eigenvalue of a first-order, nonlinear, ordinary differential equation with specified boundary conditions. Refs. [10] and [21] contain a detailed review of a number of methods for obtaining an approximate, closed form solution for this eigenvalue. The eigenvalue is a constant which in addition to depending on known thermodynamic, kinetic and transport properties (all of these properties are in turn temperature dependent) of the particular mixture, depends also on the mass burning velocity being the unknown parameter to be

determined. A solution to the first-order boundary value problem will exist only for a particular value of the constant eigenvalue.

According to [10] and [21], the method of Johnson and Nachbar [8,9] is the most accurate technique for the solution of one-dimensional laminar flame problems since it permits a rigorous determination of an upper and a lower bound for the eigenvalue.

This method, which was originally developed for the deflagration of a solid propellant, may be applied to the case of a gaseous laminar flame without modification. In [9], it has also been extended to include an iterative procedure which would converge monotonely to the approximate eigenvalue between the upper and lower bounds.

This is the method used in the present analysis of laminar flames in H_2S-air mixtures. The method will also be modified to include the presence of water sprays and water vapor in the gas mixture.

2.2 FORMULATION OF THE EIGENVALUE PROBLEM

The theory developed here will be applicable to the phenomenological mass-action law for a one-step, forward (back reaction will not be considered), chemical reaction involving an arbitrary number of species, in arbitrary initial ratios and with specific reaction rate coefficients dependent upon the temperature in the form of the Arrhenius law.

We have to consider in this problem a deflagration-wave flame front (Fig. 1), which may be a curved surface, moving

through a uniform, pre-mixed gas.

It is assumed that the energy release takes place in a very thin front. The velocity of the flame front is in the direction of the normal to the surface and is time-independent (local flow is laminar at the flame front). The analysis considers the problem as one-dimensional, the frame of reference being the coordinate direction normal to the surface. The flame surface itself can be considered fixed in this frame of reference, while cold gases flow from negative infinity ($x = -\infty$) into the stationary flame surface and hot gases move away from the flame surface to reach an equilibrium flame temperature at positive infinity ($x = +\infty$), (Figs. 1 and 2). Hence, we have "cold boundary" conditions at $x = -\infty$ and "hot boundary" conditions at $x = +\infty$.

$x = 0$ is the ignition plane or the plane where the ignition temperature is obtained. The ignition temperature, T_i, is defined as the temperature at which the chemical reaction begins, i.e. at the end of the pre-heat zone as illustrated in Fig. 2. The mathematical statement of this problem is defined as the classical laminar flame problem.

For a solution to the classical laminar flame problem to exist, the chemical source function must strictly vanish at the cold boundary temperature; even admitting this unrealistic hypothesis (unrealistic, because of the use of the Arrhenius expression for the reaction rate), the solution for the

eigenvalue can be non-unique. To circumvent this cold boundary difficulty, the modified laminar flame problem was considered in order to obtain approximate, or numerical solutions.

The modification consists of either assuming that the chemical source function has an ignition temperature below which the combustible will exhibit no reaction, or, that there is present a "flame holder" which acts both as a heat sink and a semipermeable membrane. The membrane is assumed to pass only the reactant molecules and to prevent back diffusion of product molecules. $x = 0$ is the point of ignition or the location of the flame holder.

Solution of the flame equations shows that the calculated burning velocity is independent of either the assumed value of the ignition temperature, or of the chosen value of heat transfer to the "flame holder" for all reasonable values of these parameters [23, p. 319]. Johnson and Nachbar [8] formulated the theory for the stoichiometric composition of the solid monopropellant and in [9], they extended the method to non-stoichiometric compositions without alteration of the final form of the equations. They used in their analysis the ignition temperature concept.

The mathematical formulation of the theory will now follow.

The governing equations considered here are for one-

dimensional, steady laminar flow in a reacting gaseous mixture i.e. for a plane deflagration wave.

We assume a forward reaction in the gaseous mixture which has a specific reaction rate coefficient k_f and involves r chemically distinct reactant species which are transformed into n-r chemically distinct reaction product species, where n and r are positive integers and n > r. All the other species in the mixture are inert and their sum will be designated by the subscript I. The reaction can also proceed in the reverse direction (with specific reaction rate coefficient, k_b), an aspect which will not be considered in the present application.

If M_K is the chemical symbol for species K in the mixture, the stoichiometric relation describing the opposing reaction is written:

$$\sum_{K=1}^{r} \nu'_K M_K \underset{k_b}{\overset{k_f}{\rightleftharpoons}} \sum_{K=r+1}^{n} \nu''_K M_K \qquad (2\text{-}1)$$

where ν'_K and ν''_K represent, respectively, the stoichiometric coefficients of species M_K for the reactant species and for the product species.

Using the parameters defined in Appendix I, the relevant laminar flow equations assuming that there is no energy transfer between the gases and the surroundings may now be

written down.

Conservation of Mass. If $\dot{w}$ denotes the chemical source function (g/cm^3 sec) for the rate of formation of the aggregate of reaction products in the forward reaction, then for species mass conservation,

$$\frac{d\dot{m}_K}{dX} = - Y_K^* \dot{w} \qquad K = 1, \ldots, r \qquad (2\text{-}2a)$$

$$\frac{d\dot{m}_K}{dX} = Y_K^* \dot{w} \qquad K = r+1, \ldots, n \qquad (2\text{-}2b)$$

$$\frac{d\dot{m}_I}{dX} = 0 \qquad (2\text{-}2c)$$

and total mass conservation is

$$\frac{d\dot{m}}{dX} = 0 \qquad (2\text{-}3)$$

where $$\dot{m} = \rho u = \text{constant} \qquad (2\text{-}4)$$

With a_K and a_I being the coefficients in the chemical equation depending on the composition prior to the reaction, and from Eqn. (2-3), the species mass fluxes at $X = 0+$ (and also in the region $-\infty < X \leq 0+$) are:

$$\dot{m}_K(0+) = \frac{a_K W_K}{W_{total}} \dot{m} \qquad K = 1, \ldots, r \qquad (2\text{-}5a)$$

$$\dot{m}_K(0+) = 0 \qquad K = r+1, \ldots, n \qquad (2\text{-}5b)$$

$$\dot{m}_I(0+) = \frac{a_I W_I}{W_{total}} \dot{m} \qquad (2\text{-}5c)$$

Conservation of Momentum. Laminar flame burning velocities are small compared with the speed of sound. Empirical burning velocities lie between 1 cm/sec and 1400 cm/sec (hydrogen-oxygen flames) with the upper limit corresponding to approximately a Mach number of .04.

This implies constant pressure deflagrations since at such low Mach numbers the pressure difference across the flame front is negligibly small, thus,

$$P = \text{constant} \qquad (2\text{-}6)$$

Conservation of Energy. We assume an adiabatic process. Viscous forces and also the kinetic energy of the flowing gases are negligible because of the low flame Mach numbers involved. In this case, there is a balance between the heat flow by conduction and the enthalpy transport. The overall conservation of energy equation becomes:

$$\frac{d}{dX}\left[\sum_{K=1}^{n} h_K \dot{m}_K + h_I \dot{m}_I - \lambda \frac{dT}{dX}\right] = 0 \qquad (2\text{-}7)$$

If T is absolute temperature, and $T = T_0$ is standard condition temperature, assuming all chemical species may be considered to have constant and equal average specific heats at constant pressure, $\bar{C}_p$, we may write for the specific enthalpies:

$$h_K(T) = h_K^0 + \bar{C}_p(T-T_0) \qquad (2\text{-}8)$$

where h_K^0, K = 1, ..., n represents the standard heat of formation at temperature T_0 for the K^{th} chemical species.

The energy released by the forward reaction, per gram of reaction products formed under standard conditions is given by:

$$q = \sum_{K=1}^{r} Y_K * h_K^0 - \sum_{K=r+1}^{n} Y_K * h_K^0. \qquad (2\text{-}9)$$

Only exothermic reactions are considered, and for these, q is positive.

The Diffusion Equation. According to Fick's law for binary mixtures, the one dimensional flux of species K due to

the gradient in concentration is,

$$Y_K U_K = -D \frac{dY_K}{dX} \qquad K=1,\ldots,n;I \qquad (2\text{-}10)$$

where U_K is the diffusion velocity of species K.

The diffusion equation for the K^{th} species with D being the common diffusion coefficient for any 2 species in the mixture (could be a multicomponent mixture) interdiffusing into each other and transported with the bulk of the flow is,

$$\dot{m}_K = \rho\, Y_K\, (u+U_K) \qquad K=1,\ldots,n;I \qquad (2\text{-}11)$$

Substituting Eqns. (2-4) and (2-10) in Eqn. (2-11):

$$\dot{m}_K = \dot{m}\, Y_K - \rho\, D \left(\frac{dY_K}{dX}\right) \qquad K=1,\ldots,n;I \qquad (2\text{-}12)$$

The conservation and diffusion equations given so far determine completely the flow problem with chemical reactions, provided, we obtain an explicit expression for the rate of production of the various species. This expression is given in Eqn. (II-1) of Appendix II.

The differential equation for Y(X), defined in Eqn. (I-8), follows from Eqns. (2-2b), (2-12) and the expression for

$Y_K(X)$ in (I-7b):

$$\frac{d}{dX}\left(\dot{m}Y - \rho D \frac{dY}{dX}\right) = -\frac{\dot{w}}{G} \qquad X > 0 \qquad (2\text{-}13)$$

From the B.C's in Eqns (2-5), it follows that Y obeys the boundary condition:

$$\dot{m}Y - \rho D \frac{dY}{dX} = \dot{m} \qquad \text{at } X = 0+ \qquad (2\text{-}14)$$

The energy conservation relation now is developed by using enthalpy relations which are useful in defining a particular dimensionless variable $\tilde{T}$ representing temperature.

The total (static) enthalpy h in the mixture is defined as:

$$h = \sum_{K=1}^{n} h_K Y_K + h_I Y_I \qquad (2\text{-}15)$$

and it follows from Eqns. (2-8) and (I-7) that h is a function of Y and T only. For Y = 0, h(Y,T) is expressed as:

$$h(0,T) = \sum_{K=1}^{r} \frac{a_K W_K}{W_{total}} h_K(T) + \frac{a_I W_I}{W_{total}} h_I(T) - Gq \qquad (2\text{-}16)$$

Now, when the divergence of the total energy flux (Eqn. (2-7)), is integrated from $X = -\infty$ to $X = 0$ and the conditions $T \to T_0$ and $\lambda(\frac{dT}{dX}) \to 0$ as $X \to -\infty$ are imposed, where T_0 is the initial or pre-ignition temperature of the mixture, then the equation

$$\left[\sum_{K=1}^{n} h_K \dot{m}_K + h_I \dot{m}_I\right]_{X=0+} - \left(\lambda \frac{dT}{dX}\right)_{X=0+} = \dot{m} h(T_0) \qquad (2\text{-}17)$$

is obtained.

Let T_i be the ignition temperature; by the use of Eqns. (2-5) and (2-16), Eqn. (2-17) can be written as,

$$\left(\lambda \frac{dT}{dX}\right)_{X=0+} = \dot{m}\left[h(0,T_i) - h(T_0) + Gq\right] \qquad (2\text{-}18)$$

The final equilibrium flame temperature T_∞ is defined here by the equation:

$$h(0,T_\infty) = h(T_0) \qquad (2\text{-}19)$$

The definition of T_∞ is basically a statement of overall conservation of enthalpy for a completed reaction. The dimensionless temperature variable $\tilde{T}$ is then defined as:

$$\tilde{T} = \frac{h(0,T) - h(0,T_\infty)}{Gq} = \int_{T_\infty}^{T} \bar{C}_p(T)\,dT \qquad Gq \qquad (2\text{-}20)$$

Since in the present study $\bar{C}_p$ is a constant effective specific heat, thus:

$$\tilde{T} = \bar{C}_p(T-T_\infty)/Gq$$

By use of the definitions of Eqns. (2-19) and (2-20), we can transform Eqns. (2-7) and (2-18) respectively into the following differential equation and boundary conditions for $\tilde{T}(X)$:

$$\frac{d}{dX}\left(\dot{m}\tilde{T} - \frac{\lambda}{\bar{C}_p}\frac{d\tilde{T}}{dX}\right) = \frac{\dot{w}}{G} \qquad X > 0 \qquad (2\text{-}21)$$

$$\frac{\lambda}{\bar{C}_p}\frac{d\tilde{T}}{dX} - \dot{m}\tilde{T} = \dot{m} \qquad \text{at } X = 0+ \qquad (2\text{-}22)$$

The result

$$\tilde{T}(X) + Y(X) = 0 \qquad X \geq 0 \qquad (2\text{-}23)$$

follows from Eqns. (2-13), (2-14), (2-21) and (2-22) by making this important assumption that the Lewis number ($Le = \lambda/\rho\bar{C}_p D$), is equal to unity or, equivalently that,

$$\lambda = \bar{C}_p \rho D \tag{2-24}$$

This assumption implies essentially that the thermal diffusivity, $\alpha = \lambda/\bar{C}_p\rho$, is equal to the mass diffusivity, D. Developments in simple kinetic theory show that,

$$\alpha = D = \nu$$

where ν is the kinematic viscosity (momentum diffusivity). Thus from kinetic theory as a first approximation:

$$Pr = Sc = Le = 1$$

where Pr, Sc and Le are the Prandtl, Schmidt and Lewis numbers respectively. Eqn. (2-23) implies that if the reaction consumes all available reactant as $X \to \infty$ (this condition is written as $Y(\infty) = 0$), then $T \to T_\infty$ as $X \to \infty$ ($\tilde{T}(\infty) = 0$). The initial value problem consisting of Eqns. (2-21) and (2-22) together with a prescribed value $\tilde{T}(0)$ has a unique solution $\tilde{T}(X)$. If, in addition, $\tilde{T}(\infty)$ is prescribed, the problem is over specified and becomes an eigenvalue problem for the determination of a certain parameter which involves the burning rate. When the dimensionless coordinate ζ defined as

$$\zeta = \dot{m} \int_0^X \frac{dX}{\rho D} \tag{2-25}$$

is introduced into Eqns. (2-21) and (2-22), and when Eqns. (2-23) and (2-24) are used, the combustion problem is reduced to the following equation and boundary conditions for $\tilde{T}(\zeta)$:

$$\tilde{T}'(\zeta) - \tilde{T}''(\zeta) = \frac{\rho D \dot{w}}{G\dot{m}^2} \tag{2-26a}$$

$$\tilde{T}'(0) = 1 + \tilde{T}(0) \tag{2-26b}$$

$$\tilde{T}(\infty) = 0 \tag{2-26c}$$

As shown in Appendix II, with the assumption of a single step, forward reaction only, Eqn. (2-26a) becomes:

$$\tilde{T}'(\zeta) - \tilde{T}''(\zeta) = \frac{(\bar{K}p)^{r_f}}{u_0^2}\, \mu(\tilde{T})\ (-\tilde{T})^{\nu} \tag{2-27}$$

where $\mu(\tilde{T})$ is defined as:

$$\mu(\tilde{T}) = \mu_f(\tilde{T}) \prod_{K=s+1}^{r} \left(\frac{a_K W_K}{GW_{total} Y_K^*} - 1 - \tilde{T} \right)^{\nu'_K} \tag{2-28}$$

The indicated product in Eqn. (2-28) is to be interpreted as 1 if $s = r$. $\mu_f(\tilde{T})$ (Eqn. (II-10)), is positive for all positive values of $(-\tilde{T})$ for which T is positive.

Since $0 \leq Y(X) \leq 1$ it follows from Eqn. (2-23) that:

$$-1 \leq \tilde{T}(\zeta) \leq 0 \qquad (2\text{-}29)$$

Hence, the product in Eqn. (2-28) is positive. Consequently, $\mu(\tilde{T})$ is positive for all $\tilde{T}$ in the interval (2-29) for which T is positive. For the case of stoichiometric proportions of the fresh mixture, which was the case treated in [8], we have in Eqn. (2-27), $\nu = r_f$ and $\mu(\tilde{T}) = \mu_f(\tilde{T})$.

In summary, the right-hand side of Eqn. (2-27), is in general, a non-linear function of $\tilde{T}$ which is positive in some left neighborhood of $\tilde{T} = 0$ and which has a zero of order ν at $T = 0$.

The dimensionless ratio $(\bar{K}p)^{r_f}/u_0^2$ which appears in Eqn. (2-27) will be denoted by Λ, the eigenvalue:

$$\Lambda = \frac{(\bar{K}p)^{r_f}}{u_0^2} \qquad (2\text{-}30)$$

Eqns. (2-26), with Eqn. (2-26a) written in the form of Eqn. (2-27) constitute a boundary value problem for $\tilde{T}(\zeta)$. For each Λ on a certain semi-infinite interval, it can be shown that this problem has a unique solution [9]. The value of $\tilde{T}(0)$ can be specified in addition to the boundary conditions of Eqns. (2-26). The symbol $\tilde{T}_i$ (the non-dimensional ignition temperature) is used to denote the prescribed value of $\tilde{T}(0)$.

Eqn. (2-27) will be generalized by replacing the function $\mu(\tilde{T})(-\tilde{T})^{\nu}$ with a function $\Psi(\tilde{T})$ which is a continuous function of $\tilde{T}$ on a finite interval $\tilde{T}_0 \leq \tilde{T} \leq 0$, $\Psi(\tilde{T}) > 0$ if $\tilde{T}_0 < \tilde{T} < 0$ and $\Psi(0) = 0$.

Therefore, the boundary value problem becomes:

$$\tilde{T}''(\zeta) - \tilde{T}'(\zeta) = -\Lambda\Psi(\tilde{T}) \qquad \zeta \geq 0 \tag{2-31a}$$

$$\tilde{T}(0) = \tilde{T}_i \tag{2-31b}$$

$$\tilde{T}'(0) = 1 + \tilde{T}_i \tag{2-31c}$$

$$\tilde{T}(\infty) = 0 \tag{2-31d}$$

A necessary condition that Eqns. (2-31) have a solution is that $\Lambda > 0$. Negative values of Λ have no physical meaning, while the value 0 can be interpreted only as a limit.

Also $\tilde{T}_i$ must be restricted to the interval determined by the following inequalities in order for Eqns. (2-31) to have a solution:

$$\tilde{T}_0 \leq \tilde{T}_i < 0 \tag{2-32a}$$

and

$$-1 < \tilde{T}_i \tag{2-32b}$$

Using the transformation:

$$u = \tilde{T}(\zeta) \qquad 0 \leq \zeta < \zeta_* \qquad \text{(II-13)}$$

the interval $0 \leq \zeta < \zeta_*$ is mapped onto the interval $T_i \leq u < 0$ and Eqns. (2-31) are reduced to a first-order boundary value problem as shown in Appendix II.

After some mathematical manipulation presented in detail in Appendix II, the following inequalities are obtained:

$$\Lambda^- < \Lambda < \Lambda^+ \qquad \text{(2-33)}$$

where Λ^-, the lower bound and Λ^+, the upper bound of the eigenvalue are found to be:

$$\Lambda^- = \left[2 \int_{\tilde{T}_i}^{0} \frac{\Psi(u)}{(1+u)^2} \, du \right]^{-1} \qquad \text{(2-34a)}$$

$$\Lambda^+ = \left[2 \int_{\tilde{T}_i}^{0} \frac{\Psi(u)}{1+u} \, du \right]^{-1} \qquad \text{(2-34b)}$$

Eqn. (2-34b) implies that $\Lambda \to 0$ (given $\Psi(-1) > 0$) as $\tilde{T}_i \to -1$ and according to Eqn. (2-34a), $\Lambda \to \infty$ as $\tilde{T}_i \to 0$. From

Eqn. (2-30) it follows that the upper bound for the eigenvalue, Λ^+ will result in a lower bound for the burning velocity, u_θ and vice versa ($\bar{K}$, p and r_f are constant for a given mixture composition).

An iterative technique for obtaining successively narrower upper and lower bounds for Λ has been developed by Johnson and Nachbar [9]. This method constitutes a truly rigorous procedure for obtaining solutions of any desired accuracy. However, for most applications, Eqns. (2-34) will be sufficiently accurate and it is unnecessary to employ the iterative method.

2.3 APPLICATION OF THE ANALYSIS TO H_2S-AIR MIXTURES

The difficulty in applying the Johnson and Nachbar method or any one of the other existing analytical methods is that they rely on the chemistry and kinetics of the combustion process. The only way to overcome this difficulty, at least in part, is by making use of chemical kinetic parameters already known for certain reactions and since they are determined by the nature of elementary reaction processes, it is possible to extrapolate their values to other similar reactions within an acceptable range of values. E.g., for a second-order reaction, values of activation energy, E, or the pre-exponential factor, BT^β, could vary within certain

acceptable limits. This fact facilitates the task of performing a parametric study if necessary and getting a best fit with experimental results.

A consistent reaction mechanism for H_2S-air combustion is still lacking. A search of the published literature on H_2S oxidation has revealed that little information is available. A good review of the chemistry of sulphur oxidation process with respect to the kinetics and mechanisms of the various processes involved is given in Ref. [24]. A comprehensive list of literature dealing with this subject is given at the end of Ref. [24] including the work of the authors Levy, A. and Merryman, E.L.

Even for reactions that are known to take place, rate constants are not available [25,26]. The lack of data prevented us from carrying out chemical kinetic calculations in order to find the effective overall activation energy and frequency factor. Those two parameters are required for the solution of the flame's eigenvalue problem.

A recent study carried out here, at McGill University, by Frenklach and Lee [27] to determine the correlation for induction times in H_2S-air and H_2S-air-H_2O mixtures by pressure measurements behind reflected shock waves, shows the overall activation energy, E, for the H_2S oxidation to be about 26 Kcal/mole. This is the value used in the present calculations and is required to determine the eigenvalue's

upper and lower limits, but leaves still the burning velocity, u_0, unknown.

The calculation of u_0 requires the knowledge of the overall frequency factor, B_f as shown in Eqn. (2-44). The procedure employed in establishing a value for B_f will shortly be explained.

The analysis in section 2.2 is applied in the present work to the stoichiometric H_2S-air mixture for which the resultant burning velocity is approximately maximum. Other compositions (on the lean or rich side of the stoichiometric composition) could be analyzed as well by simple extensions of the approach used here based on the general equations and mathematical formulation of the eigenvalue problem shown in section 2.2 and Appendix II.

The overall stoichiometric reaction to be considered here is:

$$H_2S + 1.536\ O_2 + 5.727\ N_2 + \text{traces of } CO_2 \text{ and A} \rightarrow$$

$$.035\ O_2 + 5.722\ N_2 + .009\ NO + .9879\ H_2O + .0094$$

$$HO + .007\ H_2 + .0048\ SO + .9952\ SO_2 + \text{traces of } CO_2$$

$$\text{and A.}^* \qquad (2\text{-}35)$$

Thus, approximately 12% H_2S and 88% air is the reactants'

---

*The chemical equation is derived from equilibrium considerations by solving simultaneously the atom balance and chemical equilibrium equations.

stoichiometric composition and the air is mainly represented by about 19% O_2 and 69% N_2 on the left-hand side of Eqn. (2-35). For our purposes, a simplified approximate equation should be sufficient:

$$H_2S + 1.5\ O_2 + 5.72\ N_2 \rightarrow SO_2 + H_2O + 5.72\ N_2 \qquad (2\text{-}36)$$

The other species appearing in Eqn. (2-35) are omitted from this equation due to their insignificant mole fraction in the mixture.

Eqn. (2-36) is a particular case of Eqn. (2-1) which was the basis for the theoretical analysis. Based on that analysis, a numerical scheme for the solution of the eigenvalue problem was developed. It involves reasonable approximations and casting the equations in a form suitable for the numerical solution, which will now be discussed.

The integration of Eqns. (2-34) for the upper and lower bounds of the eigenvalue requires the evaluation of the function $\Psi(\tilde{T})$ (or $\Psi(u)$ if the transformation $u = \tilde{T}(\zeta)$ of Eqn. (II-13) is used) at each step in the integration process. Using the definition of $\Psi(\tilde{T})$ in Eqn. (2-27), together with Eqn. (2-28), where $s = r$ for the stoichiometric case and the definition of $\mu_f(\tilde{T})$ in Eqn. (II-10), then,

$$\Psi(\tilde{T}) = \left[\frac{\bar{W}(\tilde{T})}{\bar{W}(0)}\right]^{r_f}\left[\frac{T(\tilde{T})}{T^*}\right]^{\beta_f+\alpha-r_f} \exp[-E_f/RT(\tilde{T})](-\tilde{T})^{\nu} \qquad (2\text{-}37)$$

Interpretation of the various parameters in the above equation as applied to the numerical scheme and some of the approximations made will now follow.

The reaction order in the stoichiometric equation (2-36) is:

$$r_f = \nu = 2.5 \tag{2-38}$$

By using Eqns. (I-7), (I-9) (with equality holding for all K), (I-10), (II-6) and (2-23), it can be shown that

$$\bar{W}(\tilde{T})^{-1} = -\sum_{K=1}^{r} \frac{GY_K^*}{W_K} \tilde{T}(\zeta) + \sum_{K=Y+1}^{n} \frac{GY_K^*}{W_K} \tilde{T}(\zeta) + \frac{1}{\bar{W}(0)} \tag{2-39}$$

is the inverse of the mixture average molecular weight, $\bar{W}$, as a function of $\tilde{T}$. $\bar{W}(0)$ here is the final average molecular weight at the hot boundary with $\tilde{T} = 0$. It is calculated in the program from the product species coefficients on the right-hand side of Eqn. (2-36). From Eqns. (2-36) and (I-10), $G = .3388$, is in this case (stoichiometric ratios) the reactant species, H_2S and O_2, initial mass fraction. Numerical tests performed, proved that the ratio $\frac{\bar{W}(\tilde{T})}{\bar{W}(0)}$ throughout the range $-1 < \tilde{T} \leq 0$ is close to unity which means that the average molecular weight does not change significantly in the reaction. It is shown in the sample computer outputs of Appendix IV. Thus assuming this ratio to be equal to one is

an excellent approximation.

The sum $\beta_f + \alpha - r_f$ in Eqn. (2-37) can to a good approximation be assumed zero. β_f, the exponent of the temperature, T, in the pre-exponential factor of the Arrhenius equation, Eqn. (II-2) is found from kinetic theory to be 1/2 since the relative velocity of the molecules is proportional to $T^{1/2}$. However, the temperature dependence of the pre-exponential term is often modified from $T^{1/2}$ to $T^{\beta f}$ (β_f = 0, $\pm$1/2, 1 etc.) according to Penner, S.S. [23, Chpt. XVII] in order to provide a better fit of the experimental data. This temperature dependence of the pre-exponential term, $B_f T^{\beta f}$, may be considered negligible in comparison with the temperature sensitivity of the term $\exp[-E_f/RT(\tilde{T})]$ in the rate expression (2-37).

In the term $\exp[-E_f/RT(\tilde{T})]$ of Eqn. (2-37), the expression for $T(\tilde{T})$ based on the definition of $\tilde{T}$ in Eqn. (2-20) becomes:

$$T(\tilde{T}) = \frac{Gq}{\bar{C}_p} \tilde{T} + T_\infty \qquad (2\text{-}40)$$

where, $\bar{C}_p$, is the effective average specific heat at constant pressure of the mixture, calculated at about the middle temperature between the initial and final temperatures ($T \approx 1200°K$) and equal to .28 cal/g °K.

q is the total heat released per gram of reactant species

calculated from Eqn. (2-9) with the reference mass fraction values, Y_K^* derived from the chemical reaction equation (2-36) and the values of the standard enthalpies of formation for the reaction species given in Table 1. The enthalpies, together with other thermochemical properties of the reactant and product species appearing in Table 1, were compiled from Refs. [28,29]. q is found to be equal to 1637.2 cal/(gram of reactant species).

T_∞, which is the final equilibrium temperature must be known in advance in Eqn. (2-40) for the integration of Eqns. (2-34) to be possible. When all the heat evolved in the combustion process is used to heat the product gases, the product temperature, $T_{\infty,a}$, is defined as the adiabatic flame temperature.

For a reacting system whose product temperature is less than 1250 °K, the products are the normal stable species. However, most combustion systems reach temperatures appreciably greater than 1250 °K and dissociation of the stable species occurs. Since the dissociation reactions can be quite endothermic, a few percent dissociation can lower the flame temperature substantially. The determination of the final temperature is therefore much more complexed and requires the use of equilibrium relationships which exist among the product composition in the equilibrium system. Here, at McGill, the final equilibrium temperature of the stoichiometric

H_2S-air flame including the dissociation reactions, was calculated by Dr. C. Guirao and is approximately equal to 2069 °K. The adiabatic flame temperature without dissociation was found in the numerical scheme of the present work to be equal to 2275 °K; 206 °C higher than the one with the dissociation effects included. The final flame temperature considered in this work was $T_{\infty,a}$ = 2069 °K.

As a result of all the definitions and assumptions made above, the expression in Eqn. (2-37) for the function $\Psi(\tilde{T})$ is approximated by:

$$\Psi(T) \simeq \exp[-E_f/RT(\tilde{T})] \cdot (-\tilde{T})^{r_f} \qquad (2\text{-}41)$$

where E_f = 26 Kcal/mole is the activation energy whose value was discussed previously in this section and R = 1.9867 cal/mole °K, is the universal gas constant.

Eqn. (2-41) is the equation used in the numerical integration of Eqns. (2-34). The integration of each of those equations is repeated four times starting every time from a different ignition temperature ($\tilde{T}_i$ = -.9; -.8; -.7 and -.6) with step increments of .01 up to $\tilde{T}$ = 0. The insensitivity of the solution to the change in the ignition temperature mentioned before in this chapter is proven to be true from our numerical results (Chpt. V). The completion of the integration yields the upper and lower bounds for the eigenvalue

(Λ^+ and Λ^- respectively).

Left to be determined now are the corresponding values of the burning velocity, u_0, using Eqn. (2-30). This can be accomplished only after the frequency factor, B_f, which appears in the expression for $\bar{K}$ has been assigned a definite value. From Eqn. (II-11) we have:

$$\bar{K} = B_f^{1/r_f} \cdot \bar{K}^* \tag{2-42}$$

where $\bar{K}^*$ is implicitly defined by Eqns. (II-11) and (2-42). With some manipulations, $\bar{K}^*$ becomes:

$$\bar{K}^* = \left\{ (T^*)^{\beta_f+\alpha-r_f} \left(\frac{RT_0}{p\bar{W}(\tilde{T}_0)} \right)^2 \frac{\bar{\lambda}}{\bar{C}_p(T_{\infty,a})^{\alpha}} \left(\frac{\bar{W}(0)}{R} \right)^{r_f} \left(\sum_{K=1}^{r} \nu'_K W_K \right) \left[\prod_{K=1}^{r} \left(\frac{Y_K^*}{W_K} \right)^{\nu'_K} \right] \cdot G^{r_f-1} \right\}^{1/r_f} \tag{2-43}$$

where the term $(T^*)^{\beta_f+\alpha-r_f}$ drops out because of the assumption $\beta_f+\alpha-r_f = 0$ which was previously discussed. $\bar{W}(\tilde{T}_0)$ and $\bar{W}(0)$ are respectively the initial and final average molecular weights of the mixture. $\bar{\lambda}$, the effective average thermal conductivity is calculated in a way similar to that of the $\bar{C}_p$ calculation and is equal to 2.693×10^{-4} cal/cm sec °K.

Now, from Eqn. (2-30) we have:

$$u_0^2 = B_f \frac{(\bar{K}^*.p)^{r_f}}{\Lambda} = B_f.\phi \qquad (2\text{-}44)$$

The above equation indicates the need to use the experimental value for the burning velocity, u_0, in the stoichiometric H_2S-air mixture in order to determine the value of B_f. Using Eqn. (2-44) with the results for the upper and lower limits of the eigenvalue:

$$\phi^- = \frac{(\bar{K}^*.p)^{r_f}}{\Lambda^+} \qquad (2\text{-}45a)$$

and

$$\phi^+ = \frac{(\bar{K}^*.p)^{r_f}}{\Lambda^-} \qquad (2\text{-}45b)$$

Then the average value for ϕ is:

$$\phi = \frac{\phi^- + \phi^+}{2} \qquad (2\text{-}45c)$$

Substituting both, the value of ϕ from Eqn. (2-45c) (p = 1 atm and is considered constant throughout the reaction zone) and the experimental value for u_0 which is about 41 cm/sec

for 12% H_2S in air mixture (stoichiometric) in Eqn. (2-44); a value for B_f, ($B_f = u_0^2/\phi$) is obtained:

For $T_{\infty,a} = 2069\ ^\circ K \rightarrow B_f = 2.8625 \times 10^{13}$

and for $T_{\infty,a} = 2275\ ^\circ K \rightarrow B_f = 9.0670 \times 10^{12}$

Both values are reasonable though a little high for bimolecular reactions [30, p. 805].

$B_f = 2.8625 \times 10^{13}$ is the value used later in the numerical computations of the burning velocities for the H_2S-air-water spray mixtures. This, of course, requires the assumption of the constancy of B_f throughout with or without water sprays in the gaseous mixture.

2.4 ANALYSIS OF THE LAMINAR FLAME PROPAGATION IN A GAS AND WATER SPRAY COMBUSTIBLE MIXTURE

The water droplets considered here are dispersed within a combustible mixture in which they are assumed to be completely inert. The ignition of the mixture and the subsequent propagation of a laminar flame causes the droplets to undergo a partial or total phase change from liquid to gas (vapor) within the reaction zone of the deflagration wave.

In flame coordinates, it can be stated that a cold, fresh

gaseous mixture with water droplets (no vapor present) is flowing from negative infinity ($X = -\infty$) into the stationary flame surface ($X = 0$) where the fraction of the droplets evaporated depends on the heat transfer rate into the individual droplet, the droplet size, its relative velocity and the surrounding thermodynamic conditions such as pressure and temperature. If there is no total evaporation, the reduced size droplets flow out of the reaction zone together with the combustion products and vapor formed to reach an equilibrium temperature at positive infinity ($X = +\infty$).

In this research we were primarily concerned with the physical and not chemical effects of the water droplets on the flame inhibition mechanism and therefore the droplets were assumed to be inert. Experimentally, this was achieved by saturating the water with H_2S prior to spraying it into the flammability tube.

The water droplet experiences both, heat and mass transfer in the reaction zone. It acts as a heat sink, absorbing some of the heat released by the reaction via sensible heat transfer from the flame front to its surface and then due to the latent heat of vaporization. Less heat is then available for heating the combustion products and since the process is considered to be adiabatic, the final equilibrium temperature is lowered.

With the boiling temperature reached, the vapor is flowing

outward from the evaporating droplets surface into the surrounding gases by diffusion. The vapor molecules diffusing into the flame front further dilute the reacting mixture and, consequently, change its effective specific heat, $\bar{C}_p$, by increasing the inert species contribution. As $\bar{C}_p$ is increasing, the heat capacity of the overall mixture increases too and the temperature is then decreased.

The spray, with many droplets contributing their share in the process, affects the magnitude of the burning velocity. The objective here is to find a way in which a theoretical estimate of the change in the burning velocity could be made with a special reference to the case of H_2S-air mixtures.

It is important to notice that the coupling between the fluid dynamical equations of motion of the gas and the statistical spray relations (Appendix III) is so complicated, that the possibility of accurately incorporating all the aspects involved appears remote and solutions can be found for only a few simple cases.

The steady state conservation equations for a gaseous mixture containing a dilute water spray along with other governing equations and necessary assumptions will now be presented:

Conservation of mass: The flow is considered one-dimensional and all droplets are assumed to have the same average velocity, $\bar{v}$, which can be expressed from the spray

statistics equations in Appendix III as,

$$\bar{v} = \frac{\int_0^\infty v\, f\, dv}{H} \qquad (2\text{-}46)$$

by integrating the product of f and v over all the velocity space and then dividing by, H, the number of droplets per unit volume per unit range of radius (Eqn. III-1). The result is a statistical average for v. The overall continuity equation then becomes,

$$\rho_g u + \rho_s \bar{v} = \dot{m} = \text{constant} \qquad (2\text{-}47)$$

ρ_g is the gas density and ρ_s, the spray density, which is in fact the mass of condensed phase per unit spatial volume:

$$\rho_s = \int_0^\infty \rho_\ell \frac{4}{3} \pi r^3 \, H dr \qquad (2\text{-}48)$$

ρ_ℓ is the water or condensed phase density and hence $\rho_\ell \frac{4}{3} \pi r^3$ is the mass of a single droplet of radius r.

Because of the low Mach number of burning velocities in laminar flames as shown in section 2.2 (Eqn. (2-6)), and

since the initial relative velocity of the droplets and the gas is zero and the velocity gradients are small, all droplets will be assumed to travel at the same velocity as the gas ($\bar{v} = u$). Estimates of the droplet acceleration based on the drag force acting on it indicate that in the present problem, this approximation is valid [10, Chpt. 11, Sec. 7]. Eqn. (2-47) now becomes:

$$\rho u = \dot{m} \tag{2-49}$$

where $\rho = \rho_g + \rho_s$ is the total density of gas plus liquid.

It should be noted here that ρ_g is smaller than the usual density of the gas because of the volume occupied by the droplets but according to the definition of a dilute spray (Appendix III), the fractional volume occupied by the droplets is small and hence it is an excellent approximation to consider ρ_g as the density of the gas mixture without water droplets.

Finally, Eqns. (2-2) and (2-5) for the species mass conservation and mass fluxes at X = 0+ apply here as well.

Conservation of momentum: The force per unit mass exerted on a droplet by the surrounding gas is denoted by:

$$F = \frac{dv}{dt} \tag{2-50}$$

Among the effects that may contribute to F, are: (i) skin friction and separation drag, (ii) gravity and other body

forces, (iii) rotation of the droplet with respect to the gas, and (iv) pressure gradients in the gas. It can be shown [33] that the first of these effects is usually the largest in sprays. For effect (i) we may express F in terms of a drag coefficient C_D through the equation:

$$F = \frac{3}{8} \frac{\rho_g}{\rho_\ell} \frac{1}{r} |u-v|(u-v)C_D \qquad (2-51)$$

F is in fact the aerodynamic drag force per unit mass of a spherical droplet of radius r. The value of C_D depends mainly on the Reynolds number

$$Re = \rho_g |u-v| 2r/\mu_g \qquad (2-52)$$

where μ_g is the viscosity of the gas. In most sprays the particles are so small that the flow about them is laminar and the classical Stokes or Oseen formulae [10, Chpt. 11] are approximately valid. In terms of the force on individual particles then, the average force per unit volume exerted on the spray by the gas can be found. In our case this force is zero because it was assumed that the relative velocity of the droplets is zero ($u = \bar{v}$).

Another term which should be accounted for due to the spray is the one describing the momentum carried to the gas by

the vapor coming from the droplets. Again a zero relative velocity implies zero momentum here.

As for the momentum of the gas flow, the assumption of a constant pressure deflagration is valid here too and Eqn. (2-6) applies.

Conservation of energy: Same as Eqn. (2-7) except that here, two more inert species take part in the process; liquid water and water vapor, hence:

$$\frac{d}{dX}\left[\sum_{K=1}^{n} h_K \dot{m}_K + h_I \dot{m}_I + h_v \dot{m}_v + h_\ell \dot{m}_\ell - \lambda \frac{dT}{dX}\right] = 0 \qquad (2\text{-}53)$$

is the energy equation where h_v, the vapor's specific enthalpy is related to h_ℓ, the liquid's specific enthalpy by the following expression:

$$h_v(T) = h_\ell + h_{fg} + C_{p_v}(T-T_b) \qquad (2\text{-}54)$$

h_{fg}, C_{p_v} and T_b are the latent heat of vaporization at $T = T_b$, the vapor's specific heat and the boiling (saturation) temperature of the liquid droplet respectively.

The diffusion equation: Eqns. (2-10), (2-11) and (2-12) apply here too with Y_K now defining any gaseous species mass fraction (including water vapor) in the overall mixture

(gas plus water). This point is further elaborated on, in Appendix III.

The droplet vaporization equation: The rate of change of the size r of a droplet is defined as:

$$R = \frac{dr}{dt} \tag{2-55}$$

and with H defined in Eqn. (III-1) as the number of droplets per unit volume per unit range of radius we have:

$$\frac{d(\rho_g u)}{dX} = -\int_0^\infty \rho_\ell \, 4\pi r^2 R H \, dr \tag{2-56}$$

where the expression on the right-hand side of the equation above is equal to the grams per unit volume per second of vapor added to the gas due to the vaporization of water droplets.

The disappearance of the liquid phase is the cause for the appearance of the vapor phase as the reaction progresses, hence:

$$\frac{d(\rho_g u)}{dX} = -\frac{d(\rho_s \bar{v})}{dX} = \dot{m}\frac{dZ}{dX} \tag{2-57}$$

where Z, the gas mass fraction, was defined in Eqn. (I-14) of

Appendix I. From Eqns. (2-56) and (2-57) then:

$$\frac{dZ}{dX} = -\int_0^{\infty} \rho_\ell 4\pi r^2 R H \, dr/\dot{m} \qquad (2\text{-}58)$$

which is basically the most general vaporization rate equation and describes the change of the parameter Z through the reaction zone. By further assuming the spray to be monodisperse, meaning all the droplets are considered to have the same average radius, $\bar{r}$, (a statistical average for r could be found the same way it was done for v in Eqn. (2-46)), Eqn. (2-58) could be written in the form:

$$\frac{dZ}{dX} = \rho_\ell 4\pi \bar{r}^2 Rn/\dot{m} \qquad (2\text{-}59)$$

where n, the number of droplets per unit volume was defined in Eqn. (III-2). The equations and assumptions discussed so far in this section and Appendix III determine completely the combustion with water sprays problem, provided, explicit expressions for $\dot{w}$ and R are obtained. The expression for $\dot{w}$ is derived in Appendix II and given in Eqn. (II-22).

It remains to find an expression for R defined in Eqn. (2-55).

A prerequisite for a comprehensive treatment of spray

problems is a thorough understanding of the evaporation (or ignition and burning in reacting sprays) mechanism of a single droplet. By now, as stated in Appendix III, the steady state, spherically symmetric evaporation or combustion of a droplet in a quiescent atmosphere is well understood. Spalding, D.B. [60], Godsave, G.A.E. [61], Blackshear, P.L.Jr. [62], who adopted Spalding's approach, and many more investigated this phenomenon.

Some important assumptions upon which the analysis of single droplet vaporization is based are as follows:

(a) The droplet surface and the differential volume in the vapor (or flame front for a burning droplet) form concentric spheres.

(b) Convection effects may be neglected.

(c) Steady-state conditions are assumed for fixed droplet sizes. One can consider the droplet surface regression to be instant and the droplet to reach the radius used in the steady-state solution. The problem is therefore defined as quasi-steady.

(d) The effect of heat transfer by radiation is neglected.

(e) The temperature of the liquid droplet is assumed to be uniform and equal to the boiling temperature, T_b. According to Penner [23, Chpt. XXII], although this assumption is questionable, it does not exert a large effect on the theoretical results. Glassman, I. [12, Chpt. 6] claims that

the surface temperature is only a few degrees below the boiling temperature.

(f) The pressure is assumed to be uniform throughout the system.

Based on the above assumptions and considering the heat and mass transfer taking place without chemical reaction in the droplet and its surroundings, the following expression is derived for R [12, Chpt. 6]:

$$R = - \frac{\bar{\lambda}}{\bar{C}_p \rho_\ell} \frac{1}{r} \text{Ln} \left[1 + \frac{\bar{C}_p (T_f - T_\ell)}{h_{fg}} \right] \qquad (2\text{-}60)$$

where $\bar{\lambda}$ and $\bar{C}_p$ are the constant average thermal conductivity and specific heat of the gas around the droplet surface which is the water vapor in the present study. T_f and T_ℓ are the free stream and the droplet surface temperatures. $T_\ell = T_b$ from assumption (e) above and $T_f = T_\infty$, the adiabatic flame temperature, (This is only an approximation since T_f is changing through the reaction zone). The expression for R in the case of a burning droplet is similar to Eqn. (2-60) with just one more term in the logarithmic brackets due to the reaction as shown in Refs. [12, Chpt. 6; 23, Chpt. XXII].

In the present study $\bar{\lambda}_v$ and $\bar{C}_{p_v}$ are calculated at the film temperature $T_\infty + T_b/2$ to be 2.75×10^{-4} cal/sec cm °K and .59 cal/g °K respectively.

Since we have a constant pressure deflagration at 1 atm. pressure and based on assumption (f), the corresponding boiling temperature for the water droplet is T_b = 373 °K (100°C) and the latent heat of vaporization, h_{fg} = 539 cal/g at that temperature. Thus, as soon as the droplet surface reaches the boiling temperature, it starts to evaporate and remains at this temperature throughout the reaction zone with the saturated vapor pressure assumed to be at 1 atm. (assumptions (e) and (f) above).

The water droplet density, ρ_ℓ, at 373 °C is .972 g/cm^3 and with this last value Eqn. (2-60) is completely defined in terms of its parameters.

From the various equations for R, [33] it is seen that in all known cases of droplet evaporation and combustion, the relation,

$$R = - \chi / r^k \qquad (2\text{-}61)$$

is valid, where the nonnegative function χ is independent of droplet size and the exponent k is always within the range $0 \leq k \leq 1$.

In Eqn. (2-60) for R, where only evaporation is considered,

$$\chi = - \frac{\bar{\lambda}_v}{\bar{c}_{pv} \rho_\ell} \text{Ln} \left[1 + \frac{\bar{c}_{pv}(T_f - T_\ell)}{h_{fg}} \right] \qquad (2\text{-}62)$$

and the exponent, k = 1. Therefore, from the definition of R in Eqn. (2-55), the resulting equation is:

$$\frac{dr}{dt} = -\chi/r \qquad (2\text{-}63)$$

which is an ordinary 1st order differential equation. With the initial radius of a droplet r_0, at time, $t = t_0$, known; its radius r, at a later time t, in the evaporation process can be determined from Eqn. (2-63) above,

$$\int_{r=r_0}^{r} r\,dr = \int_{t=t_0}^{t} -\chi\,dt$$

Both sides of this equation are integrated to give the following relation:

$$r^2 - r_0^2 = -\chi(t-t_0)$$

or

$$r^2 = r_0^2 - \chi(t-t_0) \qquad (2\text{-}64)$$

This is the most common form of the evaporation rate equation (or burning rate equation for the case of reacting droplets) with χ referred to as the "evaporation coefficient" or "evaporation constant". Eqn. (2-64) has also been verified

by many experiments to hold for both, evaporation and burning of single droplets [12, chpt. 6; 23, chpt. XXII]. It is an empirical relation confirmed by theory as well. It is also important to note that for $r = 0$ in Eqn. (2-64), $\Delta t = t - t_0$ is the time it takes for the total evaporation of the droplet whose initial radius was r_0.

As it stands now, everything is set for the formulation of the eigenvalue problem. The unknown dependent variables of the problem are $\bar{r}$, ρ, u, Z, T and Y_K while the initial values $\bar{r}_0$, ρ_0, Z_0, T_0 and $Y_{K,0}$ are controllable by the experimental conditions. From the governing equations and the governing physical conditions as stated, it can be shown that a system of first-order differential equations (energy, diffusion and evaporation rate) and algebraic equations (equation of state, mass, momentum, etc.) will be sufficient to solve for those unknowns.

An additional boundary condition here will be $Z \to Z_\infty$ as $X \to \infty$ ($Z_\infty = 1$ for total evaporation). The other boundary conditions remain the same as in Eqns. (2-31) for the case without water spray.

The representation and computation of the eigenvalue problem is quite complexed, making it impossible to get a closed form solution. Instead, a simplified model which is basically the modified Johnson and Nachbar method will be presented here. The procedure in section 2.2 had to be

extended in order to incorporate the presence of water droplets in the mixture. Accordingly, a numerical scheme was developed, very similar to the one outlined in section 2.3, for the stoichiometric H_2S-air mixture with water sprays of various droplet size distributions and densities.

To start with, it is required to calculate Z_0 and Z_∞, the initial and final mixture gas mass fractions respectively. The knowledge of these two parameters is an indication of the amount of water evaporated in the process.

Eqn. (I-16) of Appendix I tells us that, $Y_v = Z-Z_0$, is the mass fraction of the vapor at any time in the reaction zone and consequently, $Y_{v_\infty} = Z_\infty - Z_0$ is the final vapor mass fraction at the hot boundary.

The values of Z_0 and Z_∞ depend directly on the initial spray parameters: (i) the initial droplet size distribution and (ii) the initial spray density, ρ_{s_0}; which are controlled experimentally. Droplet size distribution curves were supplied by the manufacturer of the nozzles used and are shown in Figs. 3-8. Since the spray was assumed to be monodisperse, it is the median volume diameter, $\bar{d}_0$, which was used as the average droplet diameter. (For the experimental details refer to Chpt. IV). The spray was also assumed to be uniformly distributed throughout the flammability tube with gravitational effects neglected. ρ_{s_0} and ρ_{g_0} can easily be calculated and then the value of Z_0 can be determined

$(Z_0 = \rho_{g_0}/(\rho_{g_0} + \rho_{s_0}))$.

The determination of Z_∞ is somewhat more complicated and depends, of course, on the extent of the evaporation.

In the evaporation rate equation, Eqn. (2-64), r_0 is known and χ, the "evaporation coefficient", is found from Eqn. (2-62), but the final radius, r_∞, of the droplet at equilibrium and the period of time elapsed from beginning to end of the evaporation process are unknown. Here, the time parameter, $\Delta t = t_\infty - t_0$, is the period through which a stationary droplet would be in contact with the moving flame front referred to as the residence time of that droplet in the flame's reaction zone. An estimate of Δt is obtained by the relation,

$$\Delta t = \delta/u_{sp} \tag{2-65}$$

where, δ, is the reaction zone thickness and u_{sp} is the spatial or observed velocity which is the flame velocity as measured in the experiments. The approach here is similar to the one employed in Ref. [7].

An estimate of δ, based on laminar flame theory [10, Chpt. 5] is given by,

$$\delta \simeq \bar{\lambda}/(\bar{C}_p \rho_0 u_0) \tag{2-66}$$

where it is assumed that in an adiabatic flame with no energy

lost downstream, all of the heat released must be conducted upstream, viz., $\bar{C}_p(T_\infty - T_0)\dot{w}\delta \simeq \bar{\lambda}(T_\infty - T_0)/\delta$, thus,

$$\delta \simeq \sqrt{\lambda/(C_p\dot{w})} \qquad (2\text{-}67)$$

And since mass conservation implies that:

$$\rho_0 u_0 = \dot{w}\delta \qquad (2\text{-}68)$$

Eliminating $\dot{w}$ between Eqns. (2-67) and (2-68) leads to the relation (2-66) for the estimate of δ which is found to be around 2×10^{-2} cm for the stoichiometric H_2S-air flame.

As to the use of u_{sp} in the relation (2-65), (the unburned gas velocity is considered to be practically zero), rather than, u_0, the burning velocity, it is justified due to the fact that u_{sp} is the axial velocity of the flame along the tube measured with respect to a stationary observer which could be assumed to ride on any stationary droplet. In other words, the flame front sweeps through the stationary droplet at the axial observed velocity, u_{sp} and not at the burning velocity which is normal to the curved surface of the flame.

Once Δt is determined, the final droplet radius, r_∞, can then be easily calculated from Eqn. (2-64). With u_{sp}, measured experimentally to be about 80 cm/sec in the stoichiometric

H_2S-air mixture, Δt, viz. Eqn. (2-65) is equal to 2.5×10^{-4} sec. Knowing r_∞, the fraction of liquid evaporated (%) is now,

$$\% F_v \text{ (by mass or volume)} = [1-(r_\infty/r_0)^3] \times 100 \% \qquad (2\text{-}69)$$

With the total mass of the water spray initially present in the tube known and the liquid fraction evaporated, calculated from Eqn. (2-69), the total mass of the vapor added is then derived. The expression for Z_∞ becomes:

$$Z_\infty = Z_0 + Y_{v_\infty} = Z_0 + \frac{\text{total vapor mass}}{\text{total mixture mass (gas plus liquid)}} \qquad (2\text{-}70)$$

Now that Z_0 and Z_∞ are known, it remains to derive the governing differential equation and boundary conditions applied to the simplified model developed presently. The following procedure is basically the same as the one represented in section 2.2 viz., Eqns. (2-15) - (2-34), but it considers in addition the effect of water droplets and water vapor in the combustible mixture. We begin by defining the total static enthalpy per unit mass of the overall mixture:

$$h = \sum_{K=1}^{n} h_K Y_K + h_I Y_I + h_v Y_v + (1-Z) h_\ell \qquad (2\text{-}71)$$

where all the variables have previously been defined. Again h can be expressed as a function of Y and T as was the case in Eqn. (2-16) but now it depends on a third variable, Z.

For Y = 0, h(Y,Z,T) can be expressed as:

$$h(0,Z,T) = \sum_{K=1}^{r} \frac{a_K W_K}{W_{total}} h_K(T) + \frac{a_I W_I}{W_{total}} h_I(T) - Gq + Y_v h_v(T) + (1-Z)h_\ell \tag{2-72}$$

Using the relation between h_v and h_ℓ in Eqn. (2-54) we can write:

$$h(0,Z,T) = \frac{1}{W_{total}} \left[\sum_{K=1}^{r} a_K W_K h_K(T) + a_I W_I h_I(T) \right] - Gq$$

$$+ (1-Z_0)h_{\ell_{T=T_b}} + (Z-Z_0)\left[h_{fg_{T=T_b}} + \bar{C}_{p_v}(T-T_b)\right] \tag{2-73}$$

where the liquid droplets are assumed to be at the boiling temperature, $T_b = 373$ °K (assumption (e) in the analysis of a single droplet).

At this point a major simplification is introduced in that h is made to be a function of T only, with $Z = Z_\infty$. Eqn. (2-73) will now be written as:

$$h(0,Z_\infty,T) = \frac{1}{W_{total}}\left[\sum_{K=1}^{r} a_K W_K h_K(T) + a_I W_I h_I(T)\right] - Gq$$

$$+ (1-Z_0)h_{\ell_{T=T_b}} + (Z_\infty - Z_0)[h_{fg_{T=T_b}} + \bar{C}_{p_v}(T-T_b)] \qquad (2\text{-}74)$$

This assumption simplifies enormously an otherwise complex problem, since Z is a variable changing in the reaction zone from Z_0 to Z_∞ the same way Y changes from 1 to 0. By relating these two parameters to the hot boundary, where Y = 0 and $Z = Z_\infty$, the need to account for the variation of Z is eliminated. This is made further possible by defining the following dimensionless variable $\tilde{T}$ as:

$$\tilde{T} = \frac{h(0,Z_\infty,T) - h(0,Z_\infty,T_\infty)}{Gq - (Z_\infty - Z_0)h_{fg_{T=T_b}} - (1-Z_0)\bar{C}_{p_\ell}(T_b-T_0)}$$

$$= \frac{[Z_0\bar{C}_p + (Z_\infty - Z_0)\bar{C}_{p_v}](T-T_\infty)}{(G-C_1)q} = \frac{\bar{C}_{p_g}(T-T_\infty)}{Jq} \qquad (2\text{-}75a)$$

Where the definition of $h(0,Z_\infty,T)$ in Eqn. (2-74) was used and where:

$$\bar{C}_{p_g} = Z_0\bar{C}_p + (Z_\infty - Z_0)\bar{C}_{p_v} \qquad (2\text{-}75b)$$

is the average gas phase specific heat per unit mass of the overall mixture. The first term on the right-hand side denotes all the reactant and inert species contribution while the second term stands for the total vapor contribution to $\bar{C}_{p_g}$.

It should be noted that without the very important assumption of $Z = Z_\infty$ = constant, the vapor term in Eqn. (2-75b) above should read, $(Z-Z_0)\bar{C}_{p_v} = Y_v\bar{C}_{p_v}$, where, Y_v is increasing in the reaction zone from 0 at the cold boundary ($x = 0$) to, $Z_\infty - Z_0$, at the hot boundary ($X = \infty$). Here it is considered constant and equal to its hot boundary value, $Y_{v_\infty} = Z_\infty - Z_0$, all the way through. Next,

$$C_1 q = (Z_\infty - Z_0)h_{fg_{T=T_b}} + (1-Z_0)\bar{C}_{p_\ell}(T_b - T_0) \qquad (2\text{-}75c)$$

is the heat lost per unit mass of the overall mixture, due to the latent heat of vaporization (1st term on the right-hand side) and due to the sensible heating of the water droplets from the room temperature, T_0, up to the boiling temperature, T_b (2nd term on the right-hand side) and finally

$$J = G - C_1 \qquad (2\text{-}75d)$$

by definition where $0 \leq C_1 < G$. Jq, in the denominator of Eqn. (2-75a) could be considered to represent the apparent

or pseudo heat of reaction per unit mass of the mixture. It has a lower value than the heat of reaction per unit mass of the mixture without water droplets, Gq, (Eqn. (2-20)), because obviously J << G in Eqn. (2-75d).

In light of the discussion of Eqns. (2-75) above, again like in Eqn. (2-20), the definition of $\tilde{T}$ in Eqn. (2-75a) is no more than a statement of overall conservation of enthalpy. Furthermore, the value for the adiabatic flame temperature, $T_{\infty,a}$, without dissociation effects considered, is derived from the overall conservation of enthalpy relation, which reads:

$$Z_0\bar{C}_p(T_{\infty,a}-T_0)+(Z_\infty-Z_0)\bar{C}_{p_v}(T_{\infty,a}-T_b) = Gq-(1-Z_0)C_{p_\ell}(T_b-T_0)$$

$$- (Z_\infty-Z_0)h_{fg_{T=T_b}} = Jq \qquad (2\text{-}76)$$

where the definition of $\tilde{T}$ in Eqn. (2-75a) was used.

The definition of $\tilde{T}$ is also used in the transformation of Eqn. (2-53), the energy equation, into the following differential equation:

$$\frac{d}{dX}\left(\dot{m}\tilde{T} - \frac{\lambda}{C_{p_g}}\frac{d\tilde{T}}{dX}\right) = \frac{\dot{w}}{J} \qquad X > 0 \qquad (2\text{-}77)$$

and with transforming Eqn. (2-18), the boundary condition for

$\tilde{T}(X)$ becomes:

$$-\dot{m}\tilde{T} + \frac{\lambda}{C_{p_g}} \frac{d\tilde{T}}{dX} = \left(\frac{G}{J}\right)\dot{m} \qquad \text{at } X = 0+ \qquad (2\text{-}78)$$

If now the differential equation for $Y(X)$ and its boundary condition in Eqns. (2-13) and (2-14) are both multiplied throughout by the factor (G/J), it follows that,

$$\frac{d}{dX}\left(\dot{m}Y^* - \rho D \frac{dY^*}{dX}\right) = -\frac{\dot{w}}{J} \qquad X > 0 \qquad (2\text{-}79)$$

with the boundary condition for $Y^*(X)$:

$$\dot{m}Y^* - \rho D \frac{dY^*}{dX} = \left(\frac{G}{J}\right)\dot{m} \qquad \text{at } X = 0+ \qquad (2\text{-}80)$$

where the new function $Y^*(X)$ is defined as:

$$Y^*(X) = \frac{G}{J} Y(X) \qquad (2\text{-}81)$$

Thus, the result,

$$\tilde{T}(X) + Y^*(X) = 0 \qquad X \geq 0 \qquad (2\text{-}82)$$

follows from Eqns. (2-77) - (2-81) by assuming again Le = 1,

implying an analogy between heat and mass diffusion, as was the case for the combustible mixture without water spray (Eqn. (2-23)).

Using the transformation $\zeta = \dot{m} \int_0^X \frac{dX}{Z\rho D}$ in Eqns. (2-77) and (2-78), together with the result in Eqn. (2-82), the combustion problem reduces to the following equation and boundary conditions for $\tilde{T}(\zeta)$:

$$\tilde{T}'(\zeta) - \tilde{T}''(\zeta) = \frac{Z\rho D\dot{w}}{J\dot{m}^2} \qquad (2\text{-}83a)$$

$$\tilde{T}'(0) = \frac{G}{J} + \tilde{T}(0) \qquad (2\text{-}83b)$$

$$\tilde{T}(\infty) = 0 \qquad (2\text{-}83c)$$

Eqns. (2-83) above are analogous to Eqns. (2-26).

In Appendix II the right-hand side of Eqn. (2-83a) is brought to a form suitable for the determination of the eigenvalue, upper and lower bounds. The procedure is the same as without water spray except for few changes in the expression of e.g. $\dot{w}$, ρ, etc. shown in Appendix II.

The final result for Λ^- and Λ^+ is:

$$\Lambda^- = \left[2 \int_{\tilde{T}_i}^{0} \frac{\Psi(u)}{(a+u)^2}\, du \right]^{-1} \qquad (2\text{-}84a)$$

$$\Lambda^{+} = \left[2\int_{\tilde{T}_i}^{0} \frac{\Psi(u)}{(a+u)_o}\, du \right]^{-1} \qquad (2\text{-}84b)$$

The "scale factor", $\bar{K}$, in the expression for the eigenvalue Λ, Eqn. (2-30) becomes now:

$$\bar{K} = B_f^{1/r_f} \left\{ \frac{(T^*)^{B_f+\alpha-r_f}}{\rho_0^{\,2}} \frac{\lambda}{\bar{C}_{pg}(T_{\infty,a})^{\alpha}} \left(\frac{\bar{W}(0)\cdot J}{R\cdot Z_{\infty}} \right)^{r_f} \cdot \left(\sum_{K=1}^{r} \nu'_K W_K \right) \left[\prod_{K=1}^{r} \left(\frac{Y_K^*}{W_K} \right)^{\nu'_K} \right] \cdot \frac{1}{J} \right\}^{1/r_f} \qquad (2\text{-}85)$$

where use was made of the explicit general expression for $\bar{K}$ in Eqn. (II-11). In the numerical scheme the relation (2-85) above is further simplified based on the assumptions previously made in section (2-3) and which resulted in the expression for $\bar{K}^*$ in Eqn. (2-43).

The integration of Eqns. (2-84) starts from $\tilde{T}_i$, the non-dimensional ignition temperature. The integrations are done for $\tilde{T}_i$ = -.9; -.8; -.7 and -.6 as for the dry H_2S-air mixtures.

In the definition of $\tilde{T}$ in Eqn. (2-75a), which has in the numerator a term accounting for the vapor added, it was assumed that the water droplets start to evaporate in the preheat zone (Fig. 2), even before reaching the ignition plane

or at the latest in the ignition flame. Thus, evaporation starts in the region $X \leq 0$ and therefore $\tilde{T}_b \leq \tilde{T}_i < 0$ ($\tilde{T}_b$ corresponds here to $T_b = 373°K$) is the range of physically acceptable values for $\tilde{T}_i$ in the integration of Eqns. (2-84).

The numerical integration is performed separately for two constant values of Z, (i) $Z^* = Z_\infty$, according to the foregoing analysis and (ii) $Z^* = (Z_0+Z_\infty)/2$ which is the value of Z, midway between Z_0 and Z_∞. In using this value, it is the approach of William, F.A. [32, p. 238] which was adopted.

With a parametric study done for both values of Z, their relative effect on the burning velocity results is discussed in Chapter V of this thesis.

CHAPTER III

MEASUREMENT OF BURNING VELOCITY

In laminar flame propagation, the fundamental parameter is the laminar burning velocity. It is the velocity normal to the flame surface as it propagates through the adjacent layers of unburned gas.

The burning velocity is determined by the thermochemical and transport properties of the combustible mixture and is therefore a fundamental constant of the particular gas mixture at a given pressure and temperature, independent of other experimental conditions. The aim of laminar flame theories is to predict burning velocity (Chpt. II).

The difficulty in measuring burning velocity is that in nearly all practical cases the flame front is not normal to the velocity of the gas stream. The flame front is either curved in propagating flames or conical in stationary ones.

There are several methods for measuring that velocity. These methods can be divided into two groups: (i) those involving stationary flames (burner methods) and (ii) those involving propagating flames.

There are limitations to the methods of both groups. For the various burner methods, the flame is stabilized on the burner rim, which acts as a sink for heat and active

species. There is also a variation in the gas velocity across the cross section of the burner tube, arising from the flow development in the tube and the interaction of this with the pressure field generated by the flame. For those burner methods, the burning velocity is equal to the component of the fresh gas flow normal to the flame front. Typical methods of this group are the Gouy's flame-area method, cone angle methods, the particle track method, etc. [12, Chpt. 4; 35, Chpt. IV; 36, 37, 50, 52, 55].

For propagating flame methods, which are of interest in the present work, the gas movements produced by the flame itself and the shape of the flame surface must be taken into account. Furthermore, non-uniform and unsteady flame propagation observed in some situations must be avoided. The tube method (used here), the spherical bomb method, the double kernel method, etc. are just a few examples of propagating flame methods [12, Chpt. 4; 35, Chpt. IV; 36-42, 49, 51, 53, 54]. Ref. [12, Chpt. 4; 35, Chpt. IV; 36, 37] include surveys and criticism of both groups of methods.

The cylindrical tube method, which was first introduced by Coward and Hartwell [40], further refined by Coward and Payman [41] and later by Gerstein et al. [42], is the method adopted for this investigation.

For an ideal plane flame front as shown in Fig. 1, the burning velocity u_0 is the velocity of the flame front relative

to the unburned gas immediately ahead of it and is defined by the relation:

$$u_0 = u_{sp} - u_u \qquad (3\text{-}1)$$

u_{sp} is the spatial or absolute velocity. It is the axial flame velocity measured with respect to a fixed observer.

u_{sp} is the velocity actually measured by using the tube method. u_u, the unburned gas velocity ahead of the flame front, can also be measured as an average value by e.g. observing the displacement of a soap bubble through an opening at the top end of the tube [42].

The velocity u_u is affected by the flame because of pressure waves propagating from the hot, expanded combustion products through the flame front into the initially quiescent unburned gas which is now set in motion. Thus, Eqn. (3-1) accounts for the fact that the flame is propagating within a moving gas but the effect of curved flame surface which is the actual case is not incorporated.

Obviously, a curved surface is larger than the cross section of the cylindrical tube in which the flame is propagating. This implies a higher rate of consumption of the combustible mixture or in other words a higher conversion rate of reactant species to product species due to a larger surface of the reaction zone.

It follows from the definition of burning velocity that:

$$\frac{\partial(\rho_0 V_u)}{\partial t} = - \rho_0 A_{f\ell} u_0 \qquad (3\text{-}2)$$

Where the relation above describes the mass of unburned gas mixture consumed per unit time. V_u is the volume of the remaining portion of the unburned gas at any time and $A_{f\ell}$ is the flame surface area. It is assumed in Eqn. (3-2) that u_0 has an average constant value over the entire curved flame surface. If ρ_0 is also constant, then

$$\frac{\partial V_u}{\partial t} = - A_{f\ell} u_0 \qquad (3\text{-}3)$$

is the expression for the volume burning rate.

Also from the definition of u_{sp} and u_u which are both axial velocities in a direction normal to the tube cross section and Eqn. (3-1), it follows that

$$\frac{\partial(\rho_0 V_u)}{\partial t} = - \rho_0 A_t (u_{sp} - u_u) = - \rho_0 \pi R^2 (u_{sp} - u_u) \qquad (3\text{-}4)$$

Where R is the radius of the cylindrical tube with cross sectional area A_t and where the right-hand side is again equivalent to the mass burning rate. Since ρ_0 is constant,

$$\frac{\partial V_u}{\partial t} = - \pi R^2 (u_{sp} - u_u) \qquad (3\text{-}5)$$

Equating the right-hand side of Eqns. (3-3) and (3-5) and substituting for u_0, we get

$$u_0 = (u_{sp} - u_u) \pi R^2 / A_{f\ell} \qquad (3\text{-}6)$$

That is the expression from which u_0 can be determined once all the parameters on the right-hand side are measured and determined experimentally. It follows from the expression for u_0 that the higher the ratio $A_{f\ell}/A_t$ the higher will be spatial propagation velocity, u_{sp}, of the flame since u_0 and u_u remain approximately unchanged. Another purely mathematical proof of Eqn. (3-6) based on Eqns. (3-2) and (3-3) is given in Ref. [37].

When, the velocity of the unburned gas u_u is negligible or zero, Eqn. (3-6) becomes

$$u_0 = u_{sp} \frac{\pi R^2}{A_{f\ell}} \qquad (3\text{-}7)$$

Coward and Hartwell [40] were the first to prove the relation in (3-7) experimentally, and acknowledged the fundamental importance of the burning velocity parameter.

By running flames through three different diameter tubes and measuring their spatial, axial speeds and the area of the flame surface, Coward and Hartwell [40] confirmed for a 10% methane-air mixture the constancy of the ratio, u_0 = volume burned per sec/area of the flame surface. This ratio is clearly equivalent to the expression in Eqn. (3-7). They concluded, therefore, that the ratio u_0 is the linear speed of flame, in a direction normal to its surface, through a gaseous mixture at rest and at constant temperature and pressure just ahead of the flame. They suggested that u_0 be described as the "fundamental speed of flame", defined here as the burning velocity.

Coward and Payman [41] whose modification was later adopted by Gerstein et al. [42] considered, also the velocity of the unburned gas ahead of the flame, u_u and therefore came up with the relation in Eqn. (3-6).

In our experiments, u_u, could be assumed close to zero because the closed top of the tube represents a zero velocity boundary with no efflux of unburned gas as would be the case with an orifice at the top. Besides, as will shortly be explained, an orifice at the bottom end was used to minimize the effects due to the back flow of expanded gases by reducing the pressure waves, and thus keeping the pressure almost constant throughout the flammability tube or both sides of the flame front. With very small pressure gradients due also

to relatively low burning velocities, and a closed boundary at the top, the bulk of the unburned gas trapped between the flame front and the top end is practically undisturbed except for the layers adjacent to the flame front and the assumption of $u_u = 0$ holds.

Although there are some drawbacks to the cylindrical tube method, it was adopted for the following reasons:

(a) The requirement for a dilute spray which is important in this study and was one of the major assumptions in the theoretical analysis of the combustible mixture with water spray (section 2.4), can be easily achieved in the relatively long and large diameter tubes used for this type of experiment as compared to the open tube or porous flameholders. In porous burners, the spray distribution which we are interested in as an experimental and study variable, is destroyed at the screen or grid on the burner mouth. As for the open tube burners, usually they are limited in size especially at the inlet tubes, and this makes it almost impossible to flow a gaseous mixture together with a water spray without a high degree of collision and coalescence of the droplets inside. Besides, in most of the burner methods, the fixed flame surface or cone angle are very important in determining the burning velocity and unevaporated droplets which still had enough inertia to flow through the flame surface could have an adverse effect on the measurements.

(b) The cylindrical tube method is easy to apply and quick to operate. The equipment necessary is also simpler and cheaper especially when a simple Plexiglas or glass tube is used.

(c) One can identify instantly on the same picture, non-uniform movement of the flame, where it occurs in the tube, the flame spatial velocity, and its shape or surface area.

(d) The photographic set-up for the direct photography of the luminous zone in the flame front is cheaper and simpler than other common methods of flame photography such as shadowgraph, Schlieren, streak or interferometry methods.

(e) One gets reproducible and comparable results.

The difficulties in applying the cylindrical tube method are:

(a) The curvature of the flame front due to effects such as cooling at the tube walls, viscosity of the burned gases, etc. [43, Chpt. E] makes it a little difficult to determine accurately the flame surface area as can be seen in Figs. 9-11. Henderson and Hill [53] have shown that the value of the flame area depends on the method used to evaluate it, and that some calculations may overestimate the value of it by 20%. The flame shape might also change due to non-uniform movement.

When comparing the pictures for methane-air flames in Fig. 9, to those for H_2S-air flames in Figs. 10 and 11, there is an obvious difference in that the surface area of the

methane-air flames is larger than that of the H_2S-air flames.

Measurements of two out of the three principal axes for both types of flame surface, in the plane of the pictures taken, have shown the methane-air flame surface to be approximately that of half a prolate spheroid and the H_2S-air flame surface, a hemisphere. In both cases the flame surface is tangent most of the time, particularly, in uniform movement of the flame to the inner wall of the tube. This was confirmed by taking pictures at different positions around the tube. In each of the two mixtures, based on the pictures in Figs. 9-11 and many more, the flame surface area was assumed constant over the entire flammable composition range.

Keeping the flammability tube in the vertical position was useful in avoiding the buoyancy effects which are significant in flames propagating in horizontal tubes and thus distorting the flame front. Friedman and Burke [45] had shown that, for any given mixture, the flame area bears a nearly constant ratio to the tube cross section, thus confirming our assumption. Gerstein et al. [42] went even further by assuming that in using the same experimental tube the flame front surface area remained constant for all of the hydrocarbons studied in their research (37 of them) which is doubtful, as was also shown in Ref. [45].

As for the shape of the flame, various concepts exist. Coward and Hartwell [40], for instance, calculated the area

of the flame front by matching it to a portion of ellipsoid symmetric about the vertical plane through the axis of the tube. Gerstein et al. [42] assumed the same shape for the flame front as Coward and Hartwell's [40] but subtracted from this surface the area of half a prolate spheroid. Guénoche and Jony [44,45] doubt both and other methods which they critically assess in [45]. According to them the flame front has the appearance of a "spoon" [44] tangent to the inner wall of the tube, which takes up some position in the tube and travels the length of the tube maintaining a costant area. Guénoche and Jouy [45] end up their discussion of the various methods for the calculation of the flame front area by concluding that the complex shape of the flame together with its luminosity and the optical limitations of the direct photography method are the main source of error in estimating the burning velocity.

(b) The flame movement could be at times vibratory and unsteady. When this occurs, the flame front undergoes changes which are undesirable in the context of determining burning velocities.

The tube with its two columns of unburned and burned gas forms a resonator that can vibrate in various modes above the fundamental frequency depending on the boundary conditions of the tube, its cross section and the mixture used. The flame front between the two columns acts like a piston from which

compression waves are emanating towards the unburned gas, while rarefaction waves are propagated backwards into the expanding burned gases. The interaction between those waves and the gas column results in acoustic vibrations. By introducing the proper boundary conditions in the tube, the vibrations can be almost completely suppressed down to the fundamental frequency and a very small amplitude. The result will be a uniform flame propagation.

Guénoche and Laffitte [47] achieved this by partially closing the bottom open end of the tube using an orifice. Guénoche, Manson and Monnot [48] showed a theoretical way to calculate the tube I.D./orifice diameter ratio on the basis of the action of the orifice on the reflection of waves reaching the ignition end of the tube. Clearly, the orifice allows the hot, expanding burned gases to flow outwards and based on acoustic impedance matching at that end for the gas column, the reflexion of waves can be very much attenuated and the pressure kept nearly constant on both sides of the flame front all along the tube. Guénoche et al. [48] established that a uniform movement of the flame is possible when:

$$3 < \text{Tube I.D./orifice diameter} < 4$$

for

$$10 \text{ mm} \leq \text{tube I.D.} \leq 26 \text{ mm}.$$

In the present work it was found experimentally that for a tube I.D. ranging from 2" (50.8 mm) to 3" (76.2 mm) a 1" (25.4 mm) diameter orifice at the bottom ignition end gave good results for both types of mixtures investigated, methane-air and H_2S-air (see Chapter IV).

(c) The stroboscopic photography method used here could be defective if the burned gas is bright enough to impress the photographic film. Here the problem arose particularly with fuel rich H_2S-air mixtures and was solved by reducing the exposure rate with decreasing the number of opened slits in the rotating disc (Fig. 14) thus getting less snap-shots of the flame front but a better and clearer separation.

Summing up it should be noted that with all the different methods for the determination of burning velocities developed so far, there is no agreement on a standardized one [37]. Laffitte [66] and Combourieu [67] have discussed experimental details and theoretical relationships for the burner, soap - bubble, explosion vessel and tube methods. They conclude by favoring the vertical tube method and present a compilation of experimental values of burning velocity for various gases. In a later review [68], they conclude that the tube method is best for burning velocities up to 80 cm/sec and that the constant volume bomb method is best for the higher burning velocities. By using the vertical tube method we measured values of burning velocities comparable to those of other

investigators. The results are discussed in detail in Chapter V of this thesis.

CHAPTER IV

EXPERIMENTAL DETAILS

4.1 THE EXPERIMENTAL APPARATUS

A schematic diagram of the experimental apparatus is shown in Fig. 12. There are three main parts:

(a) The flame apparatus and its affiliated gas supply and exhaust systems;

(b) The water supply system;

(c) The photographic set-up.

Figure 12 illustrates the apparatus used for the H_2S-air experiments. To insure the reliability of the cylindrical tube method a test series of experiments with methane-air mixtures was performed in a similar but simpler apparatus prior to the H_2S-air experiments. Our set-up in terms of the flame apparatus and water supply system is similar to the one used by Sapko et al. [7]. The key experimental variables of our study were the droplet size distribution and the spray density (water mass concentration) at various gaseous mixture compositions.

A detailed description of each of the three main parts of the system now follows*:

---

*The units used in this chapter and the following ones will be from both the SI and the British system of units, where reference to manufactured items employed in the experiments is made based on the manusfacturer's specifications. Otherwise, e.g. for the numerical analysis it is strictly the SI system of units which will be used.

(a) The flame apparatus: Since hydrogen-sulfide is a highly toxic gas, it was important to have a seal-tight, leakage proof apparatus and an efficient ventilation system.

The H_2S-air experiments were initially conducted in a Plexiglas tube, 7.68 cm O.D., 6.7 cm I.D. and 135 cm long. Unfortunately, the H_2S-air flames caused sulfur to deposit on the tube walls especially in fuel rich mixtures, thus making the tube walls opaque to the point at which the flame could not be observed by photographic means unless the tube was thoroughly cleaned. The cleaning was made easier by inserting a glass tube 6.32 cm O.D., 5.82 cm I.D. and 122.5 cm long into the Plexiglas tube. The glass tube could be easily removed whenever necessary.

As shown in Fig. 12, there was a dove tail type sliding plate mechanism between the flammability tube at the top and the flow inlet section at the bottom designed to switch from the flowing in of the mixture position to the ignition position and vice-versa, by shifting sideways the flow inlet section relative to the static flammability tube. The flow inlet section was a 19 cm long Plexiglas tube with the same O.D. and I.D. as the flammability tube.

The sliding mechanism is shown in detail at the two positions in Fig. 13. Delrin end shoes were glued to the bottom of the flammability tube and top of the flow inlet tube using a special resin. The end shoes were clamped to

the upper and lower plates of the sliding mechanism by aluminum top and bottom clamp flanges with "O" rings between them to avoid any possibility of leakage. The top static plate which was connected to the flammability tube was an aluminum piece with a hole of diameter equal to the tube's I.D. in the center and two stopper pins, one on each side, for fixing the bottom sliding plate in the required position. The bottom sliding plate which was made out of Teflon (Teflon is a self-lubricating material and was chosen for this reason) was connected to the flow inlet tube. It served as the moving part and had two holes corresponding to the two positions of the plate: filling and ignition. The larger hole with diameter equal to the tube's I.D. was to connect the flammability and the inlet tubes into one uniform tube, 160 cm long as shown in Fig. 13. In this position the two gases were flowed in from the bottom in the desired proportions and mixed in the tube over a certain period of time, ensuring this way good mixing. The smaller hole, 2.54 cm in diameter, provided the orifice necessary to ensure uniform propagation of the flame as described in Chapter III. It was brought to the bottom center of the flammability tube just prior to the ignition by sliding the bottom plate to the second position and thus disconnecting and blocking the inlet tube as shown in Fig. 13.

The orifice size required was initially determined

experimentally for methane-air flames in a flammability tube of 7.62 cm (3") I.D.. A 2.54 cm (1") diameter orifice gave the best results. Although the tube's I.D. was a bit smaller for the H_2S-air flames, the same size orifice was used and the resulting movement of the flame was mostly uniform.

The desired mixture composition was flowed into the flammability tube from a gas metering system comprising of two manometers, one for the fuel and one for the oxidizer as illustrated in Fig. 12. The two manometers had to be calibrated for any of the gases flowed through (methane, hydrogen-sulfide and air) and then curves of volumetric flow rate (cc/sec) vs manometer readings could be plotted for each of the gases used. The calibration was done at a flow pressure in the second stage of the pressure regulator of 10 psig using the soap bubble method. Depending on the required composition, the fuel gas and air were flowed into the flame apparatus at 10 psig delivery pressure via a 1/4" T connection at pre-set volumetric flow rates which were determined from the calibration curves. E.g. for 12% H_2S in air mixture, 19.1 cc H_2S and 140 cc air per second were flowed into the tube corresponding to manometer readings of 13.2 and 73 respectively. Those readings represent the difference in the liquid levels inside the manometer U shape tube. Both, the fuel and air were coming via one 1/4" tube into the flame apparatus where they got further mixed by purging the tube's volume a few

times over (10 times on the average) and due to the turbulent action of the flow just outside the 1/4" inlet tube. Homogeneous mixing was ensured this way for any desired mixture composition.

The top of the flammability tube was closed with a tapered rubber cap which also served as a pressure release valve, in that the cap was designed to pop out before any accidental build-up of pressure in the tube could damage the tube itself. The top cap had a 1/4" center hole from which a 1/4" flexible tube led to the inlet of a bunsen burner also shown in Fig. 12. The burner was positioned near one of the ventilation outlets. The mixing took place at constant atmospheric pressure and hence the excess gas, while preparing the mixture, was fed from the 1/4" center hole in the top cap straight into the burner. In this way the H_2S-air mixture was burned to its combustion products and the free H_2S eliminated.

The ignition source was located at the bottom of the flammability tube (Fig. 12) about 1 cm above the Delrin end shoe and consisted of a 0.5 cm spark gap, the spark being produced by the discharge from a 30 KV triggering module transformer between a pair of brass-copper electrodes.

The flame apparatus was enclosed in a transparent Plexiglas fume hood designed so as to ensure that any unburned or burned gas flowed to the ventilation outlet right above the hood.

All the tubing used for the H_2S gas was 1/4" stainless steel. Copper and Tygon (P.V.C.) tubing reacts with H_2S leading to degradation of the tubing.

(b) The water supply system: For the methane-air experiments, water at room temperature was pressurized with nitrogen gas (N_2) in a 4000 cc steel reservoir and was fed through 1/4" stainless steel tubing to the spraying nozzle located at the top of the flammability tube. For the H_2S-air experiments, the water was saturated in a 4000 cc flask with H_2S prior to filling the pressure reservoir in order to avoid interaction between the H_2S and water before the mixture was ignited. H_2S is known to dissolve easily in water and with the water saturated by H_2S, the droplets were rendered inert, (for more details, see section 4.2 (b)).

A schematic of the H_2S-air water supply system is shown as part of the whole assembly in Fig. 12. Mounted on the line from the reservoir to the nozzle were a strainer, a pressure gauge calibrated with dead weights, a solenoid valve and a timer which could provide a delay up to 15 sec. The timer controlled the period in which the solenoid valve was open for water flow. The spray was turned on by a manual switch activating the solenoid valve. Up to 15 sec of spraying the solenoid was de-activated by the timer limit switch. For more than 15 sec of spray flow, the solenoid was de-activated with the same manual switch used to activate it and the time

was measured independently. Being able to control the spraying time allowed us to get different spray densities or water mass concentrations and learn their influence as a variable of study on the propagating flame.

For the H_2S-air experiments, the water was fed through Spraying Systems Co. stainless steel hydraulic atomizing nozzles of the 1/4 LN series. These nozzles produce hollow cone spray patterns with the finest possible atomization using hydraulic pressure alone (no air). Flow capacities and spray angles for any given type of nozzle in the series and a given pressure are summarized in Table 2 from the manufacturer's specifications. Also shown in Figs. 3-6 are the manufacturer's curves of particle size (microns = μm) vs accumulated volume percentage for the whole range of 1/4 LN nozzle series at various pressures up to 500 psi. Curves of the particle median volume diameter (μm) vs pressure (psi) appear in Figs. 7 and 8. These curves are all based on Log-Normal size distribution of the water droplets in the spray.

The maximum pressure limit specified by the manufacturer for those nozzles is 1000 psi and the higher the pressure, the smaller are the spray particles produced as can be seen from the size distribution curves. It is observed in Fig. 7 that for finer nozzles (finer than 1/4 LN 4), increasing the pressure above 300 psi up to 1000 psi, does not reduce almost at all the particle size median volume diameter. In the

present set-up, 350 psi was the maximum allowable pressure in the water steel reservoir used. Located at the reservoir's outlet was a safety valve designed to protect the system from excess pressure.

At the bottom of the flame apparatus (the bottom of the flow inlet tube) was located a 1/4" draining valve to get the accumulated water out of the system.

(c) The photographic set-up: As shown in Fig. 14, a 30 cm diameter aluminum disc with two rectangular slits (10 x 2.85 cm^2), 180 ° out of phase and covered with black cardboard on both faces to avoid reflection was mounted on the shaft of a 27 V D.C. motor. The motor was powered by a D.C. - fixed, converted to variable - Hammond power supply, especially built for this purpose.

The disc rotated in front of a Polaroid Land camera mounted on a tripod with a TACUMAR lense (f 1:1.8, 85 mm focal length) which was fitted into the camera box.

The film used was Polaroid type 47 rated at 3000 ASA.

The flames were run in front of an open shutter in a dark room. The shutter was opened or closed by means of a black plate which could be slid to the required position. Every time a slit swept in front of the lense, an exposure was recorded on the film. This way successive exposures of the luminous flame front could be recorded on one picture. For slower or too bright flames, one slit was covered and only

one used. With the rpm of the D.C. motor kept virtually constant, the use of one slit only, rather than two, resulted in fewer flame fronts recorded on the film and hence a better and clearer separation of successive exposures. This way, also a higher accuracy in the measurements was ensured.

As to how the flame speed was deduced from the pictures please refer to section 4.2.

4.2 EXPERIMENTAL PROCEDURES

(a) Methane-Air

The methane-air experiments were designed to give some insight into the various problems which could arise before proceeding with the H_2S-air experiments.

Extensive research has been done on the combustion properties of the methane gas. The burning velocities of methane-air flames have been measured by many investigators in a variety of methods [37; Chpt. V in this thesis], thus, by comparing our results with other sources, we were able to confirm the reliability of the cylindrical tube method used in this work. A detailed discussion of the results is given later in Chapter V.

The apparatus used for the methane-air experiments was essentially the same as the one used for the H_2S-air experiments and described in section 4.1 but simpler. It had no sliding

mechanism, no water saturation system and the unburned exhaust gases could be safely flowed outside to the free atmosphere and not through a burner. It was basically a flammability tube which had a diaphragm with the 2.54 cm (1") diameter orifice clamped to the bottom and which could be removed whenever filling the tube with the mixture. The orifice size was, as mentioned before, determined experimentally by observing flames in different methane-air mixture compositions for various orifice sizes until a uniform flame propagation in all compositions was observed for the 2.54 cm diameter orifice.

Experiments in methane-air mixtures for which, the flammable range is 5% - 15% methane in air [29], were done over the range of 6% - 13% methane in air, the stoichiometric composition being at 9.5%. Few experiments (three to four) were performed at each composition beginning at 6% methane in air and going up by 1% increments thereafter. In addition experiments at the stoichiometric composition were performed. Photographs were taken of each flame using the photographic set-up described in section 4.1 and illustrated in Fig. 14.

The rotational speed of the disc (rpm) was calibrated against the voltage output of the D.C. power supply to the motor using a strobe light. We found that for a rotational speed of 275 rpm, the number of flame front exposures appearing on each picture was sufficient for the purpose of measurements

and analysis at all the methane-air and H_2S-air compositions. The framing rate was fixed at that value for all the experiments with maximum 3% up and down swings in the rpm.

In each of the experiments, the tube volume was purged approximately ten times with the appropriate gas mixture, the 1/4" inlet tube removed and replaced by the diaphragm with the 2.54 cm diameter orifice. The mixture was then ignited and the upward propagation of the flame recorded on the film.

On each of the pictures obtained, such as those shown in Fig. 9, it was the spatial-velocity, u_{sp}, or the observed axial flame velocity as it is defined, which was measured. On the Plexiglas tube were glued two black markers and with the distance between them measured on the tube and on the picture, the magnification ratio, M.R., could be determined. The separation distance between two successive flame fronts, s, was measured using a Vernier caliper while viewed through a magnifying glass. For uniform flames, one value of s was sufficient but in the case of non-uniform flames, s was measured in the sections of maximum uniform movement between three or four consecutive flame fronts and then averaged. The spatial velocity was obtained using the following relation:

$$u_{sp} = \frac{S \times M.R. \times rpm \times \eta}{60} \text{ cm/sec} \qquad (4\text{-}1)$$

where rpm stands for the rotations per minute of the rotating disc and η is the number of open slits used (1 or 2 in the present study). Eqn. (4-1) is just an expression of the separation distance divided by the time elapsed, t, between two successive exposures in seconds where

$$t = \frac{60}{\text{rpm} \times \eta} \text{ sec} \qquad (4\text{-}2)$$

The spatial velocity, u_{sp}, was determined this way for all the experiments performed in this study.

In the next experimental phase, water sprays were added to the gas mixture. Water from the nitrogen-pressurized reservoir was dispersed into the top of the flame tube through Spraying Systems Co. UNIJET nozzles with full cone spray tips (the hollow cone type nozzles were used in the H_2S-air experiments). Both, the nozzle size and pressure were varied to obtain different droplet size distributions.

The effective spray volume left in the tube from which in turn the spray density could be calculated, was determined by the difference between the mass of water input to the tube and the mass of water collected at the tube drain as was done in [7]. This was accomplished via a calibration procedure for the various nozzles used in the methane-air and H_2S-air experiments. After wetting the tube's wall, the specific nozzle to be calibrated was turned on for a predetermined

period of time at a preset pressure. Once the spray was turned off, after waiting a few seconds for the bulk of the drain to come out mainly from the tube's wall, its volume was measured. The difference between the spray input volume known from the manufacturer's nozzle specifications given in Table 2 and the volume of water accumulated in the drain was then calculated to give the amount of water left inside the tube. Those measurements for various nozzles, pressures and time durations were reproducible to within 5% on the average.

With the nozzles calibrated, the experiments with methane-air mixtures over the range of 6% - 13% methane in air were repeated but this time with water sprays. Mixing of the fuel (methane or H_2S)-air-water constituents was affected by the turbulent spray action coming out from the atomizing nozzle.

An example of a series of experiments performed with methane-air-water spray mixtures and discussed in Chapter V is the series in which a UNIJET TG 0.4 full cone spray tip nozzle was used. It had an orifice diameter of .022" through which the water was sprayed at a pressure of 100 psi and corresponding flow capacity of .13 gallons/min (8.2 cc/sec). The spray was on for the last 10 sec of flowing in the mixture, just prior to the ignition. The experiments were repeated as before, a few times for each methane-air composition. Essentially, the same procedure was applied to all the

experiments with water sprays for both, methane-air and H_2S-air mixtures and for various spray parameters.

It should be noted that the full cone nozzles did not produce as fine a spray as the hollow cone nozzles which were used in the H_2S-air mixtures. The particle size median volume diameter for the TG 0.4 nozzle at 100 psi was 300 microns (μm) compared to e.g. 52.5 microns for the 1/4 LN .6 hollow cone nozzle at the same pressure of 100 psi.

Most of the spray was lost to the tube's wall. The spray hit the wall at a short distance from the nozzle depending on the spray cone angle, thus most of the drained water came from the flow along the tube's internal surface. Examples of spray angles for given nozzle size in the 1/4 LN series and pressure are shown in Table 2.

(b) H_2S-Air

The apparatus for the H_2S-air experiments described in section 4.1 and shown in Fig. 12, was more complicated than the one used for the methane-air experiments due to the necessity of isolating the toxic H_2S.

First, a series of dry flame experiments was performed for different compositions beginning at 7% H_2S in air, going up by 1% increments up to 16% (Stoichiometric composition for H_2S-air flames is 12%) and then at 20% H_2S in air. The flammability limits of H_2S-air mixtures range between 4% and

44% H_2S in air [29].

The same experiments were repeated with water sprays. Three calibrated nozzles, the 1/4 LN .6 (the finest in the 1/4 LN series with .016" nominal orifice diameter), 1/4 LN 3 and 1/4 LN 8 were used in these experiments at various pressures (up to 300 psi) and flow time durations (up to 60 sec), for a given mixture composition. Also here, each experiment was repeated at least three times for each composition.

There were two more series of experiments carried out. One series was designed to determine the relationship between the spray density (water mass concentration) and the maximum burning velocity for a constant droplet size distribution, throughout. For these experiments, the 1/4 LN .6 nozzle was used at 100 psi with spraying times from 10 sec up to 60 sec. The other series of experiments was designed to investigate the droplet size distribution vs the maximum burning velocity relationship, with the spray density being constant.

Since H_2S dissolves easily in water, the water had to be pre-saturated with H_2S in order to prevent H_2S from being absorbed in the water, thus leading to a shift in mixture composition to the lean side. Such a shift before igniting the mixture would have implied that besides the influence of water on the flame, there would also be the influence due to

the change in the percentage of the H_2S gas present in the mixture.

The saturation process took place in a 4000 cc ball type glass flask shown in Fig. 12 with the H_2S gas bubbling through the water from the bottom of the flask via a special grid to ensure efficient saturation. The gas bubbled through the water to the top of the flask and out to the bunsen burner. A change of color in the bunsen burner flame from blue to violet, for a while, served as an indication that the water became saturated. Once saturated, the water was flowed down to the steel water reservoir from which it was pressurized out and into the spraying nozzle.

For each run the mixture was metered through the flow inlet tube which together with the bottom (Teflon) sliding plate were then in the filling position (Fig. 13). Towards the end of the filling process, the spray was turned on, then, after a predetermined period of time, the gas and spray flow were both stopped and the excess water drained out. The bottom sliding plate was then moved to the ignition position (Fig. 13) with the flow inlet tube now blocked so as to avoid flash back. With the orifice in position, the mixture was now ignited and the resulting flame photographed.

It should be noted that with increasing the H_2S or methane concentration, the brightness of the flame increased too. The higher flame luminosity required the reduction of

the photographic lense aperture, otherwise, the pictures became smeared by the luminous tail of the burned products, overriding the flame front exposures.

Also, the amount of sulfur deposited on the tube wall increased with increasing H_2S concentration, e.g. for the 20% H_2S in air flame, a sulfur cloud was practically formed and the glass tube had to be cleaned after every run.

CHAPTER V

RESULTS AND DISCUSSION

Throughout Chapters II to IV in the present study of laminar flame propagation, it was shown that for a given combustible mixture at a certain pressure and temperature, the burning velocity is a constant.

Changes in the burning velocity magnitude can be due to physical, chemical or a combination of both effects. Here, the experiments and numerical computations were done primarily with the aim of determining the relative change of burning velocity as a function of: (i) mixture composition, (ii) type of water spray.

The results presented in this work deal with the physical aspects of the introduction of water spray in a combustible mixture. With the water assumed to be an inert species in the mixture, the physical effects of the water spray directly influencing the magnitude of the burning velocity are: (i) the extent of the heat removed from the flame front and absorbed by the water droplets via sensible heating and vaporization, (ii) the dilution capacity of the vapor. Both effects are strongly dependent on the type of water spray introduced and will be discussed in the context of the results obtained.

Initially the discussion concentrates on the overall experimental results for the burning velocities in methane-air and hydrogen sulfide-air mixtures without and with water sprays. Following this is a discussion of the maximum burning velocities in H_2S-air stoichiometric mixtures as a function of two important spray parameters: (i) the droplet size distribution, (ii) the spray density. For this part, both experimental and numerical results are discussed.

A general computer program was developed to solve for the value of burning velocity in any stoichiometric mixture with or without water spray. Numerous runs were undertaken to establish the burning velocity, flame temperature and other physical parameters for the H_2S-air stoichiometric mixtures as a function of the water spray used. All of the numerical computations were repeated twice for two constant reference values of the parameter Z, the gaseous mass fraction:

$$Z^* = Z_\infty \quad \text{and} \quad Z^* = (Z_0+Z_\infty)/2.$$

The experimental burning velocities were determined by using the relation (3-7): $u_0 = (\pi R^2/A_{f\ell})\, u_{sp}$. Based on a careful examination of the experimental pictures (Figs. 9-11) and the analysis of the flame surface area, $A_{f\ell}$, given in Chapter III, we have the following:

For the

$$CH_4\text{-air flames} \longrightarrow u_0 = .36 \cdot u_{sp} \qquad (5\text{-}1)$$

and for the

$$H_2S\text{-air flames} \longrightarrow u_0 = .5 \cdot u_{sp} \qquad (5\text{-}2)$$

where $A_{f\ell}$ was considered to be the surface area of a semi prolate spheroid and a semi sphere for the CH_4-air and H_2S-air flame fronts, respectively.

The thorough investigation undertaken here gives a deeper insight into the general problem of two phase flow with mass transfer and heat transfer between the phases. The simple theoretical model developed is very instrumental in predicting roughly, the physical inhibitive effect of water in combustion systems. To the best of our knowledge, the results obtained for the H_2S-air mixtures with water sprays are published here for the first time.

A discussion of the results which are summarized and illustrated in tables and figures at the end of this thesis, will now follow.

5.1 OVERALL BURNING VELOCITY RESULTS

(a) Methane-Air

Figs. 15-17 relate to the burning velocities in CH_4-air and CH_4-air-H_2O mixtures. As noted previously, the comparison of our results with other sources served as an indication of

the reliability of the cylindrical tube apparatus.

The burning velocity as a function of the equivalence ratio, ϕ defined as the fuel/oxidizer ratio divided by the stoichiometric fuel/oxidizer ratio, is illustrated in Fig. 15. The burning velocities we obtained for flames in CH_4-air mixtures without water sprays are compared in Fig. 15 with results obtained by other investigators [39,40,49-51] who used various measurement methods. For all the curves, the burning velocity reaches its maximum value around the stoichiometric composition. Our curve fits somewhere in the middle with the maximum burning velocity, $u_{0_{max}}$, at 9.25% CH_4 in air equal to 36.3 cm/sec. (The stoichiometric ratio is at 9.5% CH_4 in air).

The ratio of $u_{0_{max}}$ for methane-air mixtures obtained from other sources, including those of Fig. 15, over the present value for $u_{0_{max}}$ (36.3 cm/sec) is illustrated in Fig. 16. The values for $u_{0_{max}}$ shown, vary from Coward and Hartwell's [40] value of 27 cm/sec up to Andrew and Bradely's [37] value of 45 cm/sec.

Andrews and Bradely [37], in deducing their value claim that unless an allowance is made for the quenching effect at the tube wall, the derived value of the burning velocity will be too small. They recommend a correction factor of 1.17, by which the burning velocity value determined from the cylindrical tube method should be multiplied. This effect which would have increased our burning velocity results for both the

CH_4-air and H_2S-air flames by 17% was not incorporated in the present study. It can be seen in Fig. 16 that our value of 36.3 cm/sec for $u_{0_{max}}$ compares very well with results obtained using the cylindrical tube method by Henderson and Hill [53] or Egerton and Lefebvre [54].

The burning velocities for CH_4-air with water spray mixtures vs the equivalence ratio, ϕ, are plotted in Fig. 17 and compared with the values for the dry CH_4-air mixtures, shown on the same figure.

The water spray is defined and identified by two parameters:

(i) The initial spray density, ρ_{s_0}, measured in milligrams of water per cubic cm of the overall mixture (mg/cm^3). It indicates the amount of water present initially in the mixture. Assuming the spray water droplets to be dispersed evenly in the tube with their total mass and volume known, ρ_{s_0}, can then easily be calculated.

(ii) The initial droplet size distribution is the other parameter defining the spray. The statistical description of the spray, in light of the simplifying assumptions made in Chapter II, is reduced to one single parameter which is the median volume diameter, MVD, denoted here by $\bar{d}_0$.

The value for $\bar{d}_0$ is found from the distribution curves in Figs. 7 and 8, where the droplet MVD is shown as a function of pressure and type of nozzle used. The MVD is a means of

expressing droplet size in terms of the volume of water sprayed, where 50% of the total volume of water sprayed is made up of droplets with diameters larger than the median value and the other 50% made up of droplets smaller than the median value.

The CH_4-air-H_2O curve in Fig. 17 is for a water spray with median volume diameter, $\bar{d}_0$, of 300 μm and spray density, ρ_{s_0}, of 5.3 mg/cm^3. A down and to the right shift of the CH_4-air-H_2O curve relative to the CH_4-air curve is observed in Fig. 17. The down shift is, of course, due to the lower burning velocities. The maximum burning velocity for the mixture with water spray is 35 cm/sec compared to 36.3 cm/sec for the dry mixture. This implies a 3.6% reduction in the peak burning velocity due to the addition of water spray.

The shift to the right is noticed by an overall horizontal displacement of the CH_4-air-H_2O curve relative to the CH_4-air curve, with lower burning velocities on the lean side and higher burning velocities on the rich side of stoichiometric, for the CH_4-air-H_2O mixtures. This could be justified by considering the probable pre-ignition adsorption of methane at the water droplets surface thus decreasing the percentage of methane in the mixture composition. This effect was found to be almost constant for any of the compositions in the experimental range of 6%-13% methane in air. On the average, about 0.4% methane was adsorbed from the initial CH_4-air composition thus displacing the curve to the right in Fig. 17.

(b) Hydrogen Sulfide-Air

The results in Figs. 15-17 are introductory and their general physical aspects are discussed in more detail with the H_2S-air mixtures.

In Figs. 18-25, the results for the H_2S-air and H_2S-air-H_2O flames are illustrated. Like Figs. 15-17 for the CH_4-air experiments, the measured burning velocities in the H_2S-air mixtures with and without water sprays are presented as a function of the equivalence ratio, ϕ, over the experimental range of 7% - 20% H_2S in air.

First, in Fig. 18 our results for the burning velocities in dry H_2S-air mixtures are compared with those of Chamberlin and Clark [58] and Gibbs and Calcote [59]. Refs. [58,59] were the only ones we could find for the purpose of comparison because of the limited amount of data in the literature about burning velocities of H_2S-air laminar flames. Our curve has its maximum value for the burning velocity, $u_{0_{max}}$, at the stoichiometric composition (12% H_2S in air), equal to 41.1 cm/sec. At the two ends of the experimental range, 7% and 20% H_2S in air, the burning velocity is 16 cm/sec and 18 cm/sec, respectively.

The results obtained for the burning velocities as a function of fuel-air ratio are typical to all gaseous combustible mixtures known. If the mixture is over-oxidized, there is excess oxygen which must be heated to the product

temperature and thus the product temperature drops from the stoichiometric value. If too little oxidizer is present, i.e. the mixture is under-oxidized or rich, then there is insufficient oxygen to burn all the fuel to its most oxidized state, the energy release is less and the temperature drops as well. The variation of the flame burning velocity with fuel-oxidant ratio follows the variation of temperature which peaks at the stoichiometric mixture ratio.

A higher temperature implies a higher reaction rate which in turn results in a higher burning velocity. The burning velocity is proportional to the square root of the reaction rate as shown in Eqn. (2-68). The flame temperature appears in the exponential term of the function $\Psi(u)$, the non-dimensional reaction rate defined in Eqn. (2-37), and from the expressions for the eigenvalue in Eqns. (2-34) it is obvious that the burning velocity depends strongly on $\Psi(u)$. Thus small changes in flame temperature can give noticeable changes in flame burning velocities.

In reality, some mixtures have their temperature or burning velocity peak slightly on the rich side of stoichiometric [12,35]. This result occurs because, if the system is slightly under-oxidized, the specific heat of the products is reduced and thus the temperature or burning velocity increased. Nevertheless, for H_2S-air mixtures, the maximum burning velocity according to Levy et al. [24] occurs slightly on the lean side

at 11.8% H_2S suggesting the possibility of some decomposition in the preflame zone. Our result of the burning velocity peaking at 12% H_2S in air is pretty close to that of Levy et al. [24].

The results of Chamberlin and Clarke [58] plotted in Fig. 18 do not include the value for $u_{0_{max}}$. The highest value they reported is 49.5 cm/sec at 10% H_2S. On the other hand Gibbs and Calcote [59] reported results (also shown in Fig. 18) for fewer compositions but included, $u_{0_{max}}$, which is according to them 40.9 cm/sec and very close to our result of 41.1 cm/sec.

Plots of burning velocities for both H_2S-air and H_2S-air-H_2O mixtures vs the equivalence ratio (7% - 20% H_2S in air) are presented in each of Figs. 19-24; the former being shown by broken lines and the latter by solid lines. Each curve for the H_2S-air-H_2O mixtures corresponds to a particular value of spray density, ρ_{s_0}, and droplet MVD, $\bar{d}_0$. It can then be compared to the curve for the dry H_2S-air mixture plotted on the same graph as was done in Fig. 17 for the CH_4-air results.

The most important and immediate observation in Figs. 19-24 is the reduction of the flame burning velocities especially in the region around the stoichiometric mixture. On the lean side, and on the rich side mainly between 14% and 16% H_2S, the water droplets do not seem to affect the flame speed too much.

Interestingly enough, chemical flame suppressants such

as halogen compounds (e.g. freons), halogenated hydrocarbons (e.g. the various halons) and inert powders are all very effective in fire fighting but their effect on the flame burning velocities is different than that of water sprays in the present experiments. Rather, those chemical inhibitors affect the burning velocities far away from the stoichiometric composition on the rich and lean sides of the mixture [12, chpt. 4]. Their effect in a large region around the stoichiometric mixture ratio is not too pronounced, hence, opposite to our results. The reason is that the high temperatures generate many radicals (e.g. O, H, OH, etc.) via chain branching and the elimination of some of them does not affect the reaction rate.

According to Glassman, I. [12, chpt. 4], halons and powders reduce the flame speeds to a certain extent even around the stoichiometric ratio. The investigators performing these experiments have argued that flame inhibition agents affect the flame burning velocity around the stoichiometric composition in the same manner that the burning velocities in the lean or rich mixtures are affected - by reducing radical concentrations. Glassman, I. [12, chpt. 4], questions this explanation, saying that the quantities of those agents added at the mixture compositions around stoichiometric, are such that they could absorb sufficient amounts of heat to reduce the temperature and thus the flame speed.

From the results in Figs. 19-24, the water droplets appear to be acting more as a heat sink and a diluent agent than as a chemical inhibiting agent.

Heat from the reaction is absorbed by the water droplets via sensible heating and vaporization. Moreover, the vapor added to the combustion process has a higher specific heat (.59 cal/g °K at about T_f = 1200 °K) than any of the reactant or product species, thus increasing the heat capacity of the overall mixture. The higher heat capacity causes a reduction in the final equilibrium temperature or equivalently a reduction in the rate of flame propagation. With heat removed from the reaction zone and the combustible mixture diluted, the mixture burning velocity could be reduced in a controlled manner down to the point where the mixture, if ignited, would not propagate a flame.

From the foregoing, it is clear that away from the stoichiometric H_2S-air mixture where the flame temperature is lower, a smaller temperature differential exists between the droplet surface and the surrounding hot gases. Less heat is then absorbed by the droplets implying that a smaller fraction of the spray is evaporated. This explains why the burning velocities on the lean and rich sides of the H_2S-air-H_2O mixtures are not reduced by the presence of the water spray as much as they are around the stoichiometric composition. It is illustrated in Figs. 19-24.

The extent to which the flame front is cooled due to the heat removed from the process depends on the initial conditions of the water spray, namely, the spray density, ρ_{s_0}, and the droplet MVD, $\bar{d}_0$. The values of, ρ_{s_0}, and, $\bar{d}_0$, for which the results in Figs. 19-24 were obtained, are indicated on each of the figures. Also indicated are the type of nozzle and pressure used to produce the particular spray.

For a water spray with $\rho_{s_0} = 1.09$ mg/cm^3 and $\bar{d}_0 = 52.5$ μm, the maximum burning velocity, $u_{0_{max}}$, in Fig. 19 is down to 33.75 cm/sec compared to $u_{0_{max}}^0 = 41.1$ cm/sec for the dry H_2S-air mixture, a reduction of 18%. Keeping the same spray density, $\rho_{s_0} = 1.09$ mg/cm^3, but with a smaller droplet MVD, $\bar{d}_0 = 40$ μm, as indicated in Fig. 20, we measured $u_{0_{max}} = 31.9$ cm/sec, a reduction of 22.5% relative to the value of $u_{0_{max}}$ in the dry mixture. This implies that a water spray containing smaller droplets is more effective in reducing the flame burning velocity for a given constant spray density. It is analyzed when discussing the results in Figs. 26-28 (section 5.2).

The results represented in Fig. 21 for $\rho_{s_0} = 1.09$ mg/cm^3 and $\bar{d}_0 = 35$ μm yield $u_{0_{max}} = 33$ cm/sec. Hence for the same spray density and smaller droplet MVD ($\bar{d}_0 = 35$ μm compared to $\bar{d}_0 = 40$ μm in Fig. 20), we get a higher value for the maximum burning velocity ($u_{0_{max}} = 33$ cm/sec compared to $u_{0_{max}} = 31.9$ cm/sec). Further in Fig. 22, for the same droplet MVD as in Fig. 21, $\bar{d}_0 = 35$ μm and a higher spray density, $\rho_{s_0} = 2.32$ mg/cm^3,

the result $u_{0_{max}}$ = 33.5 cm/sec is even higher than that of Fig. 21.

This contradiction could be explained by realizing that water was sprayed at a nozzle pressure of 300 psi in the experiments of Figs. 21 and 22 compared to 100 psi and 200 psi in those of Figs. 19 and 20, respectively. Due to the high pressure combined with the tube wall effect, the droplets collisions and coalescence are increased in rate and intensity. It results in shifting the droplet size distribution towards the larger droplets more than at the lower pressures and thus reducing the water spray effectiveness in slowing down the flames.

In Figs. 23 and 24, results for larger droplet MVD and higher spray densities are shown. ρ_{s_0} = 6.48 mg/cm^3 with $\bar{d}_0$ = 80 μm and ρ_{s_0} = 5.71 mg/cm^3 with $\bar{d}_0$ = 145 μm are the water spray initial conditions for the results of Figs. 23 and 24, respectively.

The H_2S-air-H_2O burning velocity curves of Figs. 19, 20 and 23 are plotted together with the curve for the burning velocities in the dry H_2S-air mixture on one graph in Fig. 25.

It shows again the important effect of the droplet size distribution . It could be expected that a higher spray density, up to a certain limit, will be as effective as a spray of lower density but with smaller size droplets. The results in Fig. 23 show that although the water mass concentration in

the mixture is increased about six times (6.48 mg/cm^3 compared to 1.09 mg/cm^3) the resulting burning velocities are still higher, e.g. $u_{0_{max}}$ = 37.15 cm/sec for $\bar{d}_0$ = 80 μm in Fig. 23, than the ones obtained with lower spray densities but smaller droplets. e.g. $u_{0_{max}}$ = 31.9 cm/sec for $\bar{d}_0$ = 40 μm in Fig. 20. This implies that although the amount of water present in the mixture plays an important role in reducing the burning velocities, its effect is not as drastic as is the effect of change in the size of the droplets.

The curves for the H_2S-air-H_2O burning velocities in Figs. 19-25, generally, do not appear to be displaced horizontally with respect to the curve of burning velocities in the dry H_2S-air mixture. This is due to the saturation of the water with H_2S before it was sprayed.

The interaction between the water droplets and the surrounding gas is similar to a heterogeneous process, which is a process taking place at a phase boundary, e.g. at the droplet surface. At the saturation limit, an equilibrium is established so that the rate of adsorption of molecules onto the surface is equal to the rate of desorption of molecules from the surface. The water droplet surfaces are thus at equilibrium with the surrounding H_2S-air mixture throughout the pre-ignition period and hence do not change the mixture's composition. This way the resulting curves for the H_2S-air-H_2O flames in Figs. 19-25 are almost not displaced at all with

respect to the curve for the dry H_2S-air flames.

In all the H_2S-air-H_2O experiments discussed so far, and those whose results are shown in Figs. 26-34, we were unable to bring the mixtures down to the limit where they would not ignite or even if ignited would then propagate a limited distance along the tube. Every mixture in the range of 7% - 20% H_2S in air, which was the range of study, did ignite and did propagate for any type of water spray introduced. Only close to the lower flammability limit (4% H_2S) at 6% H_2S and below did the mixture not ignite, no matter what water spray was used. Sometimes it was hard to ignite even a 7% H_2S mixture. Setting the 30 KV trigger transformer at its highest energy output to the ignition electrodes did not help.

It was shown [12, chpt. 4] that reduction of the radical concentrations in the pre-ignition reactions or near the flammability limits can have remarkable consequences on the ability to initiate combustion. In these cases the radical concentrations are such that the chain branching factor is very close to the critical value for ignition. Any reduction could prevent the explosive condition from being reached. In our experiments, the quenching effect of the tube wall could be considered minimal because its I.D. was large enough (5.82 cm I.D.) to avoid almost completely that effect. The relatively easier ignition of the 6% H_2S in air mixtures without water sprays was a proof of that.

It seems that the major contributing factor to the reduction of radical concentrations in the present experiments are the water droplet surfaces similarly to what many believe is the mechanism of various antiknock compounds in combustion systems [12, chpt. 4].

In the inerting experiments reported by Sapko et al. [7], a combination of steam and fine water droplets (< 10 μm) was used where the steam helped to atomize the secondary water.

For a water saturation temperature of 60°C, Sapko et al. [7] determined the amount of water liquid plus water vapor (81 plus 19 mole-percent respectively assuming 100% saturation) in terms of mole-percent necessary to prevent ignition and subsequent propagation beyond a certain limit, of methane-air flames over the entire flammability range. E.g. for the stoichiometric methane-air mixture they got an inerting limit of 28 mole-percent at 60°C.

Comparing the results of Sapko et al. [7] to ours, it should be noted that the finest water spray produced in the present experiments had a droplet MVD of 35 μm compared to less than 10 μm diameter droplets reported in [7]. Besides, there was no vapor introduced with the spray and all the water sprays were at room temperature. Sapko et al. [7] made several attempts to extend the inerting data down to room temperature but with little success because of nozzle flow limitations and excessive droplet loss on the walls of the flammability tube.

It is understood that the closer the water droplet temperature is to the boiling point, the sooner it will start to evaporate in the flame reaction zone and thus more of it will evaporate. A larger fraction evaporated will remove more heat from the flame front and further reduce the flame burning velocity to the point in which the mixture will not be able to sustain a propagation.

It is also shown in [7] that water droplets of less than 10 μm are effective in inhibiting the propagation of methane-air flames. In the present study, the residence time of a water droplet in the H_2S-air flame reaction zone was found in section 2.4 to be 2.5×10^{-4} sec. Since the final radius, r_∞, for a completely evaporated droplet is zero, it is deduced from Eqn. (2-64) that only droplets with a maximum initial diameter of 10 μm or less will completely evaporate within 2.5×10^{-4} sec, in the H_2S-air flame reaction zone.

Our numerical calculations have shown that for a water spray with droplet MVD, $\bar{d}_0$ = 10 μm and density, ρ_{s_0} = 1.09 mg/cm^3 in the stoichiometric H_2S-air mixture, the burning velocity is close to zero. In this case, from a total of 291.3 calories of heat released per gram of the mixture, 220.5 cal/g (75.7%) is removed by the water spray heating and evaporating. Thus, extrapolation of the above result indicates that water sprays with both $\bar{d}_0 \leq 10$ m and $\rho_{s_0} \gtrsim 1.00$ mg/cm^3 would inhibit flames in any H_2S-air mixture composition.

5.2 EXPERIMENTAL AND NUMERICAL RESULTS FOR THE H_2S-AIR-H_2O MAXIMUM (STOICHIOMETRIC) BURNING VELOCITIES

It has been shown in section 5.1 from our experimental results and those of other investigators [12,24,35] that the assumption of the maximum burning velocity occurring at the stoichiometric H_2S-air composition is an excellent one.

$u_{0_{max}}$, is a critical parameter in that a flame propagating at the maximum burning velocity is the most difficult to suppress by both, chemical and non-chemical agents. Since the effectiveness of these agents (including water) is measured by the relative reduction of the flame burning velocity for a given concentration, the largest concentration of these agents will be required for a mixture composition yielding the maximum burning velocity as was also shown in [7] for the case of water in methane-air mixtures.

The effect of the water sprays in terms of ρ_{s_0} and $\bar{d}_0$ on the value of $u_{0_{max}}$ and the other related physical parameters was extensively investigated. The experimental and numerical results are illustrated in Figs. 26-34 and summarized in Tables 3-10 of this thesis. In Appendix IV, two sample computer outputs for both mixtures with and without water sprays are presented. With some minor modifications based on the theoretical analysis of Chapter II, the numerical scheme can be extended to non-stoichiometric mixtures.

The effect of each of the two spray parameters, ρ_{s_0} and $\bar{d}_0$, on the results will now be discussed:

(a) Varying the Droplet Size Distribution for a Given Constant Spray Density

We have shown previously that the smaller diameter droplets are more effective in reducing the burning velocity of the H_2S-air flame.

In Fig. 26, both, the experimental and theoretical curves are plotted, where the maximum burning velocity, $u_{0_{max}}$, is represented as a function of the droplet MVD, $\bar{d}_0$, for a given constant spray density, ρ_{s_0}. The experimental curve shows $u_{o_{max}}$ to increase continuously from 31.9 cm/sec at $\bar{d}_0$ = 40 μm to 39.3 cm/sec at $\bar{d}_0$ = 145 μm, while ρ_{s_0} = 1.09 mg/cm^3 and is constant. With increasing droplet size the curve flattens and approaches asymptotically the value of $u_{0_{max}}$ for the dry H_2S-air flame (41.1 cm/sec). At the limit where the droplets will be very large, their effect will be nullified and the flame will propagate at $u_{0_{max}}$ = 41.1 cm/sec.

The two theoretical curves in Fig. 26 are represented in the form of upper and lower bound curves and the corresponding average value curves, all plotted from the numerical results summarized in Tables 3 and 4 for $Z^* = Z_\infty$ and $Z^* = (Z_0+Z_\infty)/2$, respectively.

All the numerical results in this study were tabulated exactly as they appeared in the computer output, with the same number of significant figures. Tables 3 and 4 show the numerical results for the upper and lower bounds of the eigenvalue and the corresponding burning velocities for each of the droplet sizes ($\bar{d}_0$) used in the experiments. Corresponding to each droplet size (e.g. 35 μm, 40 μm up to 145 μm) there are four sets of results for four ignition temperatures, tabulated in non-dimensional form ($\tilde{T}_i$ = -.9, -.8, -.7, -.6) and the equivalent in degrees Kelvin. As already mentioned (section 2.2) the resultant eigenvalue is independent of the choice of the ignition temperature [23, p. 319] in the range $-a < \tilde{T}_i < 0$ (a = 1 when no water droplets are present in the mixture by Eqns. (2-32)). This is confirmed by our results since for any given droplet size the four sets of eigenvalues and burning velocities are almost identical.

Also given in Tables 3 and 4 for each droplet size is the final equilibrium temperature, $T_{\infty,a}$. It is the adiabatic flame temperature calculated from the overall conservation of enthalpy relation in Eqn. (2-76). In deducing $T_{\infty,a}$, defined here also as the ideal flame temperature, dissociation effects were neglected. It has been pointed out in section 2.3 that dissociation reactions are quite endothermic and in reality the flame temperature will be lower, especially at high temperatures where more heat is absorbed due to the higher rate

of dissociation reactions.

We have shown the higher burning velocity to be tied up with a higher flame temperature. Thus, by using the adiabatic flame temperature without considering dissociation (Eqn. (2-76)), in the numerical computations, we should expect higher values for the resulting burning velocities or have the theoretical curves (of $u_{0_{max}}$ vs $\bar{d}_0$) above the experimental curve. As illustrated in Fig. 26, (It applies also to Figs. 30 and 31 as well), indeed, both theoretical curves except for a small part (mainly of the curve for $Z^* = Z_\infty$) in the region of the smaller droplet sizes, are above the experimental curve. The reason for that part of the theoretical curves being below the experimental curve in Fig. 26 has probably to do with the choice of certain parameters in this parametric study such as e.g. the frequency factor and also because of possible experimental errors incurred such as e.g. the determination of the flame surface area.

Moreover, when $Z^* = (Z_0+Z_\infty)/2$, all the results for $u_{0_{max}}$ and $T_{\infty,a}$ are higher than when $Z^* = Z_\infty$ as can be observed in Figs. 26 through 32. This is because $Z^* = (Z_0+Z_\infty)/2$ which is a middle value between Z_0 and Z_∞, represents a smaller gas mass fraction than $Z^* = Z_\infty$. A smaller gas mass fraction implies less evaporation which in turn causes the flame to propagate faster and at a higher temperature.

The theoretical curves of Fig. 26 show the same trend

as the experimental one (refer also to results in Tables 3 and 4), namely, increasing burning velocities with increasing droplet sizes up to the limit where the burning velocity value in the dry mixture is reached.

The increasing gap between the theoretical curves (especially the one for $Z^* = (Z_0+Z_\infty)/2$) and the experimental curve with increasing droplet size could be attributed to the fact that at higher burning velocities and hence higher temperatures, the dissociation reactions are accelerated. The difference, then, between the actual flame temperature and the ideal one is larger than their difference for the smaller droplet sizes and lower burning velocities where the actual flame temperature approaches the ideal one.

Table 9 summarizes the experimental and numerical values of the maximum burning velocities, $u^e_{0_{max}}$ and $u^c_{0_{max}}$ respectively, for each of the droplets MVD generated in the experiments. The percentage discrepancy corresponding to the gap between the experimental and theoretical curves in Fig. 26 is also given. The second part of Table 9 relates to the varying spray density and constant droplet MVD experiments. The values of $u^c_{0_{max}}$ are the average between the upper and lower bound values.

From the foregoing analysis of the results reported in Tables 3, 4 and 9 and illustrated in Fig. 26, it is clearly

indicated that a finer water spray is more effective in reducing the maximum burning velocity. This stems from the fact that for a given spray density smaller droplets will increase the effective surface area of the spray per unit volume of the mixture. An increased contact surface between the cooler water droplets and the hotter surrounding gases means that for a given heat flux into the droplets more heat will be absorbed per unit time. Therefore, with a higher heat flow rate, more of the spray will be evaporated with the heat absorbed via the sensible heating of the water droplets and latent heat of vaporization. Besides, since more vapor is added, the mixture's heat capacity will be further increased via dilution. The net result will be a further decrease of the flame temperature and hence the burning velocity.

In Figs. 27 and 28, the results for the adiabatic flame temperatures from Tables 3 and 4 are plotted versus the droplet size for $Z^* = Z_\infty$ (Fig. 27) and $Z^* = (Z_0+Z_\infty)/2$ (Fig. 28). Those results show clearly the increase in the flame temperature with increasing droplet size.

Plotted also, on Figs. 27 and 28, are the curves for what we define in the present study as empirical adiabatic flame temperatures. These temperatures were found numerically to give back the experimental values of the maximum burning velocities. This was done by substituting trial values of T_∞ in the definition of $\tilde{T}$, ($\tilde{T} = \bar{C}p_g(T-T_\infty)/Jq$ from Eqn. (2-75a))

and then integrating the eigenvalue equations, Eqns. (2-84), in which $\tilde{T}$(or u) is the variable of integration. Thus, we fitted values of final equilibrium temperatures in order to get back the experimental values of $u_{0_{max}}$, e.g. for $\bar{d}_0$ = 80 μm and $Z^* = (Z_0+Z_\infty)/2$ (ρ_{s_0} = 1.09 mg/cm^3 = constant) the ideal adiabatic temperature, $T_{\infty,a}$, is 1977.6°K and the empirical adiabatic temperature, $T_{\infty,e}$ is 1910°K. This value of T_∞, when used in the numerical computations will yield the corresponding measured burning velocity, $u_{0_{max}}$ = 37.15 cm/sec.

The results of the empirical adiabatic flame temperatures which are probably closer in value to the actual flame temperatures are illustrated in Figs. 27 and 28. It is easily observed that the position of the $T_{\infty,a}$ curve with respect to the $T_{\infty,e}$ curve in each of the figures, corresponds exactly to the relative position of the $u^c_{0_{max}}$ curves to the $u^e_{0_{max}}$ curve, respectively, in Fig. 26. Therefore, the fact that a variation in the flame temperature is followed by a variation in burning velocity or vice-versa, is confirmed by our numerical results.

The results for $T_{\infty,a}$ and $T_{\infty,e}$ with varying droplet size and also with varying spray density are summarized in Table 10, and the percentage discrepancy between the two values in each case is given, as it was done with the maximum burning velocity results in Table 9.

Finally, the effect of varying the spray droplet size

distribution on various mixture and combustion parameters was computed and the results summarized in Table 5. Since the spray density is kept constant at 1.09 mg/cm^3, the initial reactant mass fraction (or "dilution" factor) G and the overall initial gaseous mass fraction including the inert species, Z_0, are also constant and equal to .1779 and .5250 respectively. The value of G for the dry flame was .3388 indicating clearly that the reactant mass fraction is reduced almost by half due to the presence of close to 50% water by mass in the mixture, ($(1-Z_0)$ is the initial water mass fraction in the mixture). Next, the values of Z_∞, F_v (%), and $\bar{K}$, the final gaseous mass fraction, the percentage fraction evaporated according to Eqn. (2-69) and the scale factor (it is a constant for a given mixture), respectively, are tabulated.

As expected, Z_∞ decreases from .5824 for $\bar{d}_0 \doteq 35$ μm down to .5285 for $\bar{d}_0 = 145$ μm, implying smaller final vapor mass fractions for coarser sprays. These results for Z_∞ and Z_0 vs $\bar{d}_0$ are plotted in Fig. 29. The curve for Z seems to approach asymptotically the constant Z_0 line at the larger droplet diameters where very little evaporation takes place. Also, the fraction of the spray evaporated decreases from 12% for $\bar{d}_0 = 35$ μm to .7 % for $\bar{d}_0 = 145$ μm. The $\bar{K}$ values are increasing with increasing droplet size and for given droplet size $\bar{K}$ is a little higher in value for $Z^* = (Z_0+Z_\infty)/2$

than for $Z^* = Z_\infty$.

(b) Varying the Spray Density with Constant Droplet Size Distribution

The effect of increasing the water spray density on the burning velocity of the H_2S-air flame for a given droplet size distribution, is to reduce it. In this sense it is analogous to the effect, although not as drastic, of decreasing the droplet size distributions for a given spray density.

This time instead of reducing the droplet size in order to increase the effective surface area of the spray per unit volume, we achieve that increase in surface area by increasing the amount of spray per unit volume while the droplet size distribution is kept constant at 52.5 μm droplet MVD.

The experimental and numerical results are summarized and illustrated exactly as it was done with the results for variation of the droplet size distribution in 5.2 (a). Most of the points brought up in that analysis apply as well to the present case.

The experimental and numerical values for the maximum burning velocities, $u_{0_{max}}$, in H_2S-air-H_2O mixtures with changing spray density, ρ_{s_0}, are given in the bottom part of Table 9, including the percentage discrepancy between them. Those results are plotted in Figs. 30 and 31.

In Fig. 30, the experimental and numerical results show $u_{0_{max}}$ decreasing with increasing the volume of water sprayed. That volume is derived from the nozzle flow rates given in Table 2. It is observed that at smaller volume input (< 20 cc water spray), the theoretical curves for $Z^* = Z_\infty$ and $Z^* = (Z_0+Z_\infty)/2$, are far steeper than at the larger volume input. This is so because increasing the volume of water sprayed above 20 cc (up to 60 cc) does not produce as large an increase in the amount of water left in the tube (defined here as the effective spray volume, V_{eff}) as it does below 20 cc. This was determined by calibrating the 1/4 LN .6 nozzle at 100 psi according to the procedures described in Chapter IV of this thesis.

In Fig. 31, the experimental and theoretical plots of $u_{o_{max}}$ vs ρ_{s_0} or equivalently V_{eff} are shown. Here as in Fig. 30, the maximum burning velocity decreases with increasing spray density. The experimental results for $u^e_{0_{max}}$ show it decreasing from 38.9 cm/sec at ρ_{s_0} = .317 mg/cm^3 down to 29.3 cm/sec at ρ_{s_0} = 1.347 mg/cm^3. In both, Figs. 30 and 31 and also from the results in Table 9, it is observed that the discrepancy between the theoretical and experimental values of $u_{0_{max}}$ is greater for the smaller spray densities where $u_{0_{max}}$ is higher. Here, as for the case of droplet size variation in 5.2 (a), since it is the adiabatic flame temperature without dissociation effects which was considered in the

numerical computations, the higher the flame temperature or burning velocity, the more pronounced will be the dissociation reactions. Therefore, the greater will be the discrepancy between the experimental value for $u_{0_{max}}$ or the corresponding actual temperature and the numerical values of $u_{0_{max}}$ or $T_{\infty,a}$ as seen in Figs. 30 and 31.

Summarized in Tables 6 and 7 (same way as in Tables 3 and 4) are the results for the upper and lower bounds of the eigenvalue and burning velocities for a given spray density, ignition temperature and the computed adiabatic flame temperature. The results in Tables 6 and 7 are for $Z^* = Z_\infty$ (Table 6) and $Z^* = (Z_0+Z_\infty)/2$ (Table 7).

Figures 32 and 33 illustrate the variation of the empirical and ideal adiabatic flame temperatures with the spray density as was done for the variation of those temperatures with the spray droplet size in Figs. 27 and 28. The temperature ($T_{\infty,a}$ or $T_{\infty,e}$) decreases with the increasing spray density, hence the more mass of water present per unit volume of the mixture, the more heat will be absorbed from the reaction and the cooler will be the flame front. The results illustrated in Figs. 32 and 33 are tabulated in the bottom part of Table 10 for each of the spray densities used. Also given in that table is the percentage discrepancy between $T_{\infty,a}$ and $T_{\infty,e}$. Here again, the temperature variation caused by the introduction of water spray has the same pattern as the burning velocity

variation.

Finally, like Table 5, Table 8 summarizes the effect of changing the spray density on various mixture and combustion parameters. By increasing the spray density from .317 mg/cm^3 up to 1.347 mg/cm^3, G, Z_0 and Z_∞ are decreasing, G from .2682 down to .1600, Z_0 from .7916 down to .4721 and Z_∞ from .8029 down to .5008.

These results for G, Z_0 and Z_∞ are plotted in Fig. 34. It is observed that while Z_0 and Z_∞ are both decreasing due to the increase in the initial water mass fraction, $(1-Z_0)$; the difference, $Z_\infty-Z_0$, is increasing as the spray density, ρ_{s0}, increases. This implies a larger amount of vapor added to the combustion process if more water is added to the mixture initially. The difference, $Z_\infty-Z_0$, represents the final vapor mass fraction in the mixture. Thus, although percentage-wise the fraction of spray evaporated, % F_v (Eqn. (2-69)), is constant and equal to 5.43%; the higher the mass of water present, the higher will be the mass of the fraction evaporated for a given constant droplet size distribution in the water spray. Those results are just another means of showing that the more water there is in the mixture with (a) constant droplet size distribution, the greater will be the reduction in the burning velocity of the flame.

One more comment should be made at this point. In reality, when increasing the spray density, especially in

confined space experiments such as ours where some flow limitations exist, the droplet size distribution of the spray will not always be constant. By increasing the volume of water sprayed into the tube, the probability of collisions and coalescence taking place among the droplets is greater. This could be due to the tube wall effect whereby more water is lost and hence more droplets could bounce back into the main stream. It is also possible that in the initial unsteady state period when the water is sprayed into the tube, later incoming droplets might collide or coalesce with droplets of a lower velocity already in the mixture. This, in turn, could cause a slight shift in the droplet size distribution.

In our experiments, due to the low flow rates used, the assumption of a constant droplet size distribution is a very good one.

CHAPTER VI

CONCLUSIONS

The primary aim of the present study is to investigate both, experimentally and theoretically, the influence of water sprays on the burning velocity of laminar propagating flames in various hydrogen sulfide-air mixtures.

For the theoretical model, the water droplets are assumed to be inert in the mixture. In other words, it is assumed that chemical interaction between the liquid droplets and the surrounding gas has a negligible effect on the combustion process. Thus, the theoretical investigation deals with the thermophysical effects of the water droplets in the reaction zone of the H_2S-air flames.

Each of the individual droplets is assumed to act as a heat sink via sensible heat transfer through its surface from the surrounding hot gases and via the latent heat of vaporization. As less heat is then available for heating the combustion products, the flame temperature drops causing a reduction in the burning velocity.

Moreover, with the liquid droplet surface undergoing a change of phase, the vapor created diffuses into the surrounding gases and dilutes the combustible mixture. This dilution leads to an increase in the heat capacity of the

H_2S-air mixture due to the addition of inert vapor, therefore, further lowering the adiabatic flame temperature and reducing the burning velocity.

The effectiveness of a water spray in reducing the burning velocity for a given mixture is shown to depend on: (i) the water spray droplet size distribution and (ii) the water spray density or equivalently the water mass concentration in the combustible mixture.

By decreasing the droplet median volume diameter for a given spray density or increasing the spray density for a given droplet size distribution, the spray surface area per unit volume is increased. With the heat flux across the reaction zone being constant (from the energy equation, Eqn. (2-53)), an increase in the spray surface area then implies a higher rate of heat transfer from the hot gases to the cooler droplets. Consequently, more of the liquid phase is evaporated and the net result is a further reduction in the flame temperature and thus in the burning velocity.

The burning velocities of flames in H_2S-air mixtures with and without water sprays were measured experimentally over the composition range from 7% to 20% H_2S in air. The results are illustrated in Figs. 18-25, 26 and 31. Without water spray the burning velocity reaches its maximum value of 41.1 cm/sec for stoichiometric H_2S-air mixture (12% H_2S in air). A water spray density, ρ_{s_0} = 1.09 mg/cm^3, and droplet

median volume diameter, $\bar{d}_0$ = 145 μm, reduces this burning velocity by only 4.4% down to 39.28 cm/sec. For the same spray density but smaller droplet median volume diameter, e.g. $\bar{d}_0$ = 40 μm, the peak burning velocity of 41.1 cm/sec is reduced by 22.5% to 31.9 cm/sec. These and more data are presented in Fig. 26 and tabulated in Table 9.

Also measured experimentally were the burning velocities with increasing the spray density for a given droplet median volume diameter, $\bar{d}_0$ = 52.5 μm. For a spray density, ρ_{s_0} = .3172 mg/cm^3, the burning velocity in stoichiometric H_2S-air mixture is 38.93 cm/sec, a reduction of about 5.3% from 41.1 cm/sec. With the spray density increased to a maximum of ρ_{s_0} = 1.3474 mg/cm^3, the burning velocity is reduced by 28.8%, down to 29.28 cm/sec. These results are illustrated in Fig. 31 and listed in Table 9.

In our experiments we were able to inert the H_2S-air mixtures only from 6% H_2S and down. Inerting limits are defined here as the combination of spray density and spray droplet size distribution that are required to prevent incipient ignitions of flammable H_2S-air mixtures from developing into self-propagating flames. Sapko et al. succeeded in inerting methane-air mixtures by using steam and fine water droplets, less than 10 μm in diameter and at 60°C. They were unsuccessful in trying to extend the inerting data down to spray at room temperature.

In the present experiments, the spray densities achieved were quite high but the smallest droplet median volume diameter that could be generated was 35 μm and the water sprays were at room temperature. Therefore, the inerting of the H_2S-air mixtures in which the burning velocities are of the same order of magnitude as those in the methane-air mixtures, did not occur beyond 6% H_2S. Extrapolation of the present experimental results indicates that with smaller droplets at a temperature higher than the room temperature, inerting of any H_2S-air composition is feasible. Inerting of the higher burning velocity H_2S-air compositions will naturally require higher spray densities for a given droplet size distribution.

The numerical scheme developed and used to calculate the burning velocities in stoichiometric H_2S-air mixtures with water sprays could be extended to include all other mixture compositions, although this would require some modifications. The final expressions for the upper and lower bounds of the eigenvalue (Eqns. (2-34) or (2-84)) would remain unchanged.

Considering the approximations and assumptions made in the theoretical analysis, the results are in good agreement with experiments as shown, for example, in Figs. 26 and 31. Comparisons between theoretical values for the burning velocity and experimental results are few and usually far between. The only published comparisons are for the simple

hydrazine decomposition flame, and even there one could argue that the agreement is fortuitous [12]. In order to calculate the burning velocity, one must know the thermophysical properties of a complex mixture at high temperatures and have accurate reaction rate data. Such data, as for example, the overall frequency factor, overall activation energy, chain reaction and their rates, etc., are in many cases not available.

In our calculations for H_2S-air-H_2O mixtures, the frequency factor ($B_f = 2.8625 \times 10^{13}$) was chosen to give the experimental value of the peak burning velocity, $u_{0_{max}} = 41.1$ cm/sec, in the dry stoichiometric H_2S-air mixture. Using this same value of B_f, computation of the burning velocities for stoichiometric H_2S-air mixtures with various water sprays yielded results which agreed reasonably well with the experimental burning velocities (Table 9).

It should be noted that the numerical results for $u_{0_{max}}$ as they appear in Table 9 are based on an ideal adiabatic flame temperature; dissociation effects are not included.

Since the burning velocity depends on the flame temperature, the adiabatic flame temperature is an important and necessary input parameter into the burning velocity calculations. For a given temperature, the corresponding upper and lower burning velocity bounds are calculated. Thus,

once the adiabatic flame temperature is known, the burning velocity can be found and vice versa. In this thesis, the experimentally measured burning velocities were used to determine the corresponding adiabatic flame temperatues, $T_{\infty,e}$. The values for $T_{\infty,e}$ shown in Figs. 27 and 28 (as a function of increasing $\bar{d}_0$) and Figs. 32 and 33 (as a function of increasing ρ_{s_0}) show the same behavior as the calculated ideal adiabatic flame temperature, $T_{\infty,a}$, illustrated in the same figures; namely, the temperature decreases with decreasing droplet sizes or increasing spray density.

Based on our calculations we would predict that a droplet of 10 μm or less will evaporate completely in the stoichiometric H_2S-air flame reaction zone. For a spray with, $\bar{d}_0$ = 10 μm, and density, ρ_{s_0} = 1.09 mg/cm^3, (47.5% water concentration by mass) the numerical computations give an almost zero burning velocity in the stoichiometric H_2S-air mixture. In this case, the total heat released per gram of the overall mixture (liquid plus gas) is 291.3 cal/g and 220.5 cal/g (75.7% of the total) of this is removed by heating and evaporation of the water droplets and subsequently by vapor dilution. By decreasing the droplet sizes or increasing the spray density, the part of the reaction heat absorbed by heating up the liquid droplets to the boiling temperature is reduced. In the case above for example from a total of 75.7% heat removed, only 12.2% went into heating the water droplets

to the point where evaporation starts; the rest was removed due to evaporation and vapor dilution.

Our calculations therefore indicate that with water sprays of less than 10 μm MVD droplets at room temperature and spray densities above about 1 mg/cm^3, inerting of the stoichiometric H_2S-air mixture and hence any other non-stoichiometric H_2S-air mixture composition, may be possible.

The complexities and efforts involved in a full and comprehensive analytical model are beyond the scope of this work. A better knowledge of the thermophysical and transport properties, and the chemical reactions for H_2S-air mixtures would be required to justify a more detailed analysis and computations.

In conclusion, an experimental and theoretical investigation of the combustion of H_2S-air mixtures with and without water sprays has been undertaken. To the author's knowledge, the results of this investigation are the most comprehensive available for this particular system at the present time.

It is hoped that this work will be at least considered as a small contribution to the scientific effort needed to further explore the interesting and mostly unknown combustion field.

BIBLIOGRAPHY

1. Krishna, C.R., Prasad, C.R. & Klemm, R.B., "Quenched Flames with Inhibitors - A Theoretical Analysis", Combustion Studies Program, Department of Applied Science, Brookhaven National Lab., Upton, New York, 1976.

2. Biordi, C.J., Lazzara, P.C. & Papp, F.J., "The Effect of CF_3Br on Radical Concentration Profiles in Methane Flames", American Chemical Society, series 16 on "Halogenated Fire Suppressants", Washington, D.C., pp. 256-294, 1975.

3. Biordi, C.J., Lazzara, P.C., & Papp, F.J., U.S. Bureau of Mines, RI 8029 (1975), RI 8222 (1977), RI 8307 (1978).

4. Liebman, A., Richmond, J.K. & Grumer, J., "Recent Developments in Passive and Triggered Explosion Barriers", Proc. 16th Internat. Conf. on Coal Mine Safety Research, Washington, D.C., p. VII, 8.1, 1975.

5. Liebman, I., Corry, J., Pr., R., & Richmond, J.K., "Extinguishing Agents for Mine Face Gas Explosions", Bureau of Mines, RI 8294, 1978.

6. Dryer, F.L., "Water Addition to Practical Combustion Systems - Concepts and Applications", Sixteenth International Symposium on Combustion, pp. 279-295, The Combustion Institute, Pittsburgh, PA, 1976.

7. Sapko, M.J., Furno, A.L. & Kuchta, J.M., "Quenching Methane-Air Ignitions with Water Sprays", Bureau of Mines, RI 8214, 1977.

8. Johnson, W.E. & Nachbar, W., "Deflagration Limits in Steady Linear Burning of a Monopropellant with Application to Ammonium Perchlorate", Lockheed Missles and Space Division, LMSD-703060, AFOSR TN-600, Sunnyvale, CA, 1960. (Later published in the Eighth International Symposium on Combustion, Williams & Williams of Baltimore, 1962).

9. Johnson, W.E. & Nachbar, W., "Laminar Flame Theory and the Steady Linear Burning of a Monopropellant", Archive for Rational Mechanics and Analysis, 12(1), pp. 58-92, 1963.

10. Williams, F.A., COMBUSTION THEORY, Addison-Wesely Series in Engineering Science, Reading, Massachusetts, 1965.

11. Mallard, E. & Le Chatelier, H.L., Ann. Mines, 4, p. 379, 1883.

12. Glassman, I., COMBUSTION, Academic Press, New York, 1977.

13. Taffanel, M., Compt. Rend., 157, 714; 158, 42, 1913.

14. Danielle, P.J., Proc. Roy. Soc., London, 126A, 393, 1930.

15. Zeldovich, Y.B., J. Phys. Chem. (U.S.S.R.) 22, 27, 1948, English translation, N.A.C.A. Tech. Memo. No. 1282, 1951.

16. Boys, S.F. & Corner, J., Proc. Roy. Soc., London, 197A, 90, 1949; Corner, J., Ibid., 198A, 388, 1949.

17. Curtiss, C.F., Hirschfelder, J.O. & Campbell, D.E., Fourth International Symposium on Combustion, pp. 190-210, Williams & Wilkins Co, Baltimore, 1953.

18. Hirschfelder, J.O., Curtiss, C.F. & Campbell, D.E., J. Chem. Phys., 57, 403, 1953.

19. Von Karman, Th., Millan, G. & Biezens, C.B., "Anniversary Volume on Applied Mechanics", pp. 55-69, N.V. De Technische Uitgeverig, H. Stam., Haarlem (Holland), 1953.

20. Von Karman, Th. & Penner, S.S., "Selected Combustion Problems - Fundamentals and Aeronautical Applications", pp. 5-41, Butterworths Scientific Publications, London, 1954.

21. Penner, S.S. & Williams, F.A., "The Theoy of Steady One-Dimensional Laminar Flame Propagation for One Step Chemical Reactions", Astron. Acta, 7, No. 1, 1961.

22. Hirschfelder, J.O., Curtiss, C.F., "Propagation of Flames and Detonations", Adv. in Chem. Phys., Vol. III, New York; Interscience Publishers, Inc., 1961.

23. Penner, S.S., CHEMISTRY PROBLEMS IN JET PROPULSION, Pergamon Press, New York, 1957.

24. Levy, A., Merryman, E.L. & Reid, W.T., "Mechanisms of Formation of Sulfur Oxides in Combustion", Environmental Science and Technology, 4(8), pp. 653-662, 1970.

25. Jensen, D.E. & Jones, G.A., "Reaction Rate Coefficients for Flame Calculations", Combustion and Flame, 32, pp. 1-34, 1978.

26. Kondratiev, V.N., RATE CONSTANTS OF GAS PHASE REACTIONS, Reference book, Nat. Stand. Ref. Data Ser., Nat. Bur. Stand. (U.S.) COM-72-10014, Washington, D.C., 1972.

27. Frenklach, M. & Lee, J.H., "Ignition Delay Time Measurements for H_2S-Air and H_2S-Air-H_2O Mixtures Behind Reflected Shock Waves, at an Initial Pressure of 1 atm", unpublished results, McGill University, Montreal, 1978.

28. Stull, D.R. & Prophet, H., JANAF Thermochemical Tables, 2nd Nat. Stand. Ref. Data Ser., Nat. Bur. Stand. (U.S.), 37, Washington, D.C., 1971.

29. L'Air Liquid, Division Scientifique, ENCYCLOPEDIE DES GAZ, Elsevier Scientific Publishing Co., Amsterdam, 1976.

30. Merryman, E.L., Levy, A., "Kinetics of Sulfur-Oxide Formation in Flames: II. Low Pressure H_2S Flames", Air Pollution Control Association, 17(12), pp. 800-806, 1967.

31. Williams, F.A., "Spray Combustion Theory", Combustion and Flame, 3, pp. 215-228, 1959.

32. Williams, F.A., "Monodisperse Spray Deflagration", Liquid Rockets and Propellants, Vol. 2 of Progress in Astronautics and Rodatry, pp. 229-264, Academic Press, New York, 1960.

33. Williams, F.A., Eighth International Symposium on Combustion, pp. 50-59, Williams and Wilkins Co., Baltimore, 1962.

34. Lu, H.Y. & Chiu, H.H., "Dynamics of Gases Containing Evaporable Liquid Droplets under a Normal Shock", AIAA Journal, 4(6), pp. 1008-1011, 1966.

35. Gaydon, A.G., Wolfhard, H.G., FLAMES - THEIR STRUCTURE, RADIATION AND TEMPERATURE, 3rd Edition, Chapman and Hall Ltd., London, 1970.

36. Linnet, J.W., "Methods of Measuring Burning Velocities", Fourth International Symposium on Combustion, pp. 20-35, Williams & Wilkins Co., Baltimore, 1953.

37. Andrews, G.E. & Bradley, D., "Determination of Burning Velocities: A Critical Review", Combustion and Flame, 18, pp. 133-153, 1972.

38. Bradley, D. & Hundy, G.F., "Burning Velocities of Methane-Air Mixtures Using Hot-Wire Anemometers in Closed-Vessel Explosions", Thirteenth International Symposium on Combustion, pp. 575-583, The Combustion Institute, Pittsburgh, PA, 1971.

39. Andrews, G.E. & Bradley, D., "Determination of Burning Velocity by Double Ignition in a Closed Vessel", Combustion and Flame, 20, pp. 77-89, 1973.

40. Coward, H.F. & Hartwell, F.J., "Studies in the Mechanism of Flame Movement", J. Chem. Soc., Part I, pp. 1996-2004; Part II, pp. 2676-2684, 1932.

41. Coward, H.F. & Payman, W., "Problems in Flame Propagation", Chem. Rev., 21, pp. 359-366, 1937.

42. Gerstein, M., Levine, O. & Wong, E.L., "Flame Propagation. II. The Determination of Fundamental Burning Velocities of Hydrocarbons by a Revised Tube Method", J. Am. Chem. Soc., 73, pp. 418-422, 1951.

43. Markstein, H.G., "Non-Steady Flame Propagation", Chap. E by Guénoche, H., "Flame Propagation in Tubes and in Closed Vessels", The McMillan Co., New York, 1964.

44. Guénoche, H. & Jouy, M., "Changes in the Shape of Flames Propagating in Tubes", Fourth International Symposium on Combustion, pp. 403-407, Williams & Wilkins Co., Baltimore, 1953.

45. Guénoche, H. & Jouy, M., "L'utilisation de la Méthode du Tube pour la Mesure des Vitesses de Déflagration", Institut Français Du Pétrole, Vol. IX, No. 10, pp. 562-572, 1954.

46. Friedman, R. & Burke, E., Industrial & Engineering Chemistry, Vol. 43, p. 2772, 1951.

47. Guénoche, H. & Laffitte, P., Compt. Rend., 222, 1394, 1946.

48. Guénoche, H., Manson, N. & Monnot, G., "La Propagation Uniforme d'une Déflagration dans un Tube Cylindrique Lisse", Compt. Rend., 226, 163, 1948.

49. Lewis, B. & von Elbe, G., COMBUSTION, FLAMES AND EXPLOSION OF GASES, 2nd Ed., p. 387, Academic Press, New York, 1961.

50. Günther, R. & Janisch, G., Combustion and Flame, 19, 49, 1972.

51. Manton, J. & Milliken, B.B., "Study of Pressure Dependence of Burning Velocity by the Spherical Vessel Method", Proceedings of the Gas Dynamics Symposium on Aerothermochemistry, Northwestern University, Evanston, Illinois, p. 151, 1956.

52. Gerstein, M., Levine, O. & Wong, E.L., "Fundamental Flame Velocities of Pure Hydrocarbons, I: Alkanes, Alkenes, Alkynes, Benzene and Cyclohexane", NACA RM E50G24, 1950.

53. Henderson, H.T. & Hill, G.R., J. Phys. Chem., 60, p. 874, 1956.

54. Egerton, A.C. & Lefebvre, A.H., Proc. Roy. Soc., London, Ser. A222, p. 206, 1954.

55. Grover, J.H., Fales, E.N. & Scurlock, A.C., Ninth International Symposium on Combustion, p. 21, Academic Press, New York, 1963.

56. Levy, A. & Merryman, E.L., "Sulfur Chemistry and its Role in Corrosion and Deposits", Engineering for Power, Transactions of ASME, 85, pp. 229-234, 1963.

57. Van Tiggelen, A. & Burger, J., OXYDATIONS ET COMBUSTIONS, Chapter VII, Première Partie, "Propriétés des Mélanges Gazeux Inflammables", Rev. Inst. Franç. du Pétrole, XIX, No. 3, pp. 394-458, 1964.

58. Chamberlin, D.S., Clark, D.R., Ind. Eng. Chem., 20, 1016, 1928.

59. Gibbs, G.J. & Calcote, H.F., J. Chem. Eng., 4, 226, 1959.

60. Spalding, D.B., "The Combustion of Liquid Fuels", Fourth International Symposium on Combustion, pp. 847-864, Williams & Wilkins Co., Baltimore, 1953.

61. Godsave, G.A.E., Fourth International Symposium on Combustion, p. 818, Williams and Wilkins, Co., Baltimore, 1953.

62. Blackshear, P.L.Jr., AN INTRODUCTION TO COMBUSTION, Chapter IV, Department of Mechanical Engineering, University of Minnesota, Minneapolis.

63. Tanasawa, Y., Tech. Rept. , Tohoku University, 18, 195, 1954.

64. Nukiyama, S. & Tanasawa, Y., Trans. Soc. Mech. Eng., Japan, 5, 62, 1939.

65. Rosin, P. & Rammler, E., Zeit des Vereins Deutscher Ing., 71, 1, 1927.

66. Laffitte, P., EXPERIMENTAL METHODS IN COMBUSTION RESEARCH, (J. Surugue Ed.), AGARD; Pergamon, Oxford, p. 5, 1961.

67. Combourieu, J., EXPERIMENTAL METHODS IN COMBUSTION RESEARCH, (J. Surugue Ed.), AGARD; Pergamon, Oxford, p. 25, 1961.

68. Laffitte, P. & Combourieu, J., Journées Internationales de la Combustion et de la Conversion de l'Energie, p. 55, Institut Français des Combustibles et de l'Energie, Paris, 1964.

TABLES

Table 1. Thermochemical Properties of H_2S-air Combustion Species at 1 atm Pressure.

Reactants	h_K^0 (Kcal/mole)	W_K	$Cp_{T=298°K}$ (cal/g °K)	$\lambda_{T=298°K}$ (cal/s cm °K)
H_2S (g)	-4.88 ± .15	34.08	.2396	3.32×10^{-5}
O_2 (g)	0	32	.2198	6.27×10^{-5}
N_2 (g)	0	28.016	.2486	6.176×10^{-5}
Products	h_K^0 (Kcal/mole)	W_K	$Cp_{T_\infty=2069°K}$ (cal/g °K)	λ (cal/s cm °K)
SO_2 (g)	-70.947	64.066	.2177	4.47×10^{-5} T=600°K
H_2O (ℓ)	-68.315	18.016	.6834	1.15×10^{-3} T=600°K
N_2 (g)	0	28.016	.3075	2.885×10^{-4} T=2100°K

Table 2. The Manufacturer's Specifications for the Spraying Nozzles.

Nozzle No.	Orifice Diam. No.	Core No.	CAPACITY GPH (Gallons per hour)									SPRAY ANGLE		
			30 psi	40 psi	60 psi	100 psi	200 psi	300 psi	500 psi	700 psi	1000 psi	40 psi	80 psi	300 psi
1/4 LN .6	.016"	110	-	-	-	.95	1.3	1.6	2.1	2.5	3.0	-	35°	65°
1/4 LN 3	.028"	220	2.6	3.0	3.7	4.7	6.7	8.2	10.6	12.5	15.0	65°	70°	73°
1/4 LN 8	.060"	225	6.9	8.0	9.8	12.6	17.9	22	28	34	40	85°	89°	91°

Table 3. Numerical Results for Varying Droplet Size ($\bar{d}_0$) and given Spray Density (ρ_{s_0} = 1.09 mg/cm^3); $z^* = z_\infty$.

$\bar{d}_0$ (μm)	$T_{\infty,a}$ (°K)	$\tilde{T}_i$	T_i (°K)	$\Lambda^+ \times 10^{-5}$	$u_{0\ max}^-$ (cm/sec)	$\Lambda^- \times 10^{-5}$	$u_{0\ max}^+$ (cm/sec)
35	1553.1	-.9	436.1	14.33327207	12.35992785	9.795848620	14.95090822
		-.8	560.2	14.33344603	12.35985285	9.796302129	14.95056215
		-.7	684.3	14.34201845	12.35615847	9.811060897	14.93931286
		-.6	808.4	14.45650671	12.30713394	9.958857830	14.82804317
40	1647.2	-.9	443.1	8.030384777	16.91232285	5.442195750	20.54396936
		-.8	576.9	8.030489588	16.91221248	5.442463652	20.54346372
		-.7	710.7	8.035938682	16.90647750	5.451684926	20.52608221
		-.6	844.4	8.108309612	16.83085879	5.543675537	20.35506700
52.5	1792.9	-.9	453.8	3.644638490	26.05506351	2.437922739	31.85733158
		-.8	602.6	3.644693911	26.05486542	2.438060274	31.85643300
		-.7	751.4	3.647740008	26.04398440	2.443081746	31.82367756
		-.6	900.2	3.687331328	25.90378836	2.492234598	31.50829511
80	1923.7	-.9	463.5	1.960843405	36.72117729	1.296418224	45.16120160
		-.8	625.7	1.960878593	36.72084781	1.296503342	45.15971911
		-.7	787.9	1.962866679	36.70224678	1.299706231	45.10404084
		-.6	950.2	1.987967198	36.46980534	1.330232995	44.58350358
145	1999.2	-.9	469	1.415988599	44.03958566	.9299626626	54.34259165
		-.8	639	1.416016788	44.03914730	.9300298802	54.34062781
		-.7	809.1	1.417622562	44.01419816	.9325834302	54.26618052
		-.6	979.1	1.437500281	43.70882517	.9564789796	53.58403175

Table 4. Numerical Results for Varying Droplet Size ($\bar{d}_0$) and given Spray Density (ρ_{s_0} = 1.09 mg/cm^3); Z^*_{ℓ} = $(Z_0+Z_\infty)/2$

$\bar{d}_0$ (μm)	$T_{\infty,a}$ (°K)	$\tilde{T}_i$	T_i (°K)	$\Lambda^+ \times 10^{-5}$	$u_{0\ max}^-$ (cm/sec)	$\Lambda^- \times 10^{-5}$	$u_{0\ max}^+$ (cm/sec)
35	1768.7	-.9	452	4.122528137	24.34780988	2.763560972	29.73768732
		-.8	598.3	4.122589091	24.34762989	2.763712971	29.73686956
		-.7	744.6	4.125915158	24.33781411	2.769219630	29.70728861
		-.6	890.9	4.169339435	24.21074143	2.823340067	29.42118227
40	1824.9	-.9	456.2	3.109561926	28.43875529	2.074062127	34.82164701
		-.8	608.2	3.109611066	28.43853059	2.074183305	34.82062982
		-.7	760.3	3.112334987	28.42608314	2.078648267	34.78321214
		-.6	912.4	3.147513173	28.26678471	2.122100256	34.42526090
52.5	1907.4	-.9	462.3	2.109067969	35.26252462	1.396426387	43.33608427
		-.8	622.8	2.109105007	35.26221500	1.396516261	43.33468978
		-.7	783.4	2.111192515	35.24477738	1.399888820	43.28245816
		-.6	944	2.137653557	35.02595856	1.432151576	42.79215892
80	1977.6	-.9	467.4	1.550959445	41.85256543	1.020548261	51.59475225
		-.8	635.2	1.550989402	41.85216124	1.020619987	51.59293927
		-.7	803	1.552692763	41.82919826	1.023338775	51.52435809
		-.6	970.8	1.573901869	41.54640778	1.048919292	50.89220504
145	2016.4	-.9	470.3	1.318633033	45.83282415	.8647146520	56.59814341
		-.8	642.1	1.318659930	45.83235672	.8647785804	56.59605138
		-.7	813.9	1.320193874	45.80572248	.8672107557	56.51663114
		-.6	985.7	1.339092680	45.48134256	.8898700973	55.79243133

Table 5. The H_2S-Air-Water Spray, Mixture and Combustion Parameters for Varying Droplet Size ($\bar{d}_0$) and given Spray Density (ρ_{s_0} = 1.09 mg/cm^3).

$\bar{d}_0$ (μm)	ρ_{s_0} (mg/cm^3)	ρ_0 (mg/cm^3)	G	Z_0	Z_∞	% F_v	$\bar{K}_{Z^*=Z_\infty}$	$\bar{K}_{Z^*=(Z_0+Z_\infty)/2}$
35					.5824	12.07	2168.5	2265.9
40					.5692	9.29	2210.3	2292.0
52.5	1.0901	2.2953	.1779	.5250	.5508	5.43	2277.1	2330.7
80					.5362	2.35	2338.3	2363.8
145					.5285	.72	2374.1	2382.3

Table 6. Numerical Results for Varying Spray Density (ρ_{s_0}) and given Droplet Size ($\bar{d}_0$ = 52.5 μm); $Z^* = Z_\infty$.

ρ_{s_0} (mg/cm^3)	$T_{\infty,a}$ (°K)	$\tilde{T}_i$	T_i (°K)	$\Lambda^+ \times 10^{-5}$	$u_{0\ max}^-$ (cm/sec)	$\Lambda^- \times 10^{-5}$	$u_{0\ max}^+$ (cm/sec)
.3172	2125.2	-.9	482.7	.8512071225	51.46014219	.5519115207	63.90780134
		-.8	665.2	.8512300579	51.45944892	.5519648427	63.90471439
		-.7	847.7	.8524672393	51.42209394	.5538859675	63.79379303
		-.6	1030.2	.8668118676	50.99483396	.5707644920	62.84346645
.6861	1960.9	-.9	468.4	1.655814482	37.63916371	1.090089964	46.38895968
		-.8	634.2	1.655847888	37.63878403	1.090170119	46.38725427
		-.7	800.1	1.657685925	37.61791137	1.093108283	46.32487022
		-.6	965.9	1.680305760	37.36385223	1.120422940	45.75671184
1.0313	1816.6	-.9	455.9	3.234934456	27.53954784	2.158964499	33.71062449
		-.8	607.1	3.234985585	27.53933021	2.159090768	33.70963873
		-.7	758.2	3.237800705	27.5273555	2.163711021	33.67362877
		-.6	909.4	3.274128526	27.37421580	2.208632556	33.32942442
1.0825	1795.9	-.9	454.1	3.588420701	26.24385578	2.399614744	32.09287010
		-.8	603.2	3.588475538	26.24365526	2.399750745	32.09196069
		-.7	752.3	3.591490330	26.23263813	2.404717773	32.05880003
		-.6	901.4	3.630639009	26.09082335	2.453295991	31.73981160
1.1882	1753.8	-.9	450.4	4.461451971	23.72160628	2.995483817	28.95000984
		-.8	595.2	4.461515717	23.72143682	2.995643292	28.94923924
		-.7	740	4.465004738	23.71216686	3.001437122	28.92128463
		-.6	884.9	4.510868044	23.59131465	3.058754430	28.64902846
1.3474	1691.8	-.9	445	6.253474995	20.28903051	4.223788664	24.68714762
		-.8	583.5	6.253556253	20.28889870	4.223994603	24.68654581
		-.7	722.1	6.257958113	20.28176182	4.231390441	24.66496218
		-.6	860.6	6.316782239	20.18710544	4.305689862	24.45122555

Table 7. Numerical Results for Varying Spray Density (ρ_{s_0}) and given Droplet Size ($\bar{d}_0 = 52.5$ μm); $Z^* = (Z_0+Z_\infty)/2$.

ρ_{s_0} (mg/cm^3)	$T_{\infty,a}$ (°K)	$\tilde{T}_i$	T_i (°K)	$\Lambda^+ \times 10^{-5}$	$u_{0\ max}^-$ (cm/sec)	$\Lambda^- \times 10^{-5}$	$u_{0\ max}^+$ (cm/sec)
.3172	2164.7	=.9	485.7	.7358932441	55.88998699	.4755170571	69.52778060
		-.8	672.2	.7359142565	55.88918908	.4755655589	69.52423502
		-.7	858.8	.7370462946	55.84625215	.4773119534	69.39693043
		-.6	1045.3	.7500164998	55.36126531	.4924851727	68.31952475
.6861	2039.6	-.9	474.3	1.192805471	45.23530050	.7798491233	55.94444848
		-.8	648.2	1.192832333	45.23479115	.7799126267	55.94217083
		-.7	822.1	1.194318960	45.20662941	.7822572910	55.85827002
		-.6	996.1	1.212228585	44.87144243	.8036262025	55.11061362
1.0313	1926.4	-.9	464	1.935399792	36.61075465	1.279100851	45.03411495
		-.8	626.5	1.935435003	36.61042162	1.279185969	45.03261663
		-.7	789	1.937415875	36.59170104	1.282375075	44.97658654
		-.6	951.5	1.962347562	36.35850864	1.312677439	44.45442688
1.0825	1909.9	-.9	462.5	2.085583495	35.43533450	1.380550599	43.55361051
		-.8	623.3	2.085620288	35.43502194	1.380639835	43.55220297
		-.7	784.1	2.087693529	35.41742271	1.383987827	43.49949270
		-.6	944.9	2.113949726	35.19678538	1.415987740	43.00516129
1.1882	1876.1	-.9	459.4	2.439476451	33.09210039	1.620098986	40.60709047
		-.8	616.8	2.439516871	33.09182624	1.620197689	40.60585355
		-.7	774.2	2.441800563	33.07634807	1.623908739	40.55942960
		-.6	931.6	2.471085237	32.87977108	1.659802363	40.11847896
1.3474	1825.7	-.9	454.8	3.108902640	29.77006243	2.074798409	36.44142515
		-.8	607.1	3.108949616	29.76983751	2.074914307	36.44040739
		-.7	759.5	3.111609551	29.75711054	2.079277664	36.40215227
		-.6	911.8	3.146338874	29.59242517	2.122208918	36.03207216

Table 8. The H_2S-Air-Water Spray, Mixture and Combustion Parameters for Varying Spray Density (ρ_{s_0}) and given Droplet Size ($\bar{d}_0$ = 52.5 μm).

ρ_{s_0} (mg/cm^3)	V_{eff} (cm^3)	ρ_0 (mg/cm^3)	G	Z_0	Z_∞	% F_v	$\bar{K}_{Z^*=Z_\infty}$	$\bar{K}_{Z^*=(Z_0+Z_\infty)/2}$
.3172	1.036	1.5224	.2682	.7916	.8029		2193.8	2211.0
.6861	2.24	1.8913	.2159	.6372	.6569		2229.0	2264.7
1.0313	3.366	2.2364	.1826	.5389	.5639		2269.4	2320.6
1.0825	3.534	2.2876	.1785	.5268	.5525	5.43	2276.1	2329.4
1.1882	3.879	2.3934	.1706	.5035	.5305		2290.4	2348.0
1.3474	4.399	2.5526	.1600	.4721	.5008		2313.4	2377.2

Table 9. Experimental and Numerical Values* of the Maximum Burning Velocities.

d_0 (μm)	Experiments $u^e_{0_{max}}$ (cm/sec)	Theory $u^c_{0_{max}}$ (cm/sec)		% Discrepancy $(u^c_{0_{max}} - u^e_{0_{max}})/u^e_{0_{max}} \times 100\%$	
		$Z^*=Z_\infty$	$Z^*=(Z_0+Z_\infty)/2$	$Z^*=Z_\infty$	$Z^*=(Z_0+Z_\infty)/2$
35	-	13.66	27.05	-	-
40	31.90	18.73	31.63	-41.3%	-.8%
52.5	33.75	28.96	39.3	-14.2%	16.4%
80	37.15	40.94	46.73	10.2%	25.8%
145	39.28	49.19	51.22	25.2%	30.4%
ρ_{s_0} (mg/cm^3)					
.3172	38.93	57.69	62.71	48.2%	61.1%
.6861	37.62	42.02	50.59	11.7%	34.5%
1.0313	34.52	30.63	40.82	-11.3%	18.2%
1.0825	33.75	29.17	39.49	-13.6%	17%
1.1882	30.00	26.34	36.85	-12.2%	22.8%
1.3474	29.28	22.49	33.11	-23.2%	13.1%

*The values of $u^c_{0_{max}}$ are averaged between $u^+_{0_{max}}$ and $u^-_{0_{max}}$.

Table 10. Numerical Values* for Adiabatic Flame Temperatures at Maximum Burning Velocities.

$\bar{d}_0$ (μm)	$Z^*=Z_\infty$		$Z^*=(Z_0+Z_\infty)/2$		$(T_{\infty,a}-T_{\infty,e})/T_{\infty,e}$ x 100%	
	$T_{\infty,a}$ (°K)	$T_{\infty,e}$ (°K)	$T_{\infty,a}$ (°K)	$T_{\infty,e}$ (°K)	$Z^*=Z_\infty$	$Z^*=(Z_0+Z_\infty)/2$
40	1647.2	1775	1824.9	1825	-7.2%	0.0%
52.5	1792.9	1835	1907.4	1855	-2.3%	2.8%
80	1923.7	1900	1977.6	1910	1.2%	3.5%
145	1999.2	1930	2016.4	1935	3.6%	4.2%
ρ_{s_0} (mg/cm^3)						
.3172	2125.2	1995	2164.7	2005	6.5%	8.0%
.6861	1960.9	1930	2039.6	1945	1.6%	4.9%
1.0313	1816.6	1850	1926.4	1875	-1.8%	2.7%
1.0825	1795.9	1835	1909.9	1865	-2.1%	2.4%
1.1882	1753.8	1787.5	1876.1	1825	-1.9%	2.8%
1.3474	1691.8	1757.5	1825.7	1795	-3.7%	1.7%

*$T_{\infty,a}$ and $T_{\infty,e}$ are the ideal and fitted adiabatic flame temperatures, respectively.

FIGURES

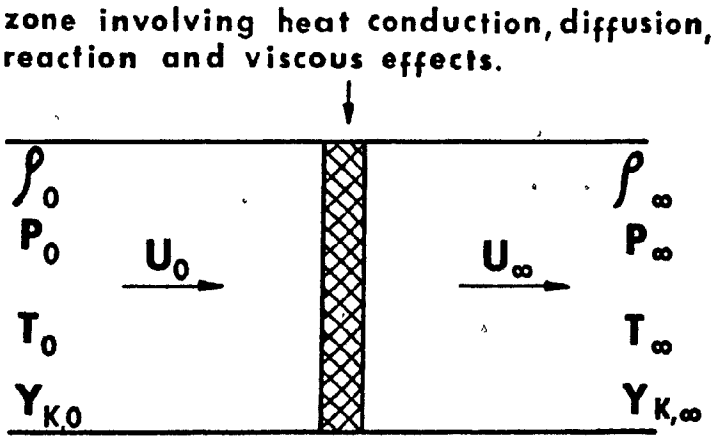

FIG. 1 SCHEMATIC DIAGRAM OF A DEFLAGRATION WAVE

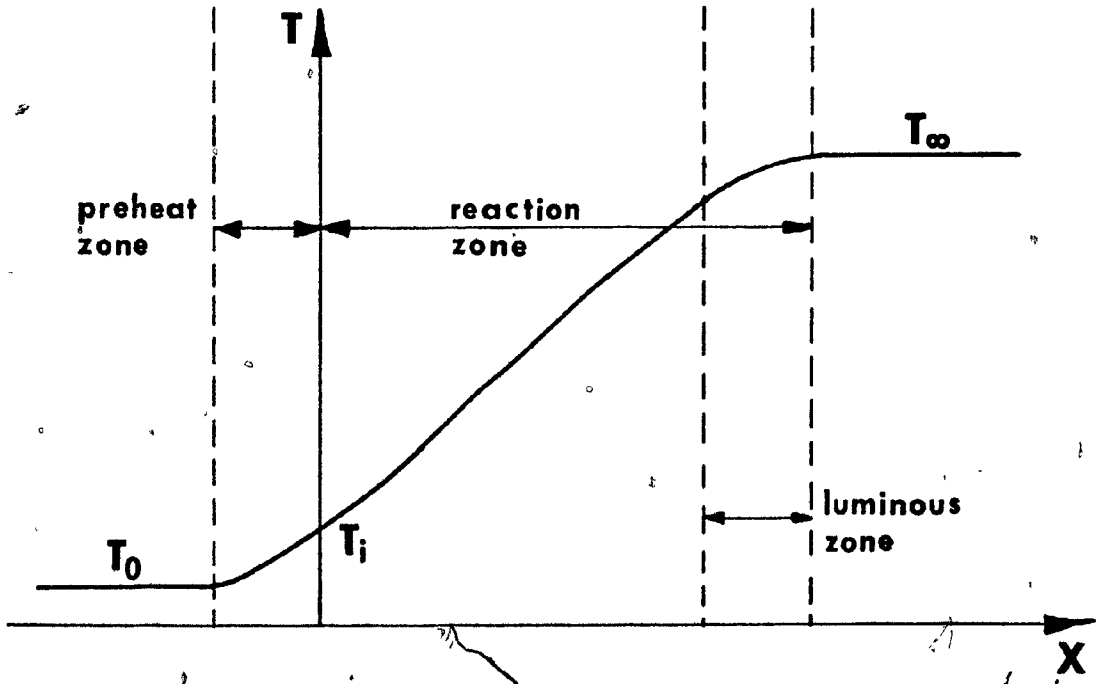

FIG. 2 TEMPERATURE REGIMES IN A LAMINAR FLAME

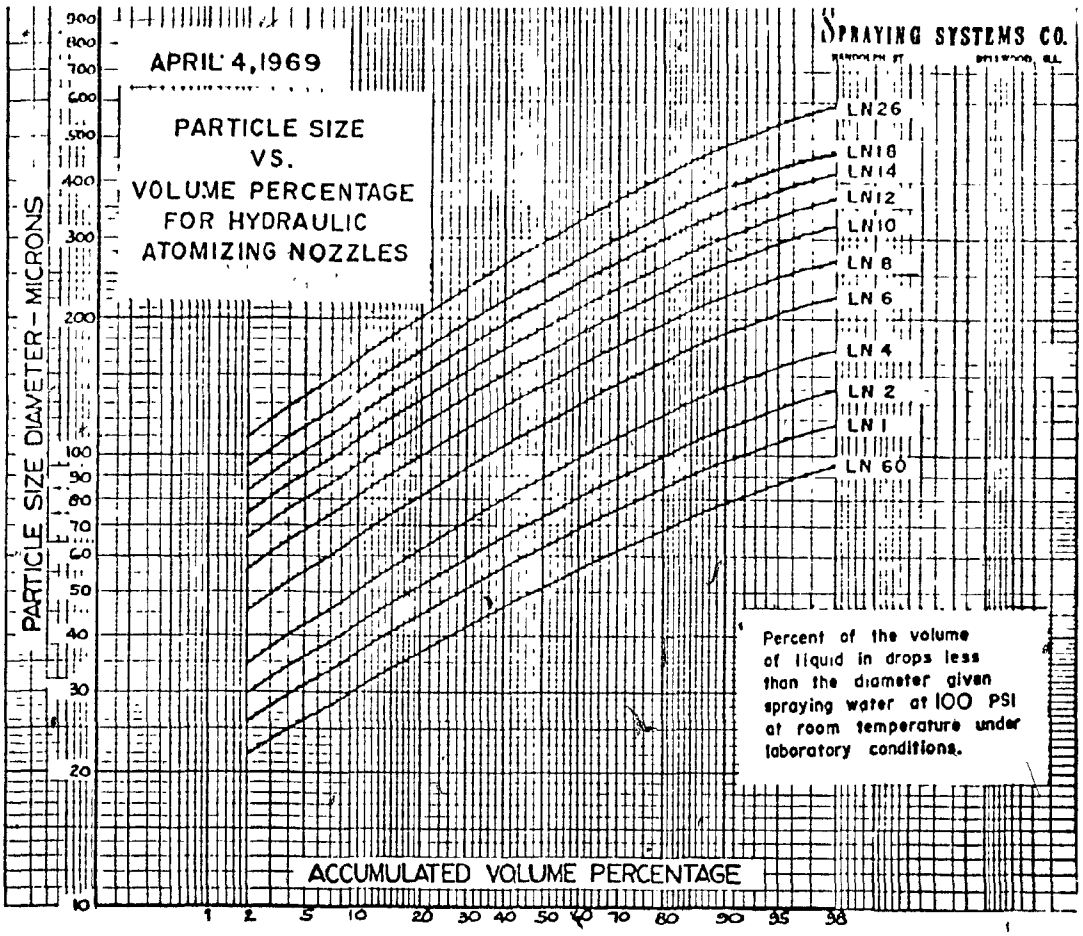
SPRAYING SYSTEMS CO.
RANDOLPH ST
BELLWOOD, ILL.
APRIL 4, 1969
PARTICLE SIZE
VS.
VOLUME PERCENTAGE
FOR HYDRAULIC
ATOMIZING NOZZLES
PARTICLE SIZE DIAMETER - MICRONS
900
800
700
600
500
400
300
200
100
90
80
70
60
50
40
30
20
10
LN 26
LN 18
LN 14
LN 12
LN 10
LN 8
LN 6
LN 4
LN 2
LN 1
LN 60
Percent of the volume of liquid in drops less than the diameter given spraying water at 100 PSI at room temperature under laboratory conditions.
ACCUMULATED VOLUME PERCENTAGE
1
2
5
10
20
30
40
50
60
70
80
90
95
98

FIG. 3

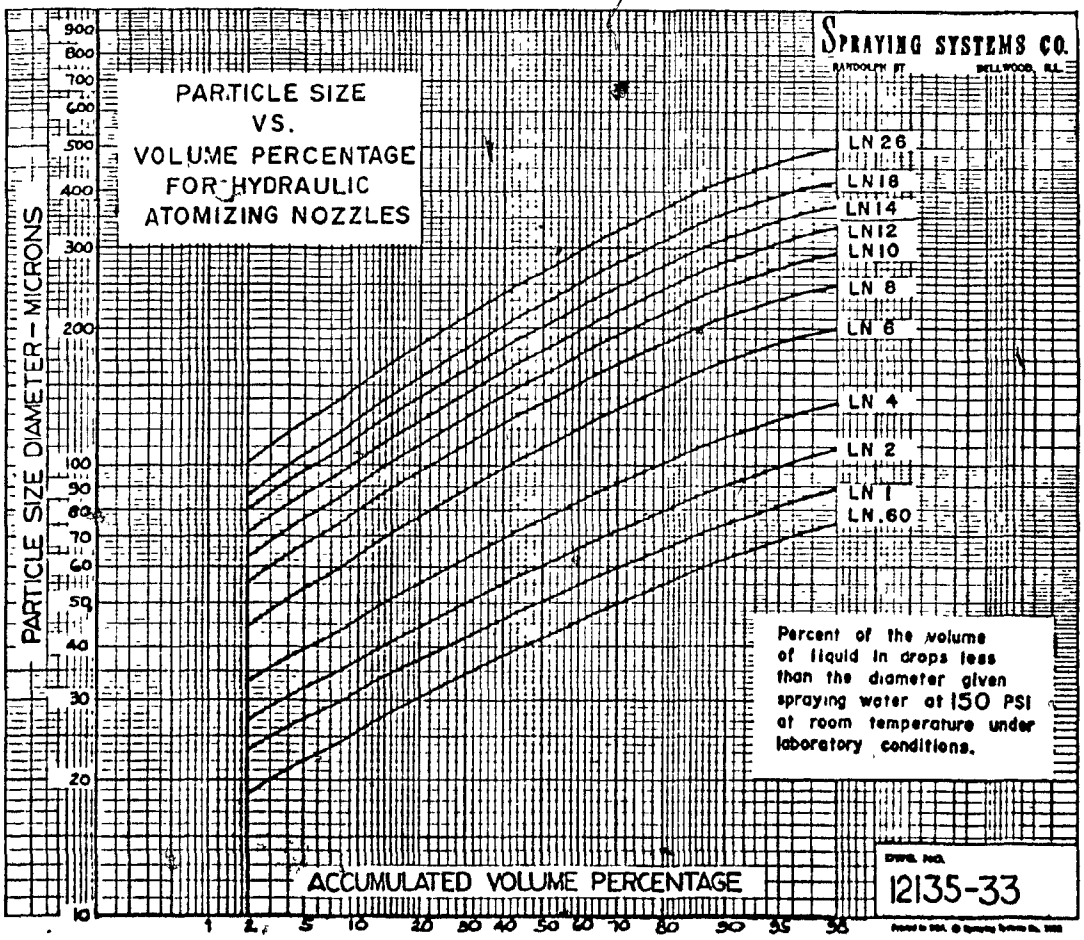
SPRAYING SYSTEMS CO.
RANDOLPH ST
BELLWOOD, ILL.
PARTICLE SIZE
VS.
VOLUME PERCENTAGE
FOR HYDRAULIC
ATOMIZING NOZZLES
PARTICLE SIZE DIAMETER - MICRONS
900
800
700
600
500
400
300
200
100
90
80
70
60
50
40
30
20
10
LN 26
LN 18
LN 14
LN 12
LN 10
LN 8
LN 6
LN 4
LN 2
LN 1
LN .60
Percent of the volume of liquid in drops less than the diameter given spraying water at 150 PSI at room temperature under laboratory conditions.
ACCUMULATED VOLUME PERCENTAGE
1
2
5
10
20
30
40
50
60
70
80
90
95
98
DWG. NO.
12135-33

FIG. 4

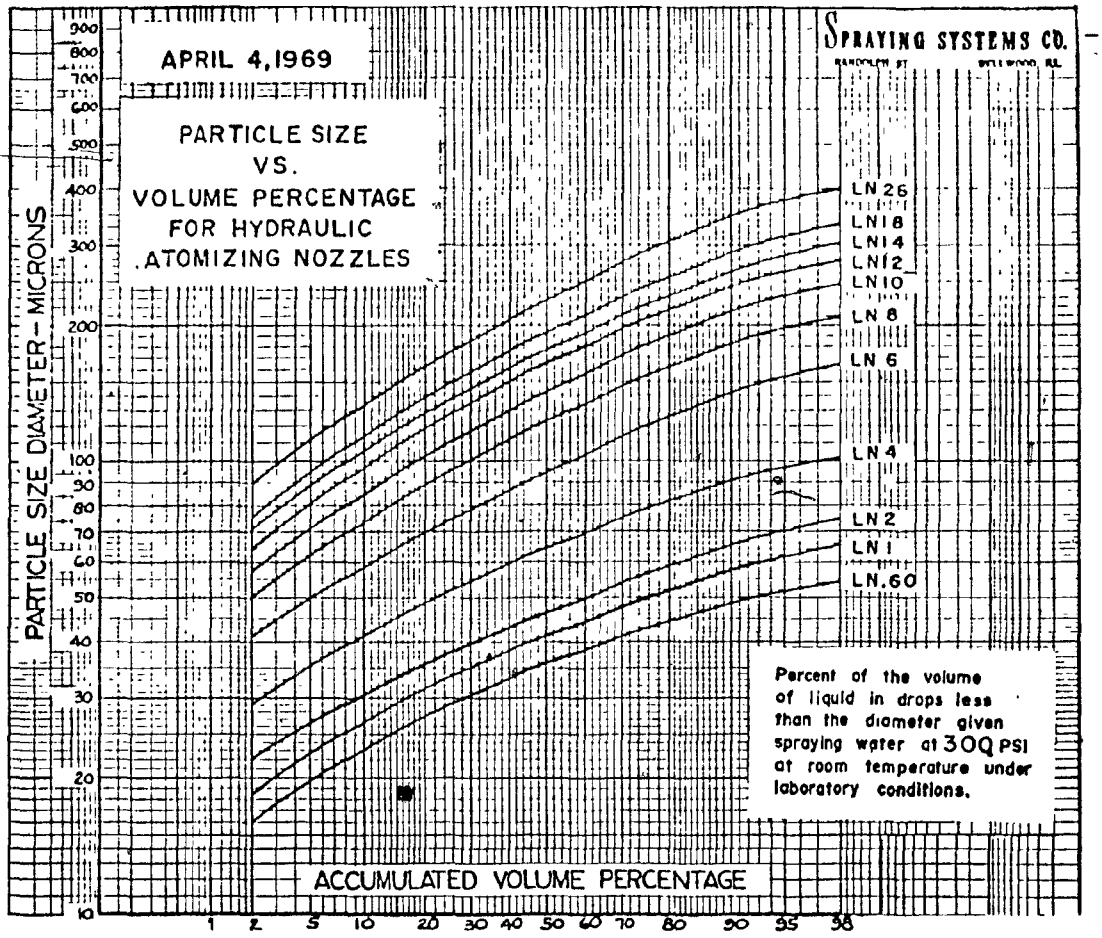
SPRAYING SYSTEMS CO.
RANDOLPH ST
BELLWOOD, ILL.
APRIL 4,1969
PARTICLE SIZE
VS.
VOLUME PERCENTAGE
FOR HYDRAULIC
ATOMIZING NOZZLES
PARTICLE SIZE DIAMETER - MICRONS
900
800
700
600
500
400
300
200
100
90
80
70
60
50
40
30
20
10
LN 26
LN 18
LN 14
LN 12
LN 10
LN 8
LN 6
LN 4
LN 2
LN 1
LN .60
Percent of the volume of liquid in drops less than the diameter given spraying water at 300 PSI at room temperature under laboratory conditions.
ACCUMULATED VOLUME PERCENTAGE
1
2
5
10
20
30
40
50
60
70
80
90
95
98

FIG. 5

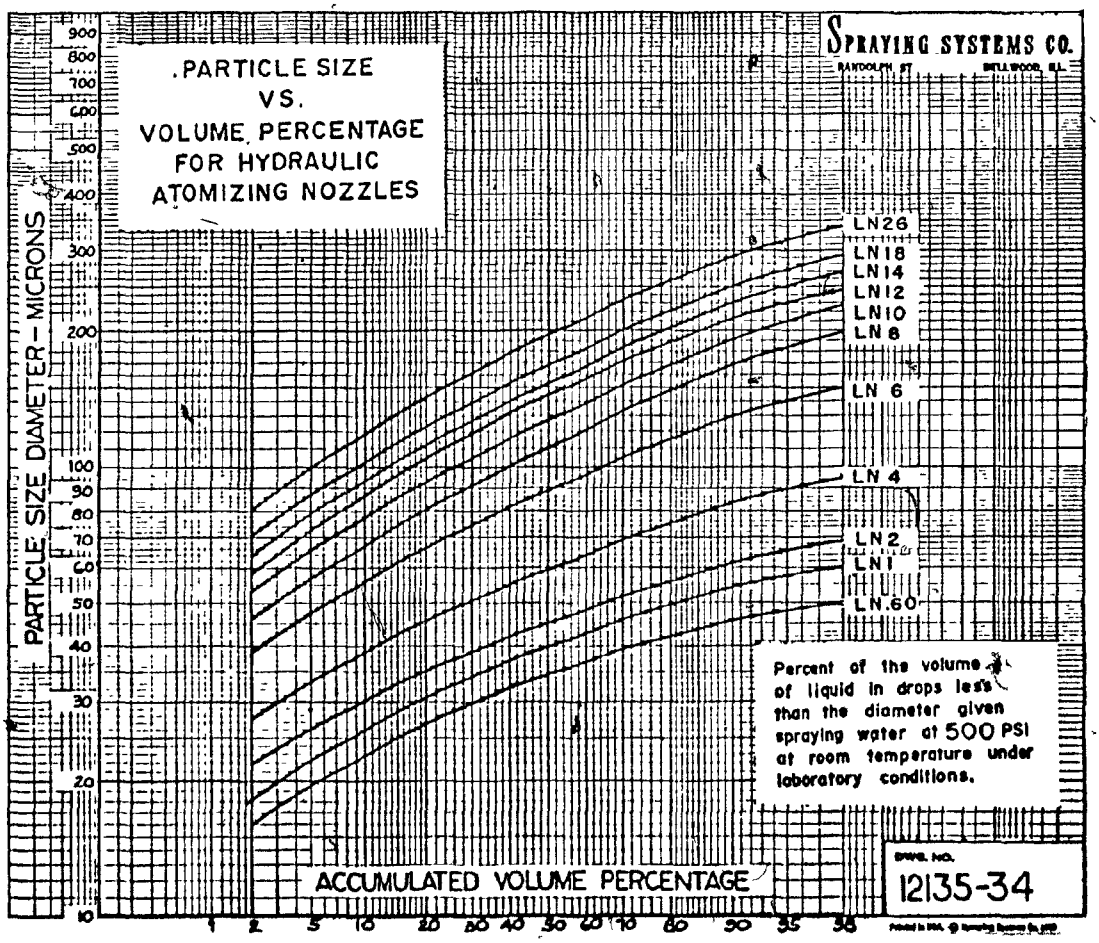
SPRAYING SYSTEMS CO.
RANDOLPH ST
BELLWOOD, ILL.
PARTICLE SIZE
VS.
VOLUME PERCENTAGE
FOR HYDRAULIC
ATOMIZING NOZZLES
PARTICLE SIZE DIAMETER - MICRONS
900
800
700
600
500
400
300
200
100
90
80
70
60
50
40
30
20
10
LN26
LN18
LN14
LN12
LN10
LN 8
LN 6
LN 4
LN 2
LN 1
LN.60
Percent of the volume of liquid in drops less than the diameter given spraying water at 500 PSI at room temperature under laboratory conditions.
ACCUMULATED VOLUME PERCENTAGE
1
2
5
10
20
30
40
50
60
70
80
90
95
98
DWG. NO.
12135-34

FIG. 6

SPRAY PARTICLE SIZE VS PRESSURE

HYDRAULIC ATOMIZING NOZZLES
CAPACITIES FROM .60 THROUGH 26
BASED ON SPRAYING WATER AT 70°F

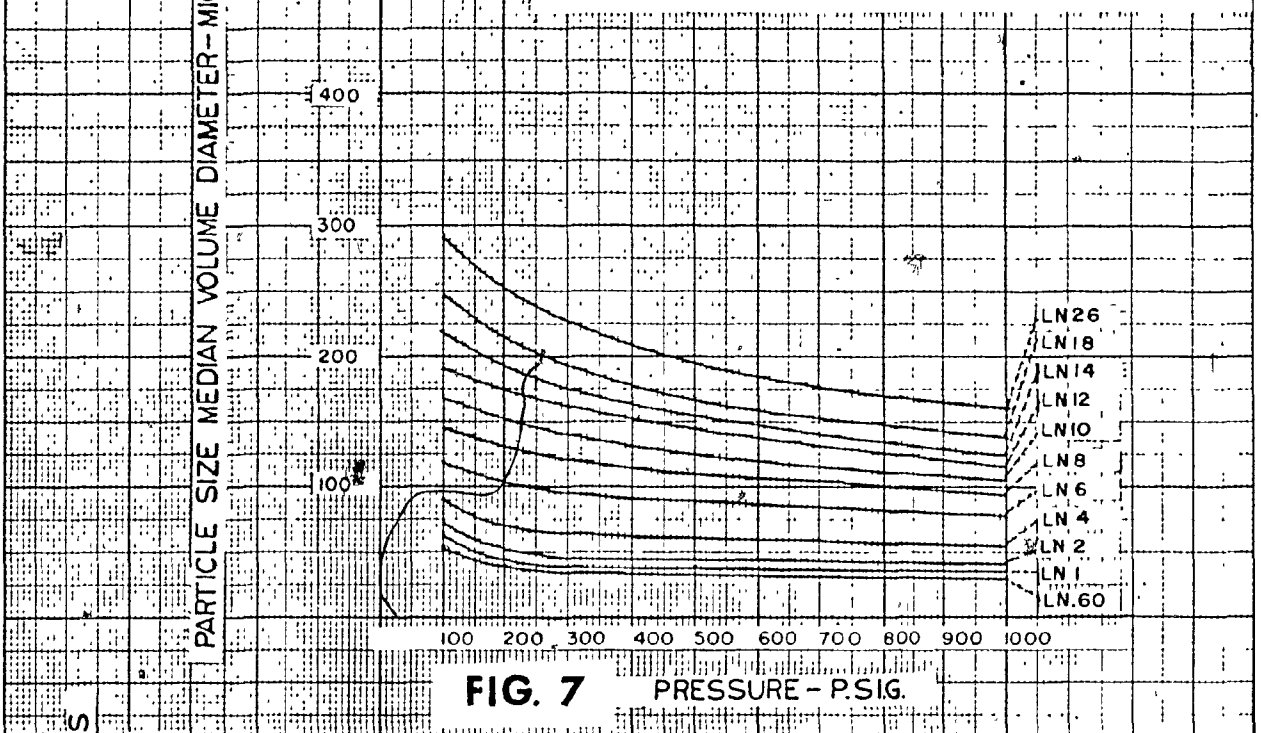

FIG. 7

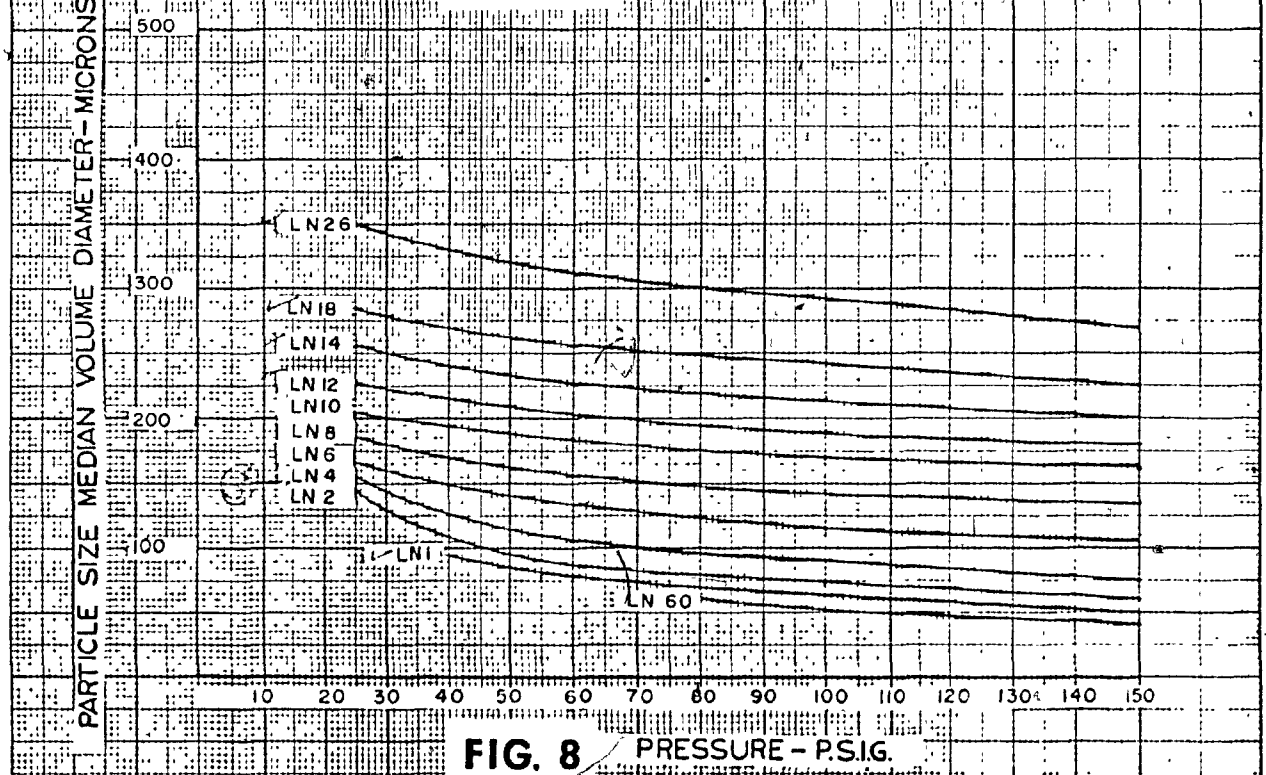

FIG. 8

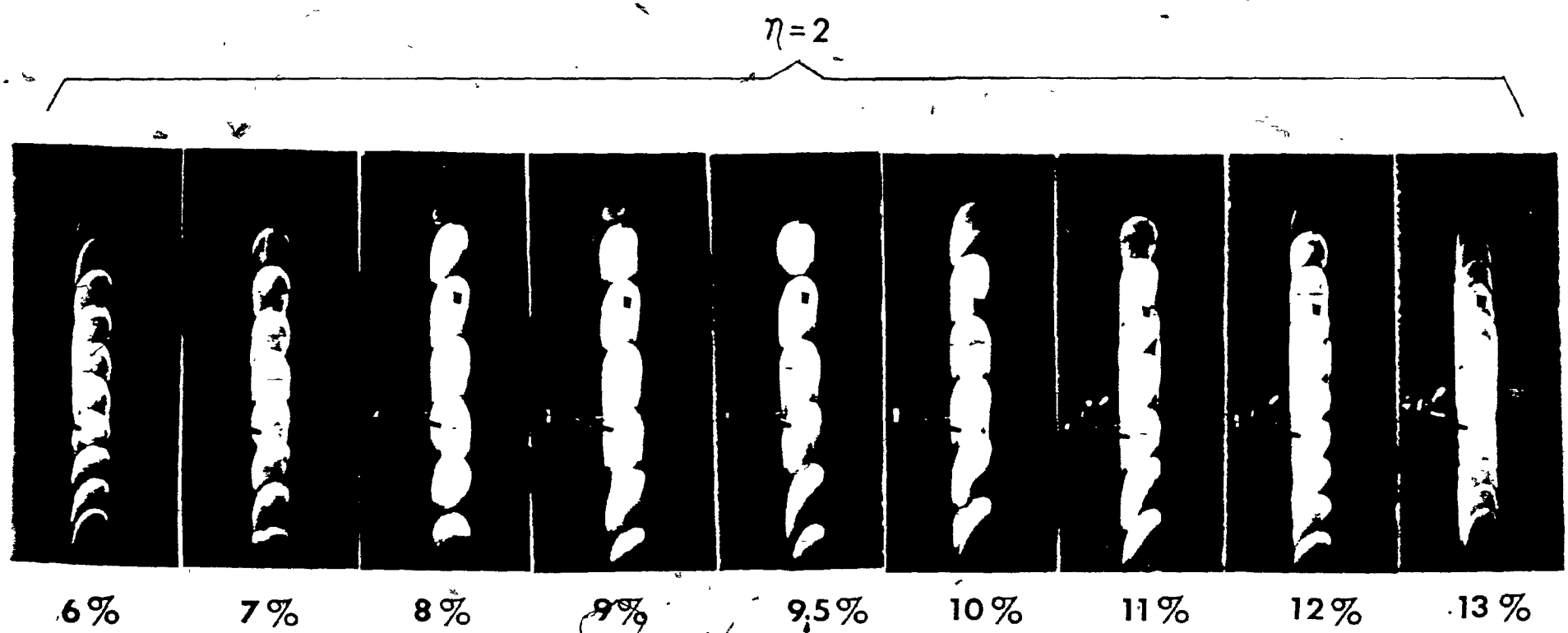

FIG. 9 FLAMES IN METHANE-AIR MIXTURES WITHOUT WATER SPRAY

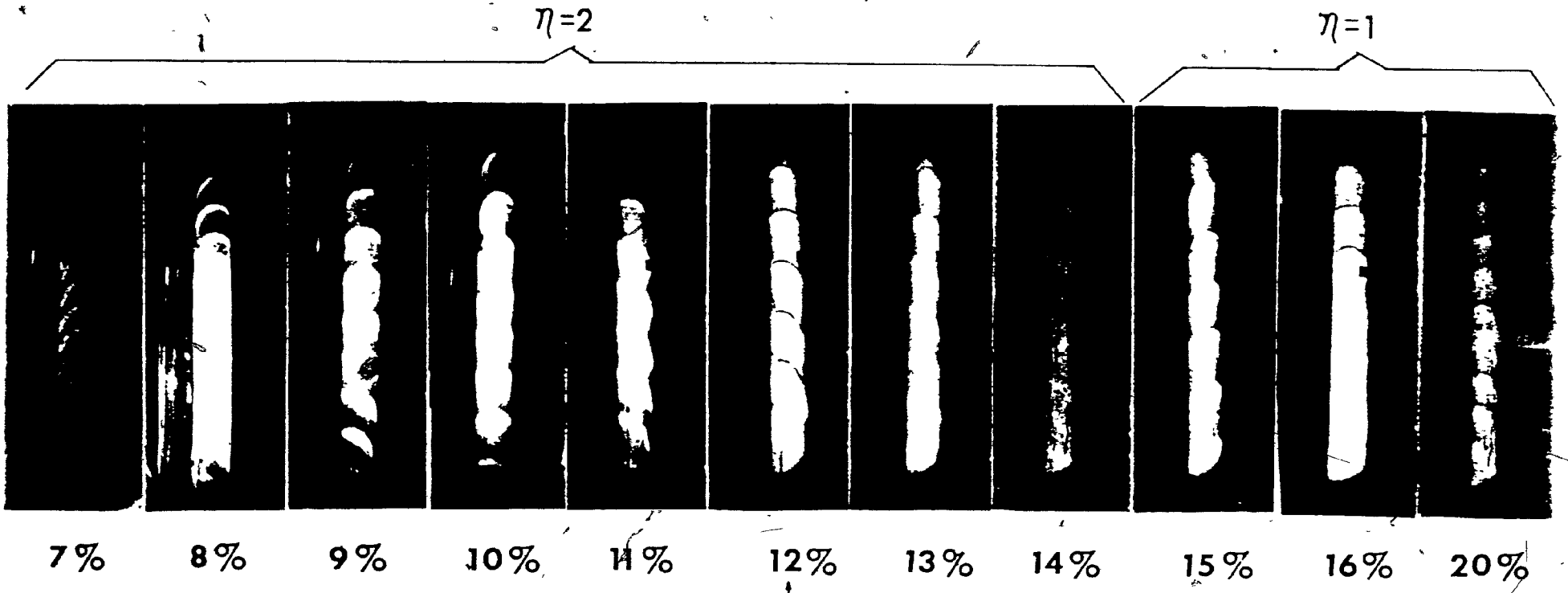

FIG.10 FLAMES IN H_2S-AIR MIXTURES WITHOUT WATER SPRAY

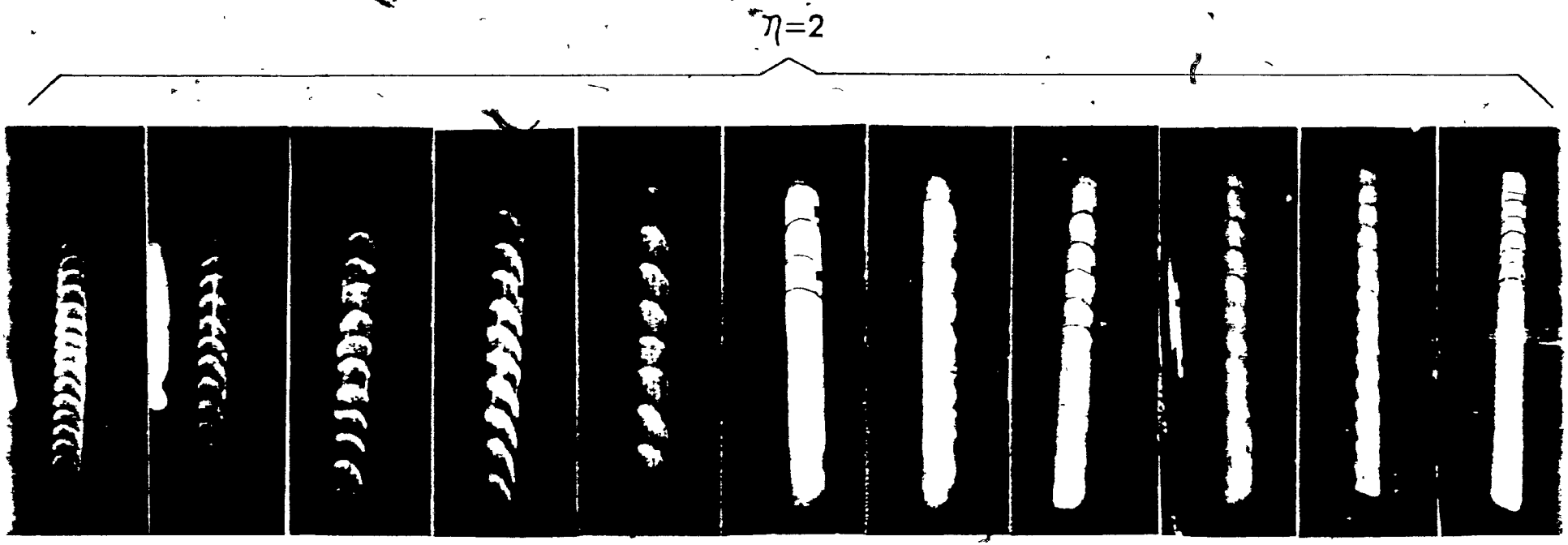

FIG.11 FLAMES IN H_2S AIR MIXTURES WITH WATER SPRAY

$\rho_{s0}=1.09\ mg\cdot cm^{-3}$; $\bar{D}_0=52.5\ \mu m$

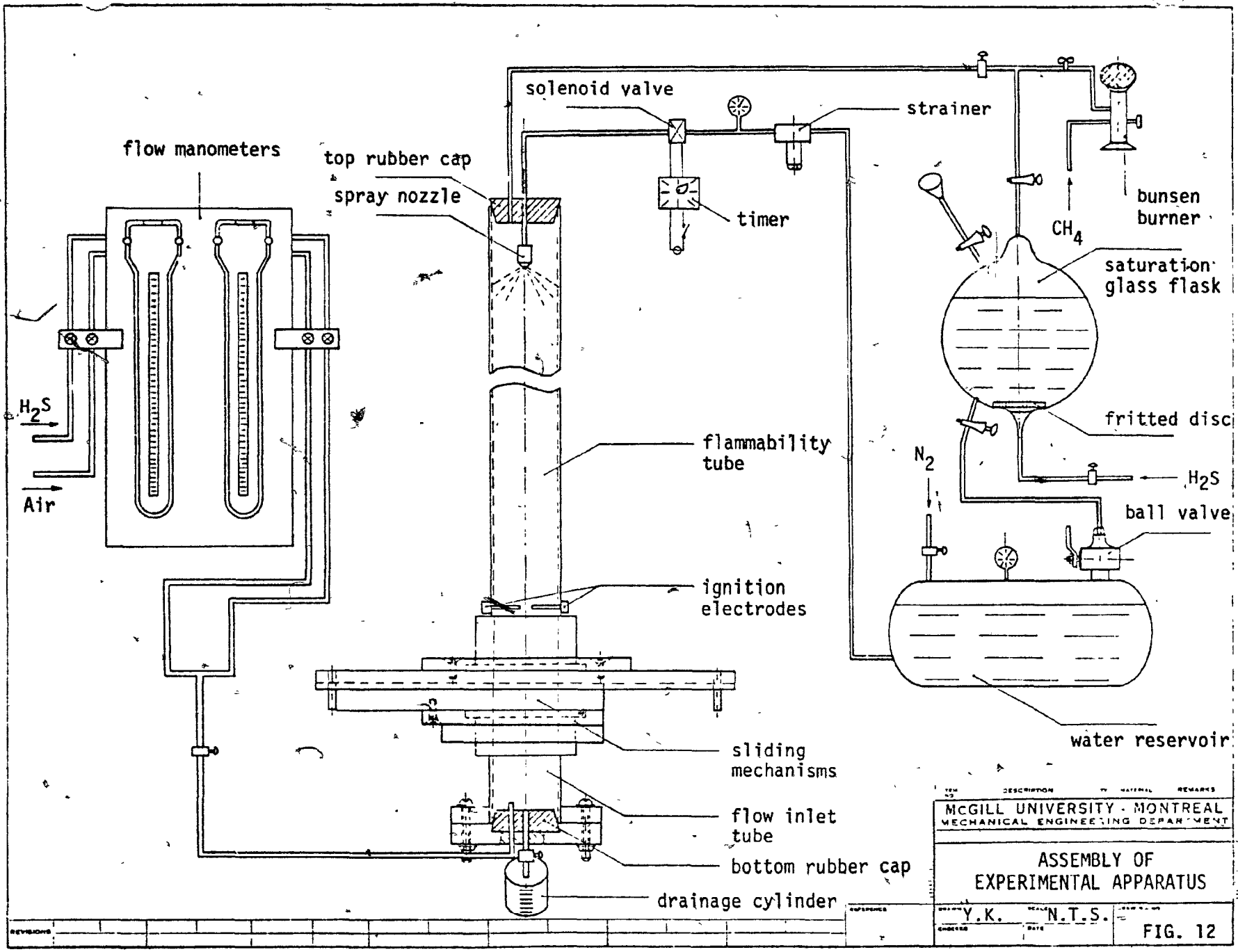
solenoid valve
strainer
flow manometers
top rubber cap
spray nozzle
timer
bunsen burner
CH_4
saturation glass flask
H_2S
Air
flammability tube
fritted disc
N_2
H_2S
ball valve
ignition electrodes
water reservoir
sliding mechanisms
flow inlet tube
bottom rubber cap
drainage cylinder
McGILL UNIVERSITY - MONTREAL
MECHANICAL ENGINEERING DEPARTMENT
ASSEMBLY OF EXPERIMENTAL APPARATUS
Y.K.
N.T.S.
FIG. 12

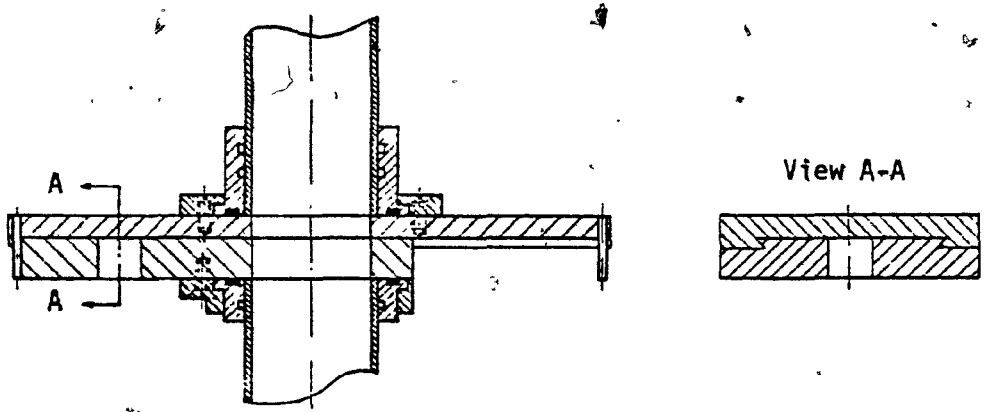

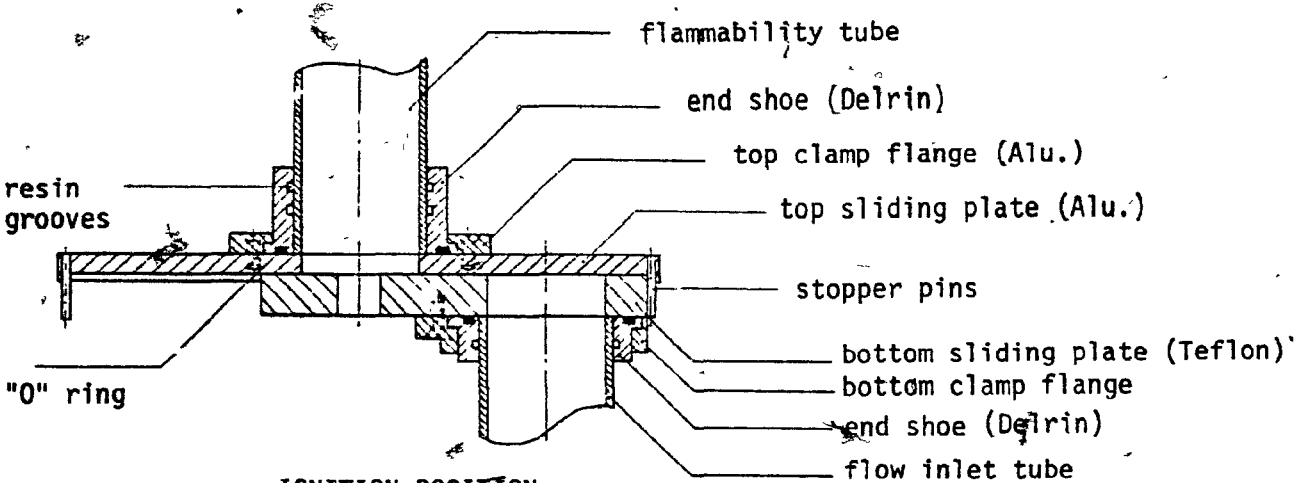

REVISIONS		REFERENCE	MCGILL UNIVERSITY - MONTREAL MECHANICAL ENGINEERING DEPARTMENT	
			DOVE TAIL SLIDING MECHANISM	
			DRAWN Y.K.	SCALE 1:2
			CHECKED	DATE
				DRAWING NO. FIG. 13

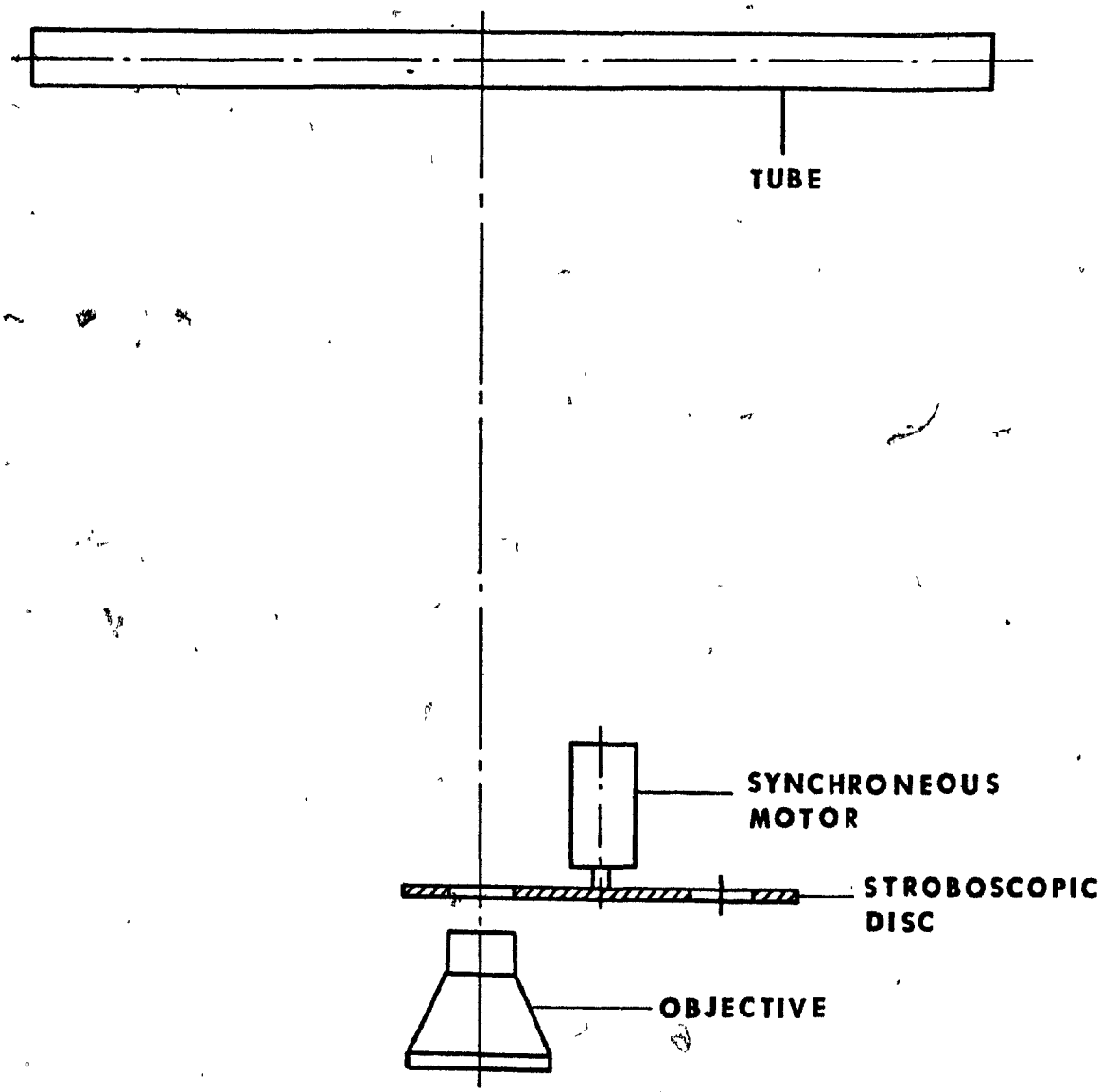

FIG. 14 SCHEMATIC OF THE PHOTOGRAPHIC TECHNIQUE

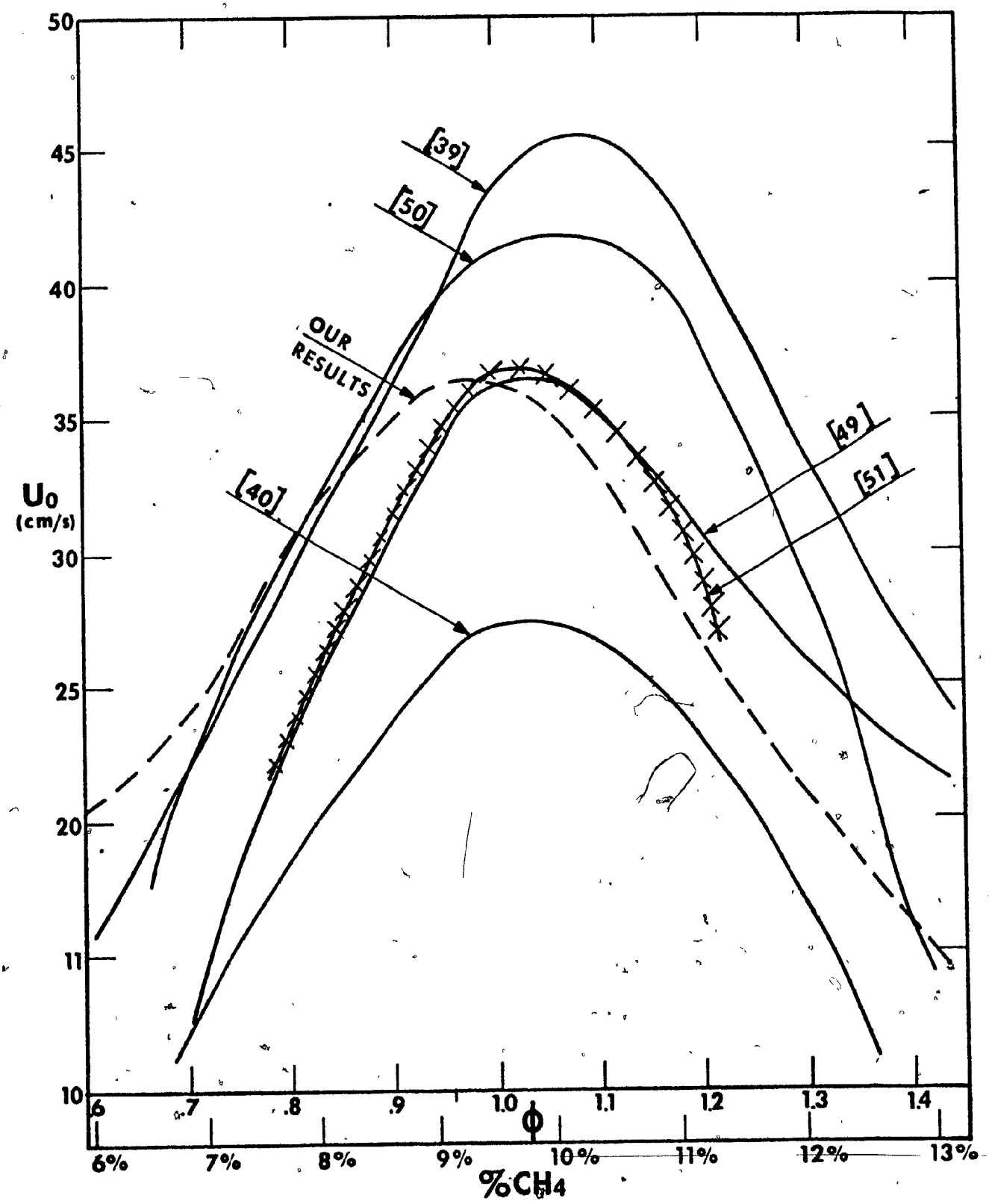

FIG. 15 BURNING VELOCITIES OF METHANE-AIR FLAMES—COMPARISON OF VARIOUS RESULTS.

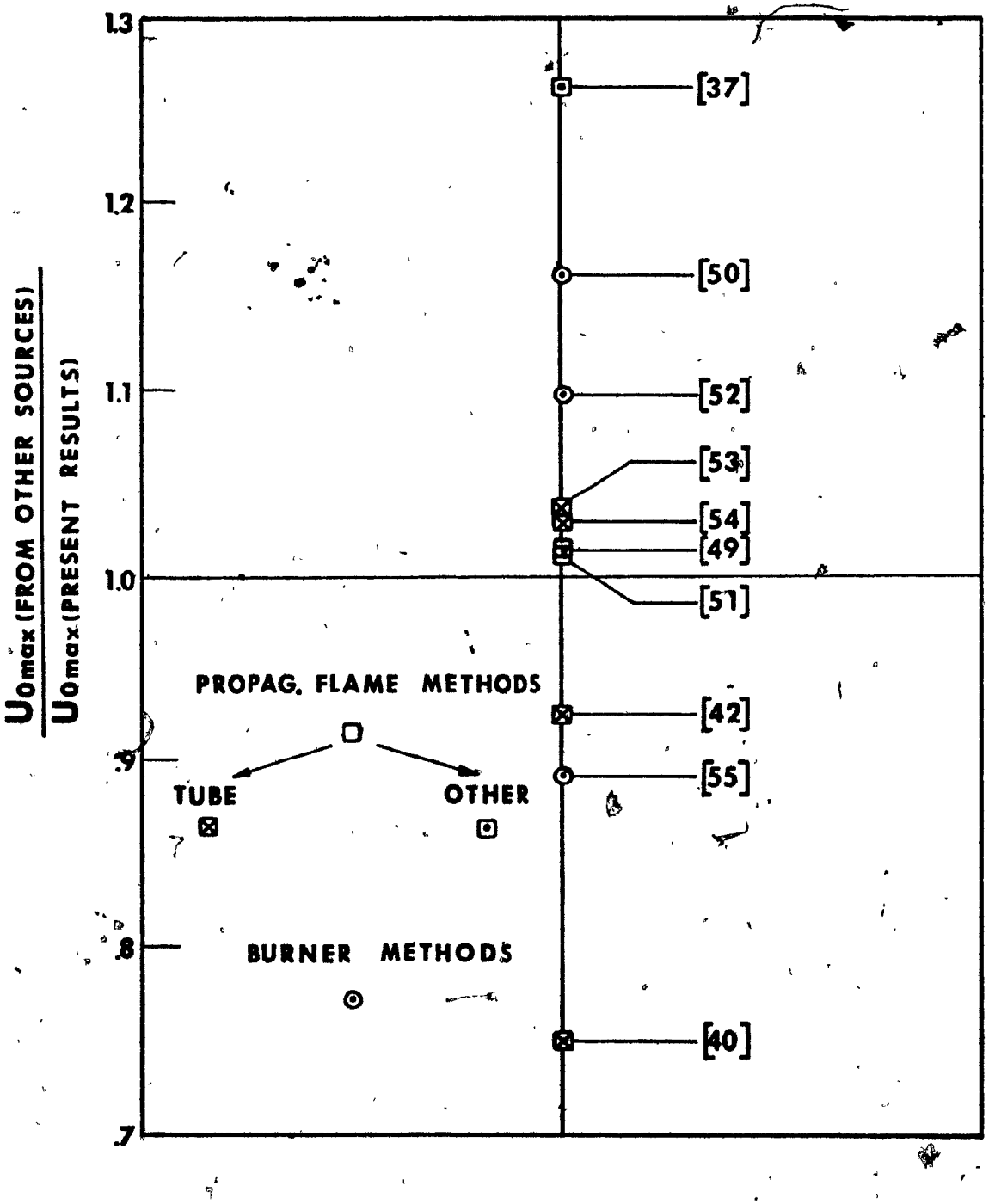

FIG. 16 SPREAD OF MEASURED MAX. BURNING VELOCITIES FOR METHANE-AIR MIXTURES

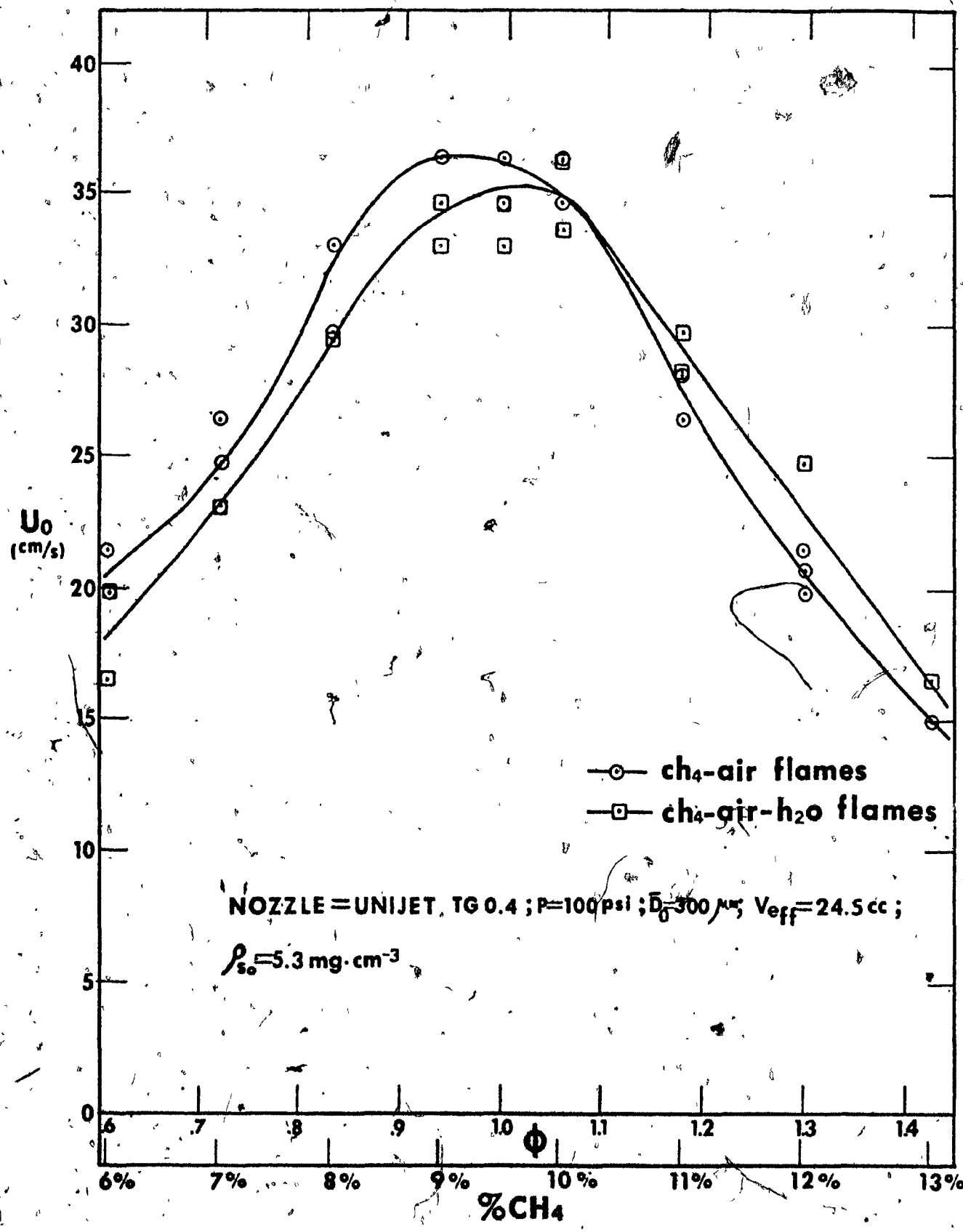

FIG. 17 BURNING VELOCITIES OF METHANE-AIR FLAMES WITH AND WITHOUT WATER SPRAYS

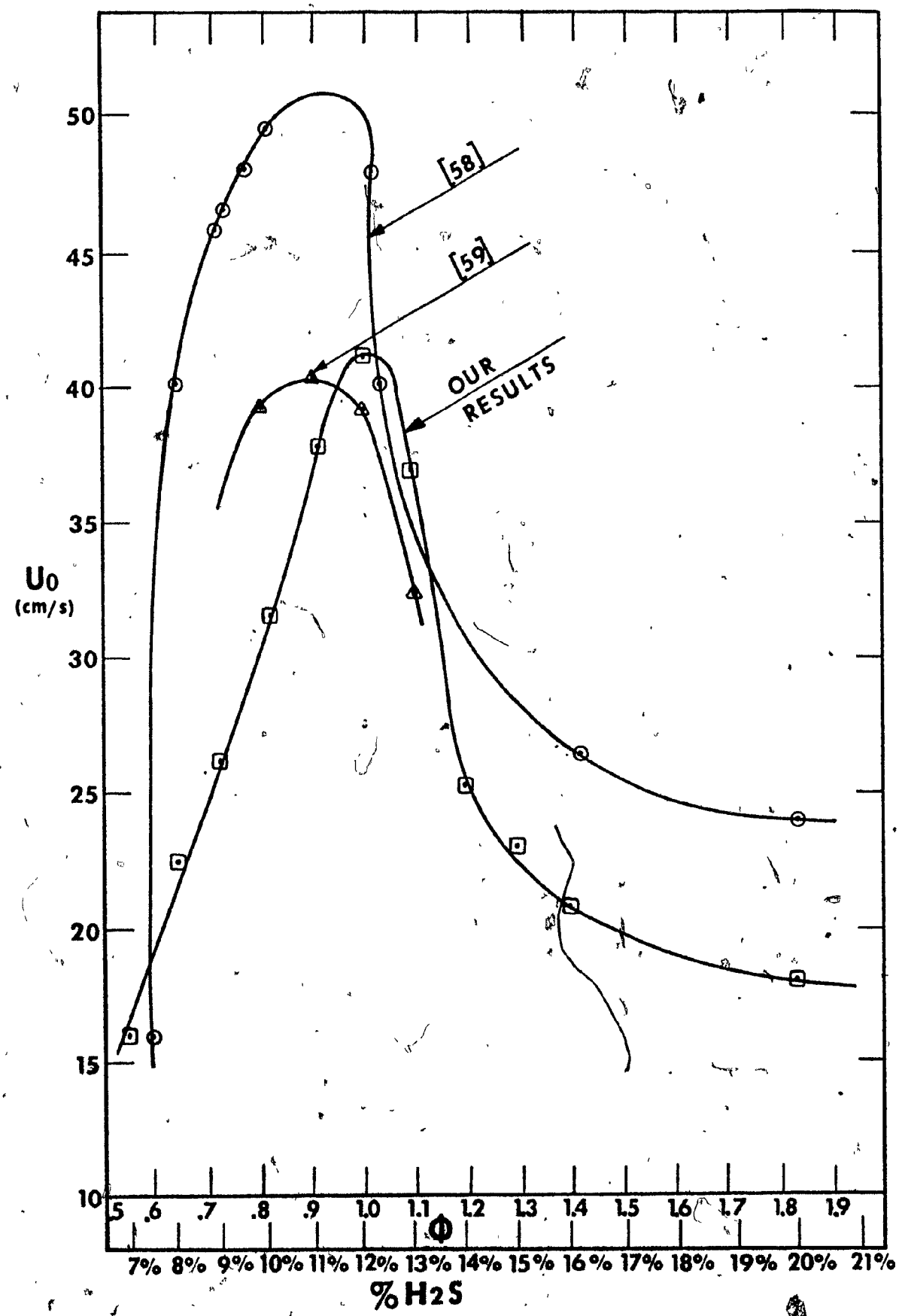

FIG. 18 BURNING VELOCITIES OF H_2S-AIR FLAMES—COMPARISON OF VARIOUS

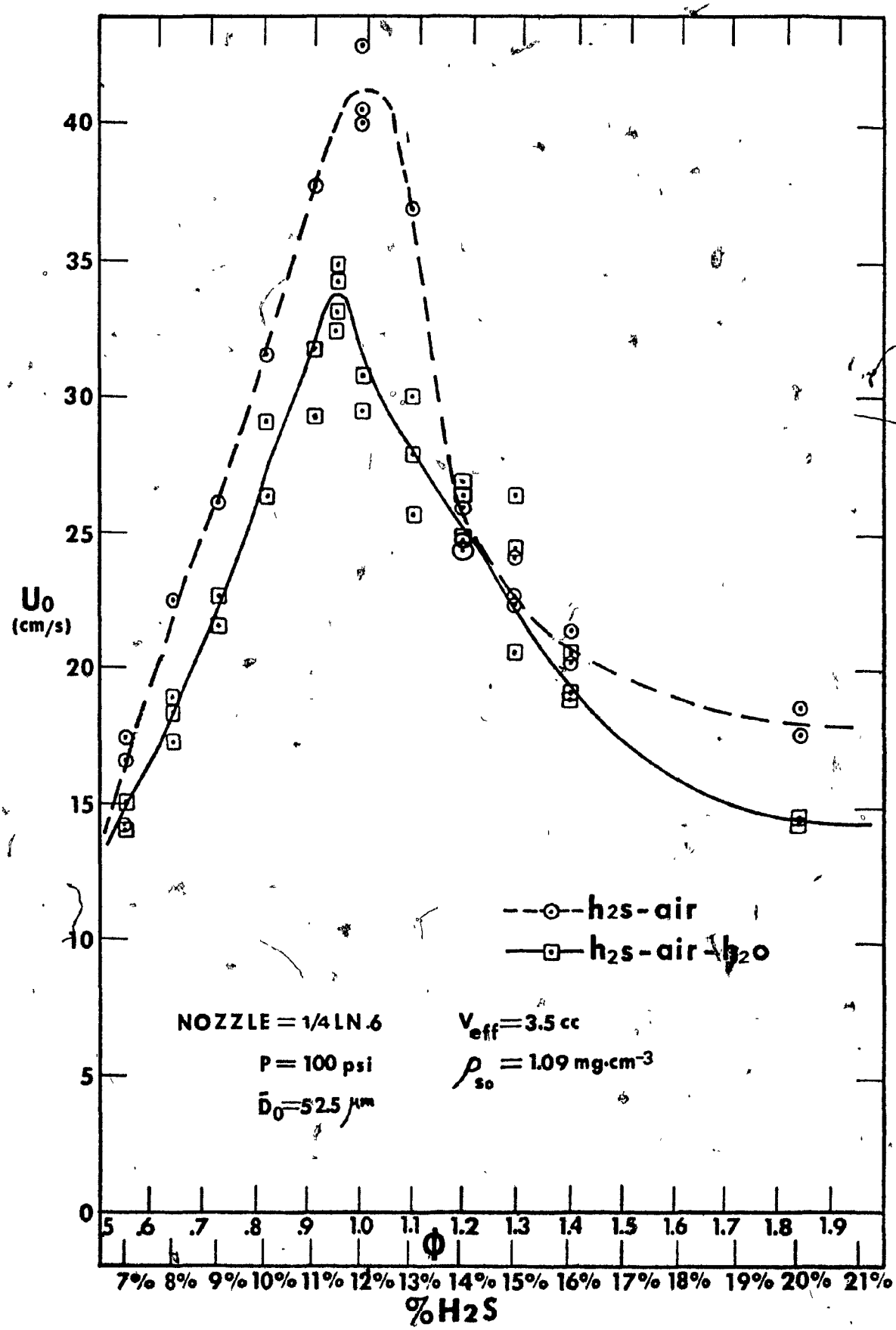

FIG. 19 BURNING VELOCITIES OF H_2S-AIR FLAMES WITH AND WITHOUT WATER SPRAYS.

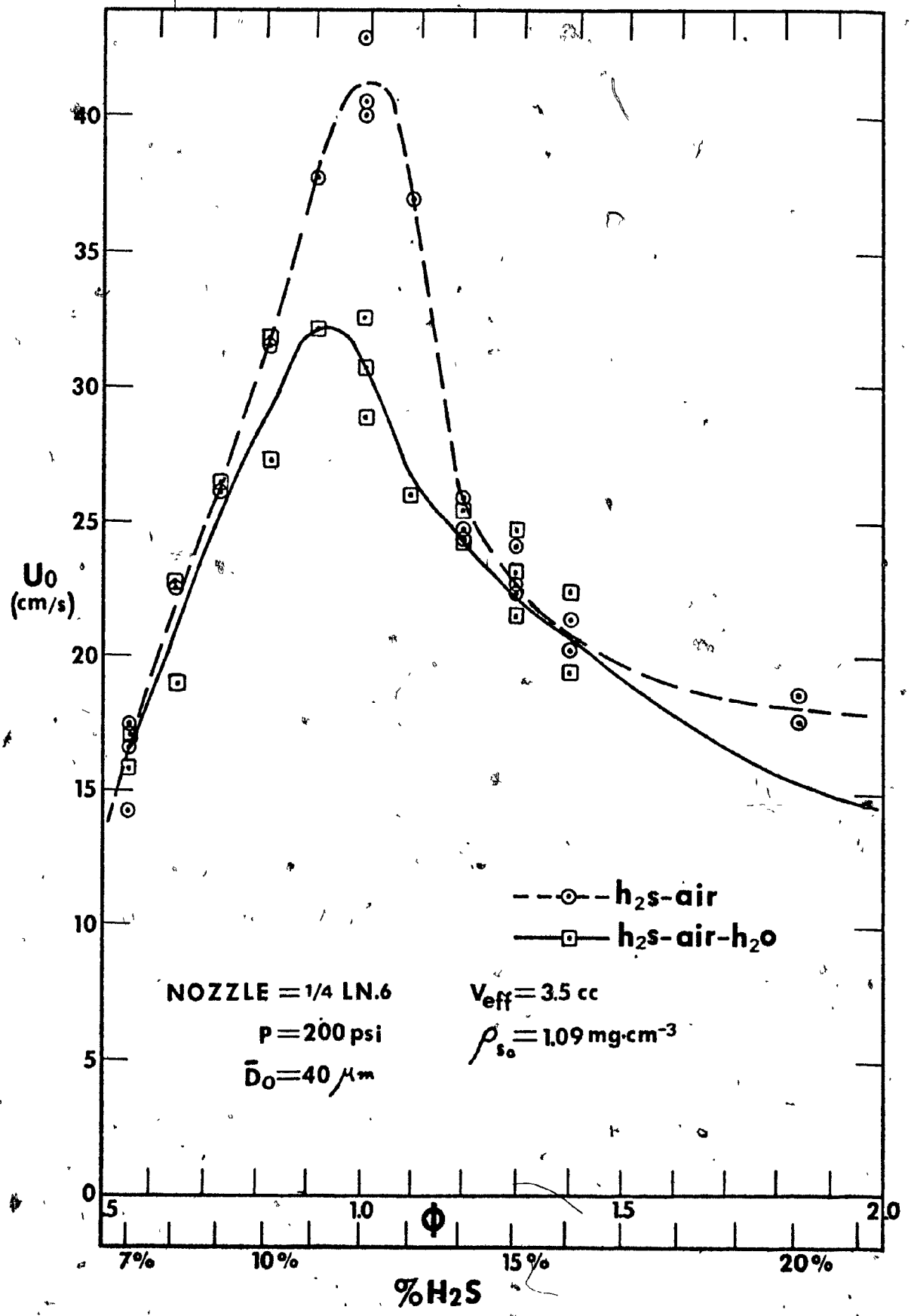

FIG. 20 BURNING VELOCITIES OF H_2S-AIR FLAMES WITH AND WITHOUT WATER SPRAYS.

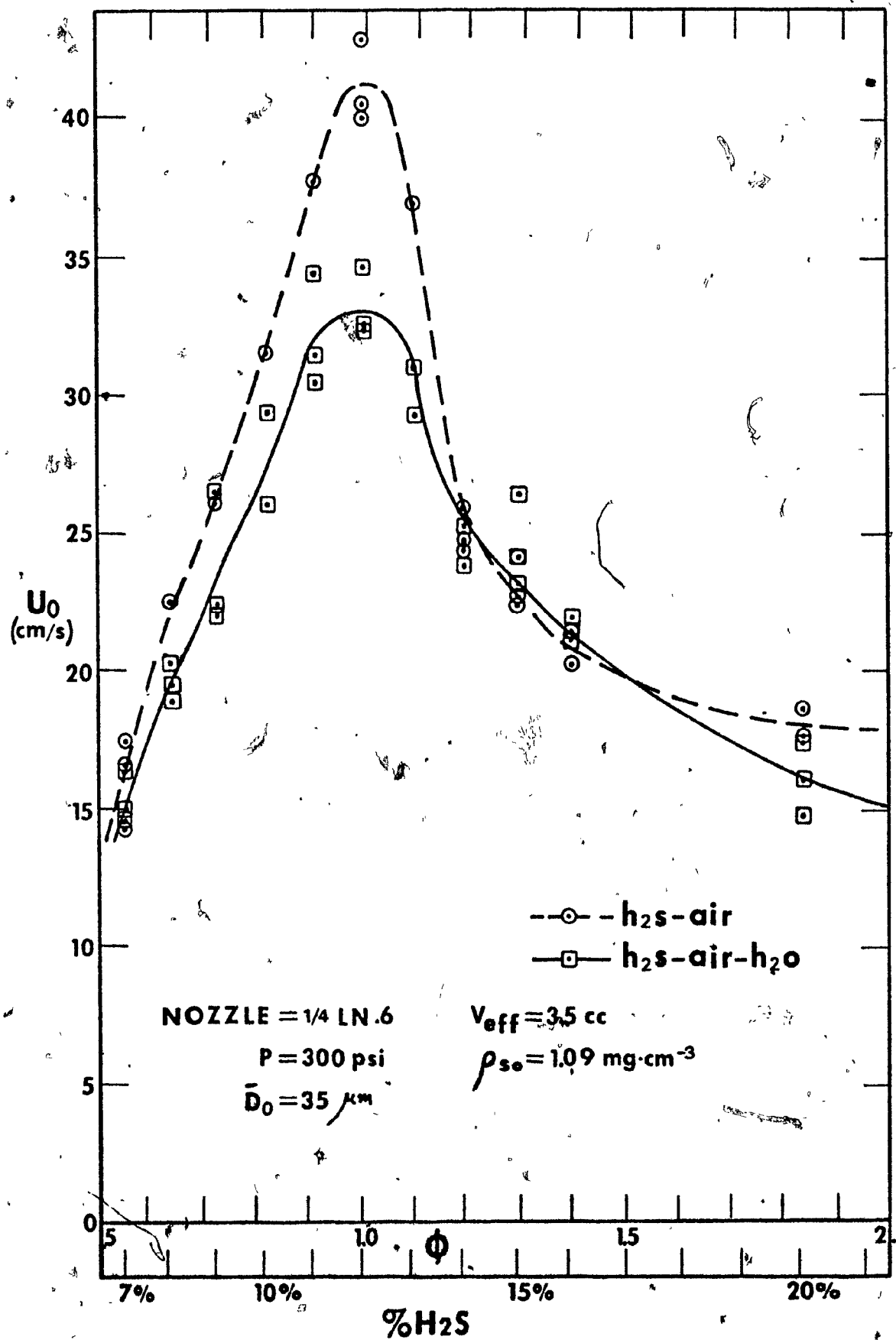

FIG. 21 BURNING VELOCITIES OF H_2S-AIR FLAMES WITH AND WITHOUT WATER SPRAYS.

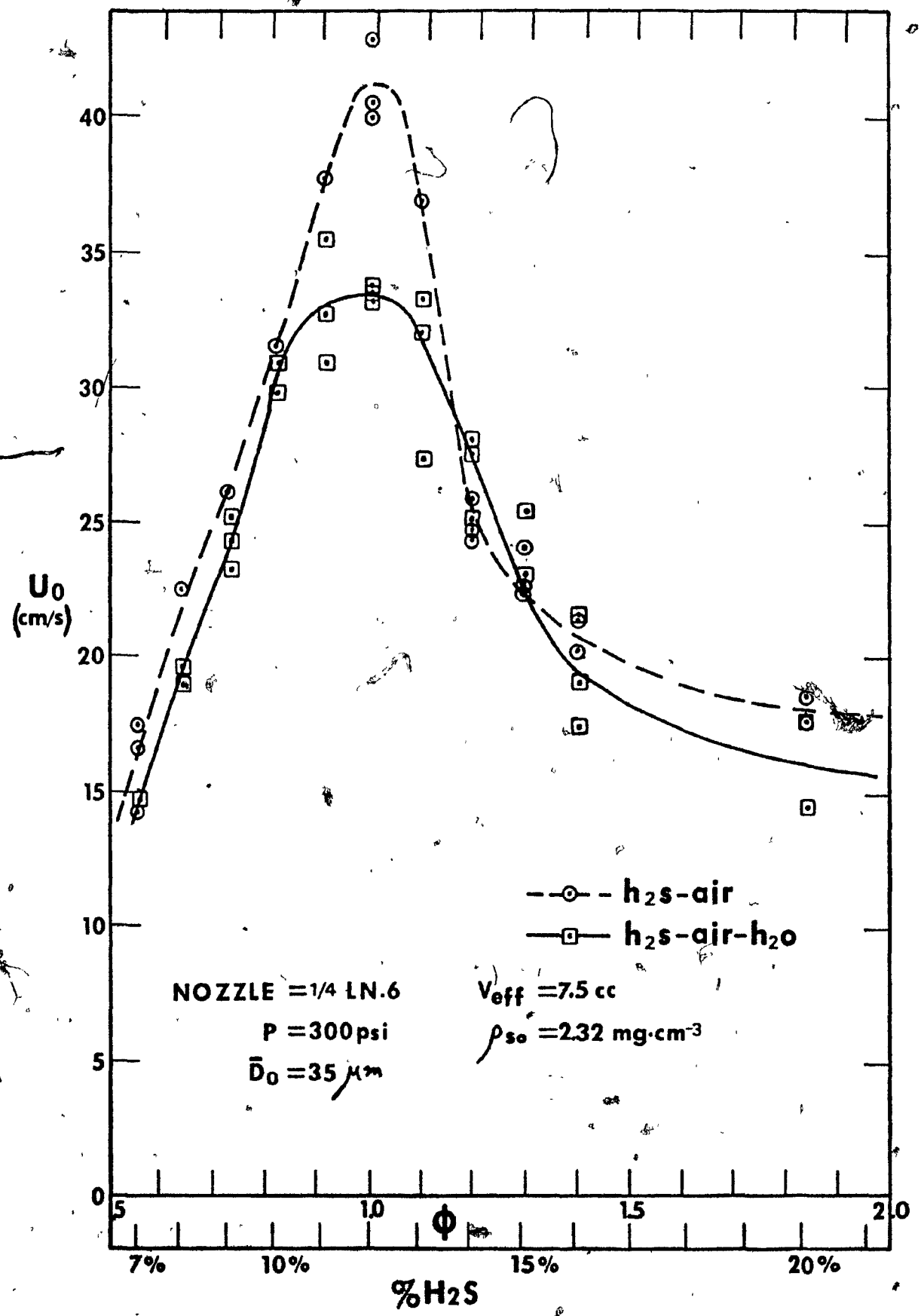

FIG. 22 BURNING VELOCITIES OF H_2S-AIR FLAMES WITH AND WITHOUT WATER SPRAYS.

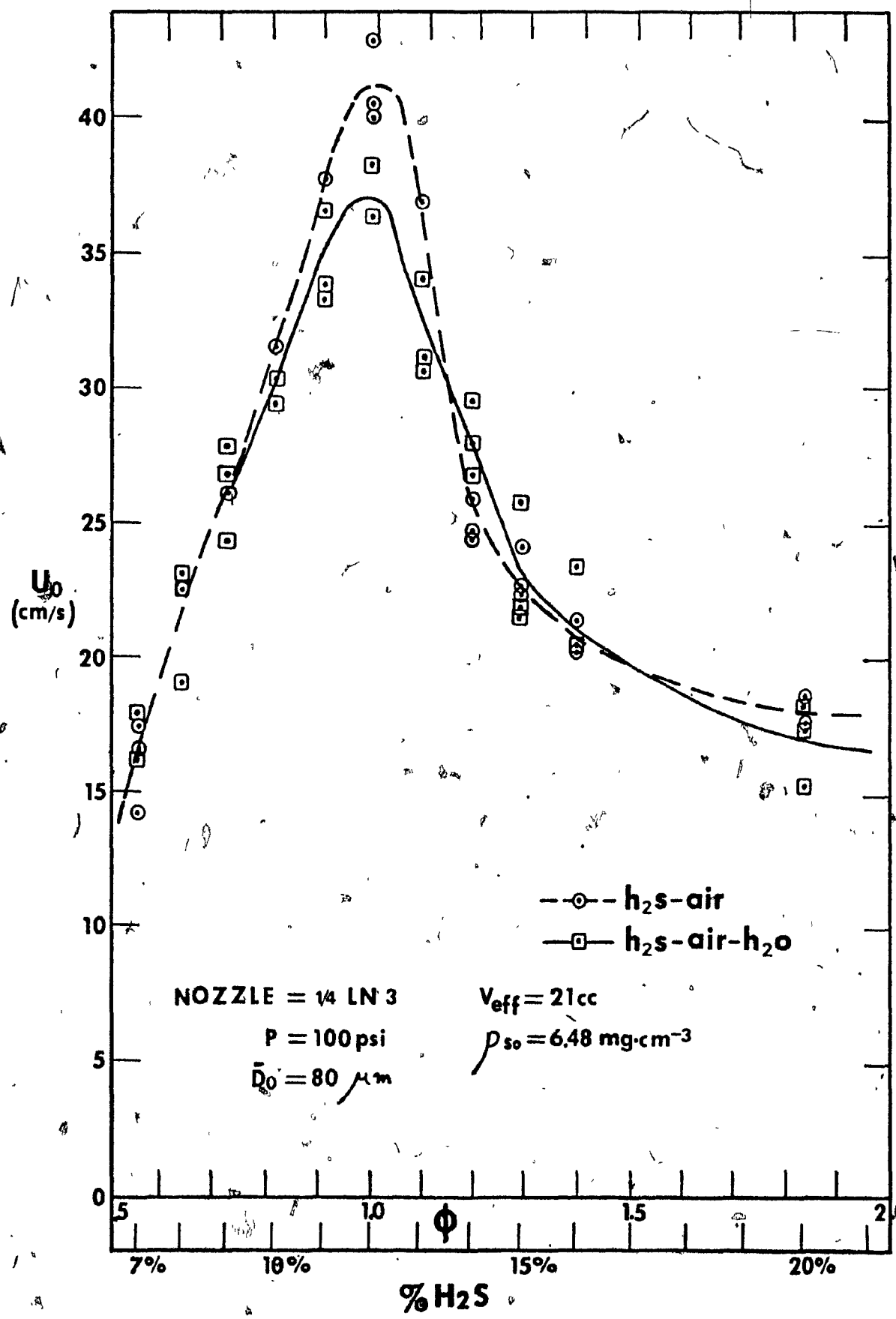

FIG. 23 BURNING VELOCITIES OF H_2S-AIR FLAMES WITH AND WITHOUT WATER SPRAYS.

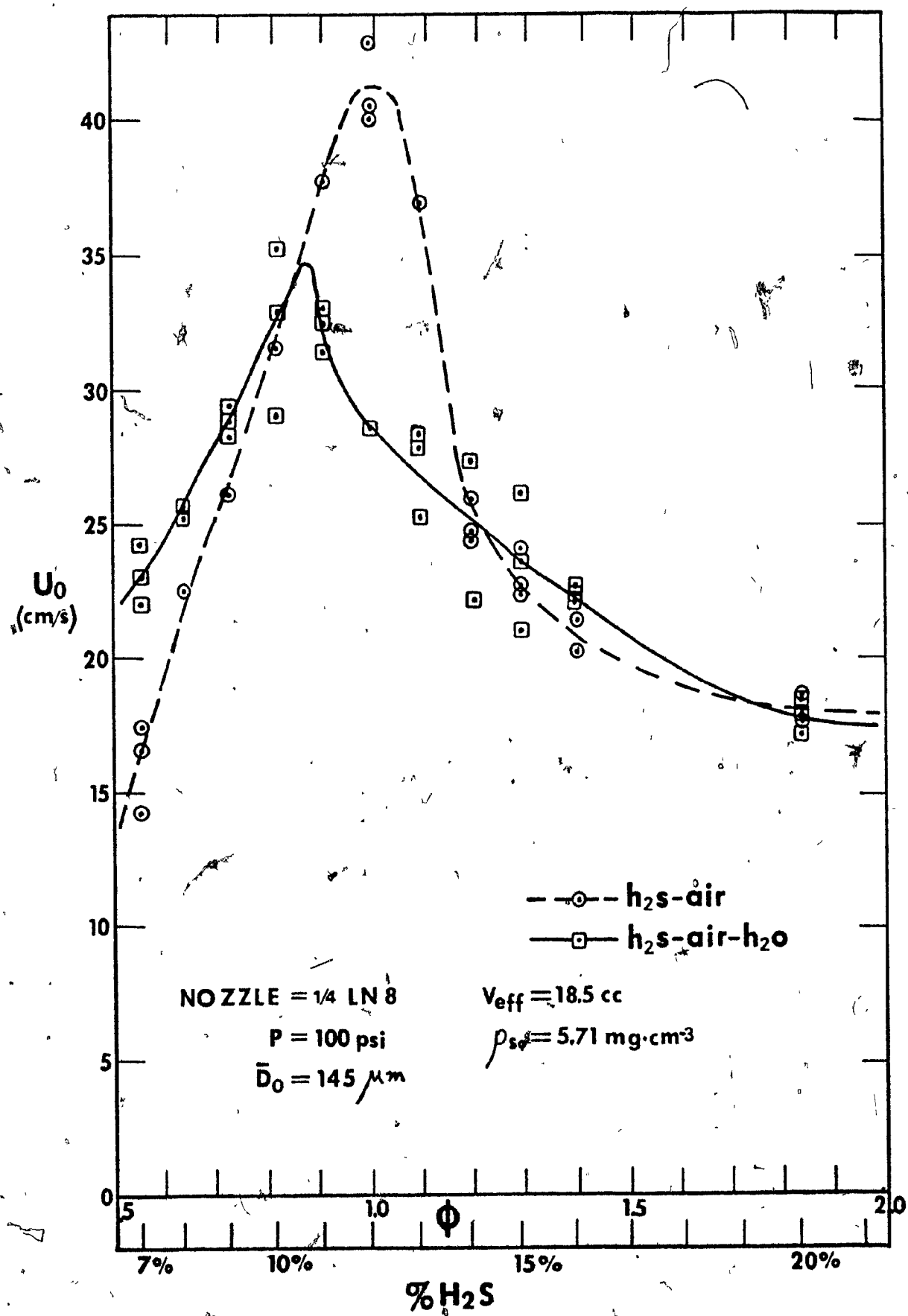

FIG. 24 BURNING VELOCITIES OF H_2S AIR FLAMES WITH AND WITHOUT WATER SPRAYS.

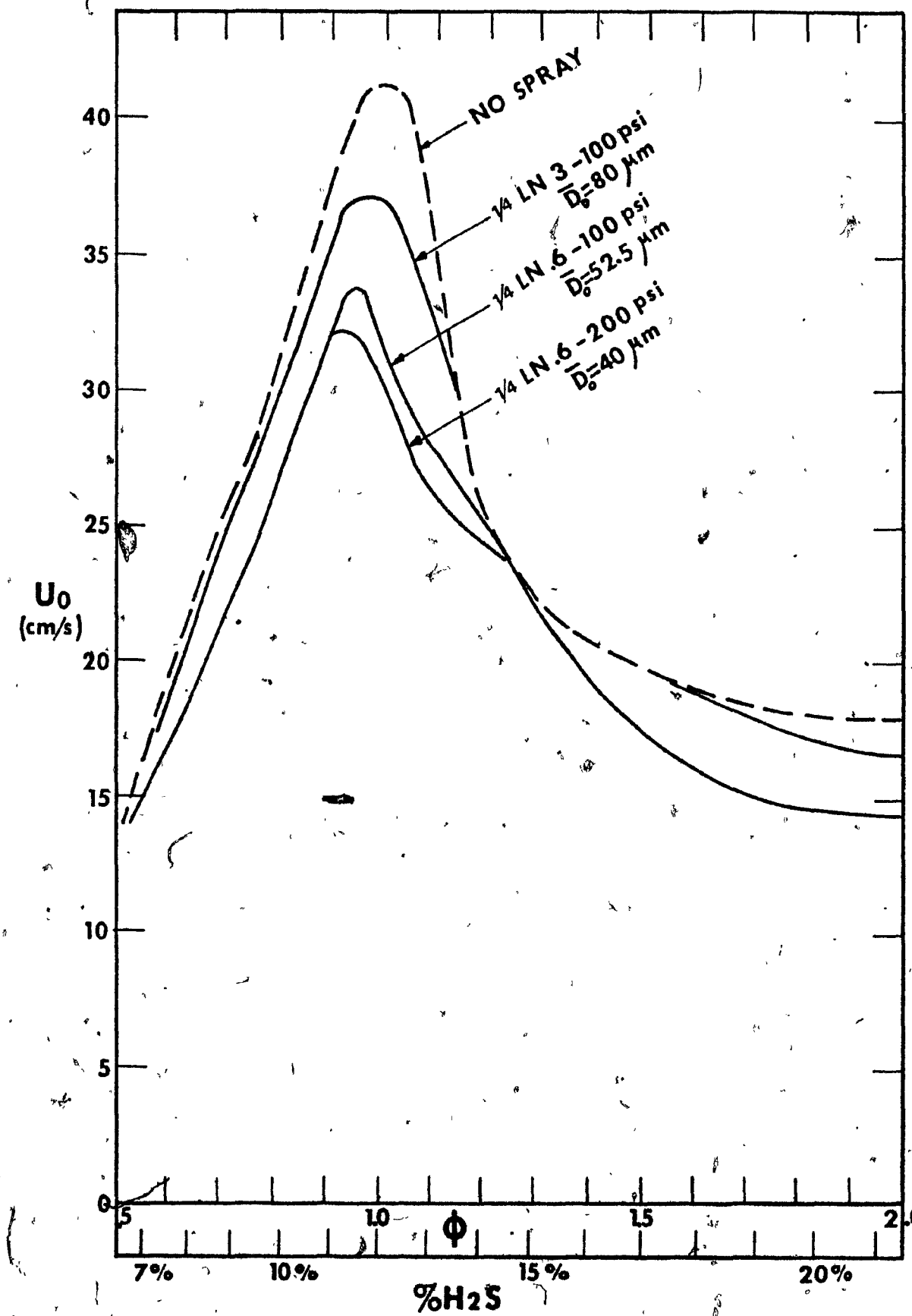

FIG. 25 COMPARISON OF PRESENT RESULTS FOR H_2S-AIR-H_2O BURNING VELOCITIES.

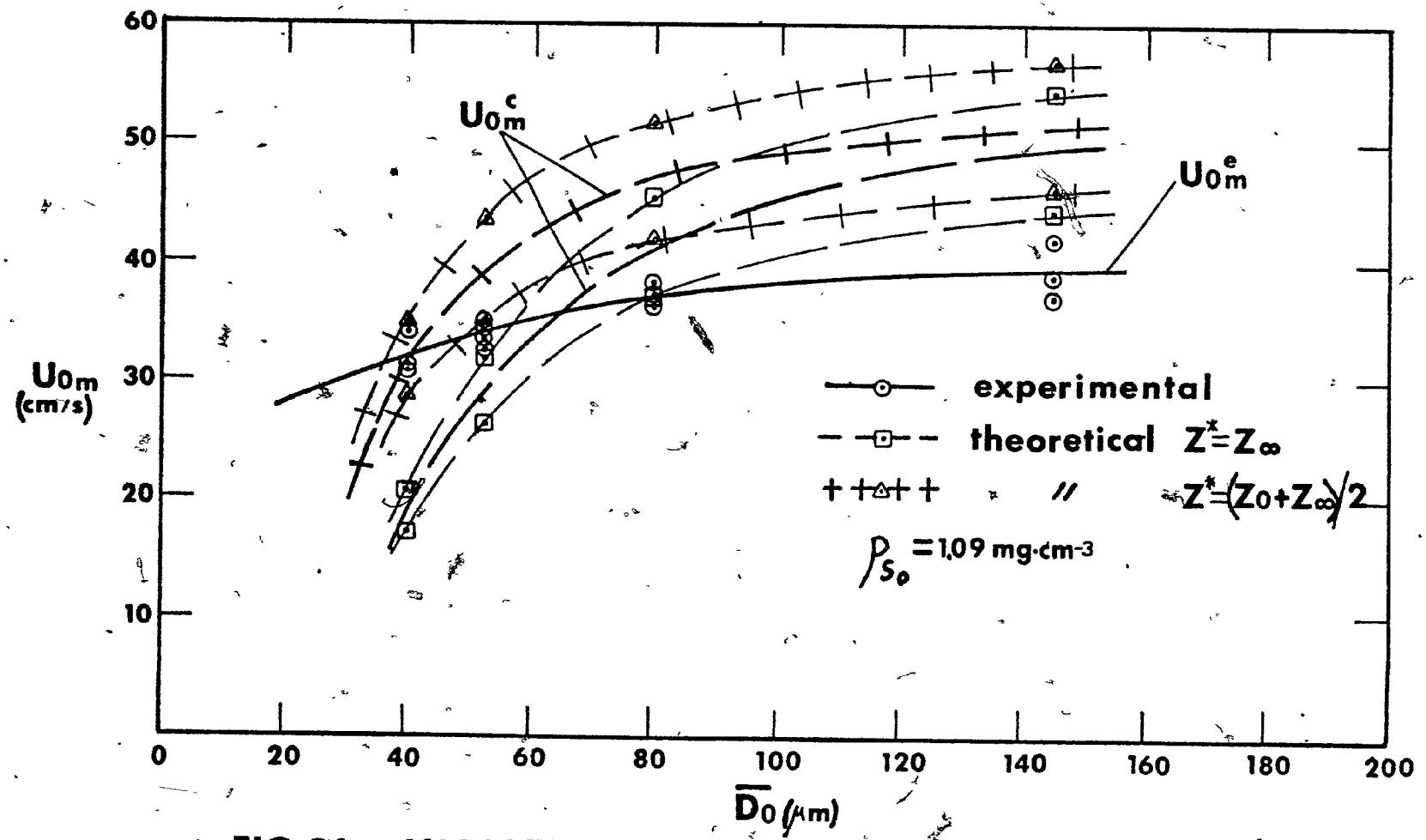

FIG. 26 VARIATION OF PEAK BURNING VELOCITY, (U_{0m}), IN H_2S-AIR-H_2O MIXTURES WITH WATER SPRAY DROPLET SIZE, $(\overline{D_0})$.

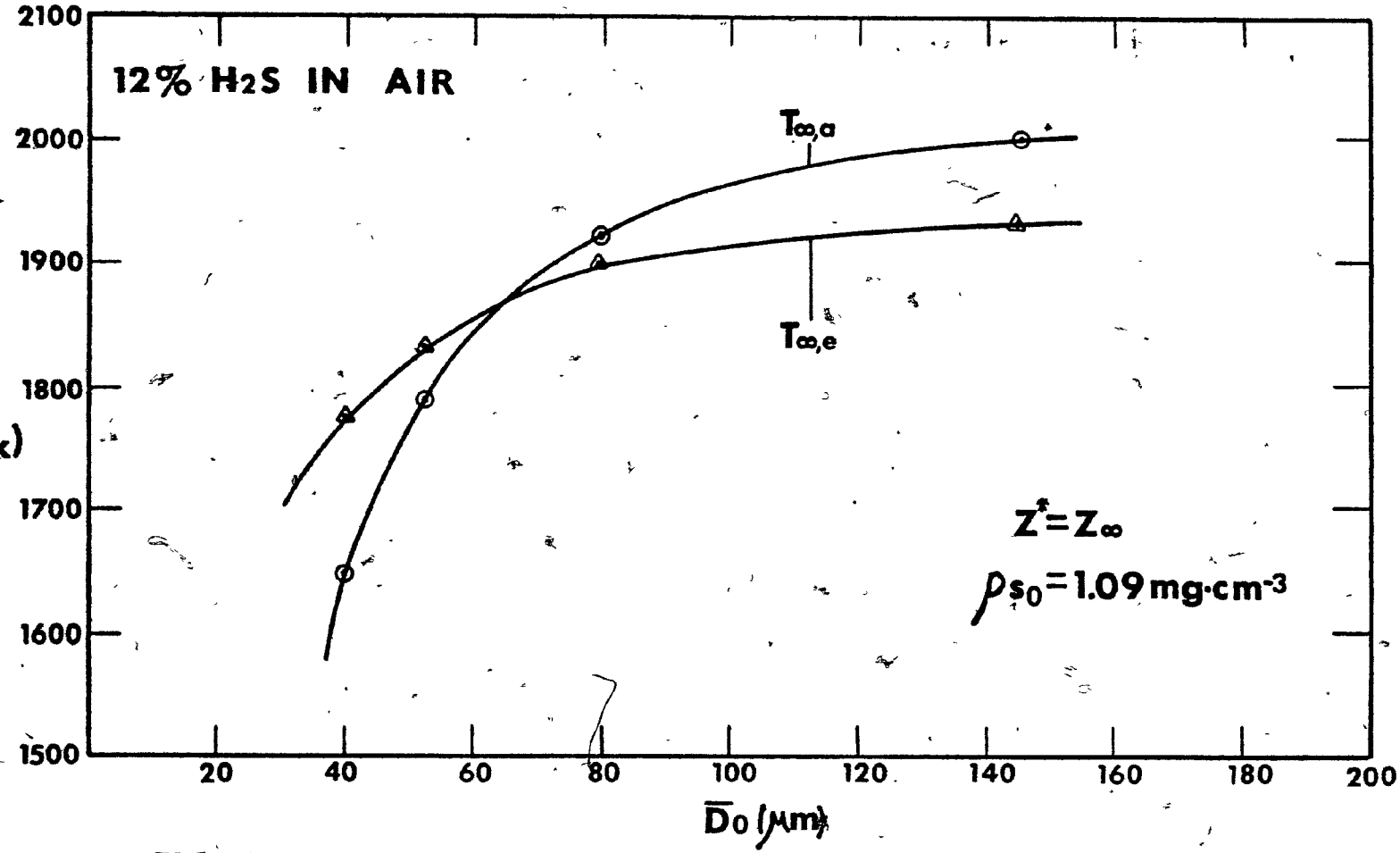

FIG. 27 VARIATION OF ADIABATIC FLAME TEMPERATURE, (T_∞), WITH WATER SPRAY DROPLET SIZE, $(\bar{D}_0)$.

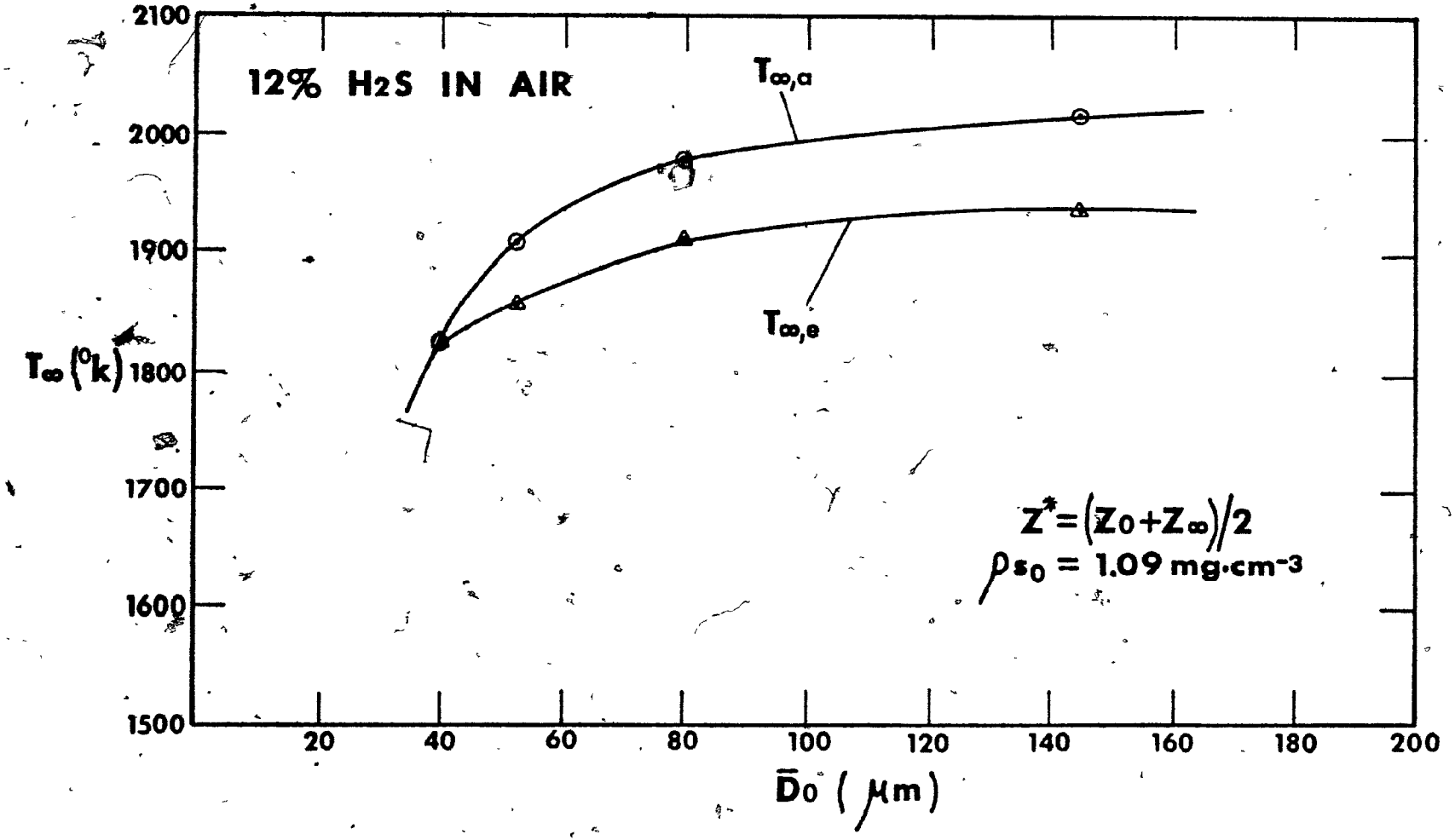

FIG. 28 VARIATION OF ADIABATIC FLAME TEMPERATURE, (T_∞), WITH WATER SPRAY DROPLET SIZE, ($\bar{D}_0$).

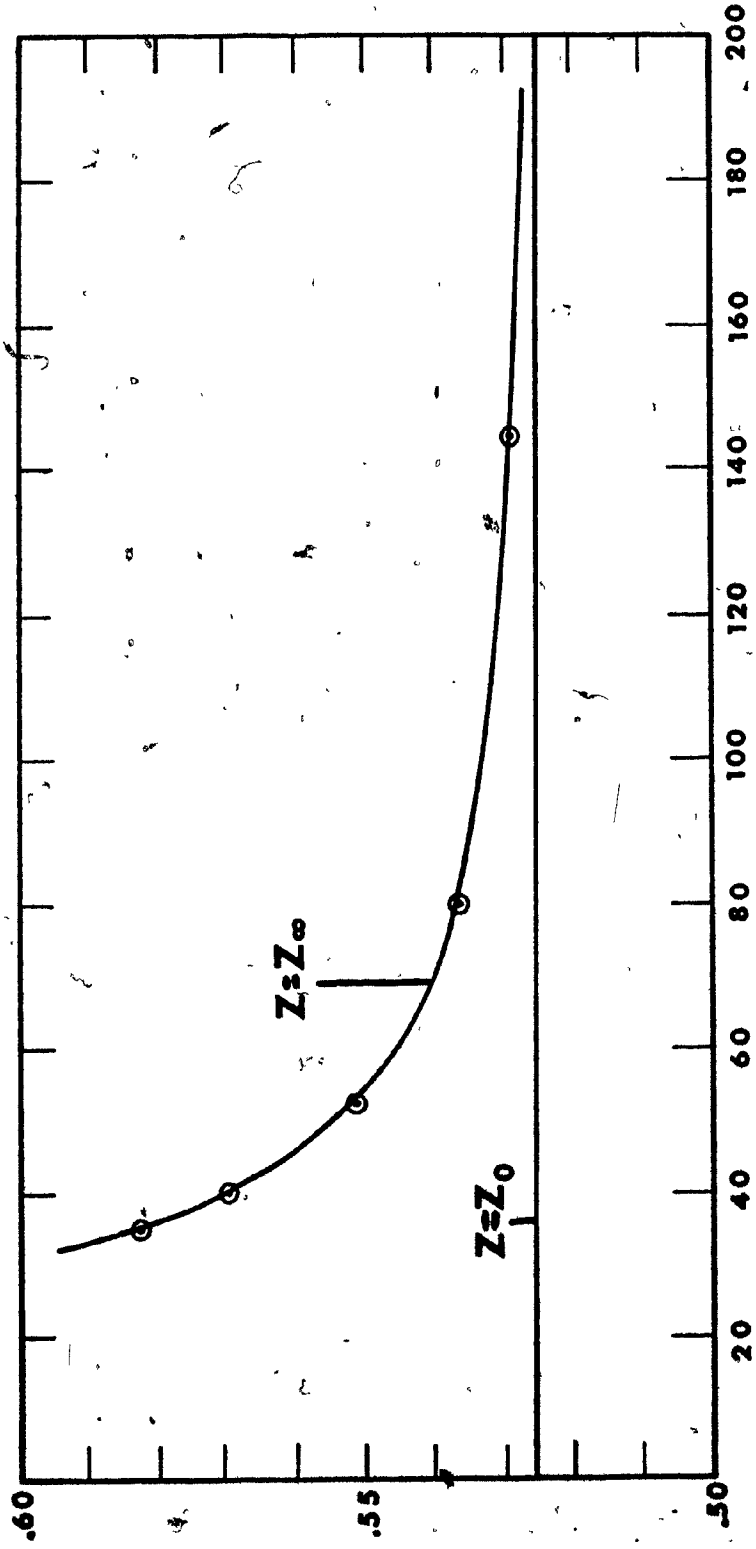

FIG. 29 VARIATION OF INITIAL AND FINAL GAS MASS FRACTIONS, (Z_0 and Z_∞) WITH WATER DROPLET SIZE, ($\bar{D}_0$).

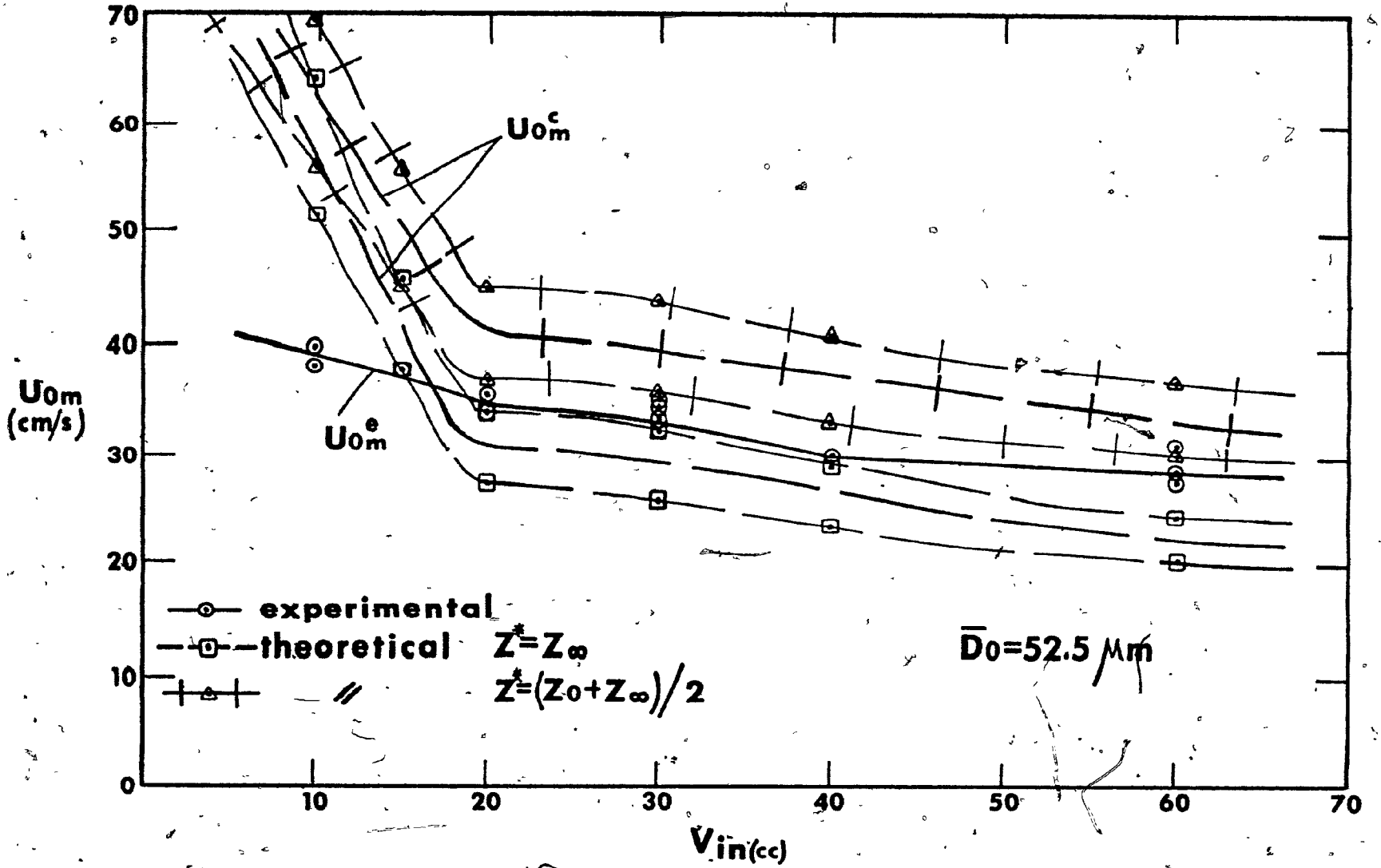

FIG. 30 VARIATION OF PEAK BURNING VELOCITY (U_{0m}) IN H_2S-AIR-H_2O MIXTURES WITH WATER SPRAY INPUT VOLUME (V_{in}).

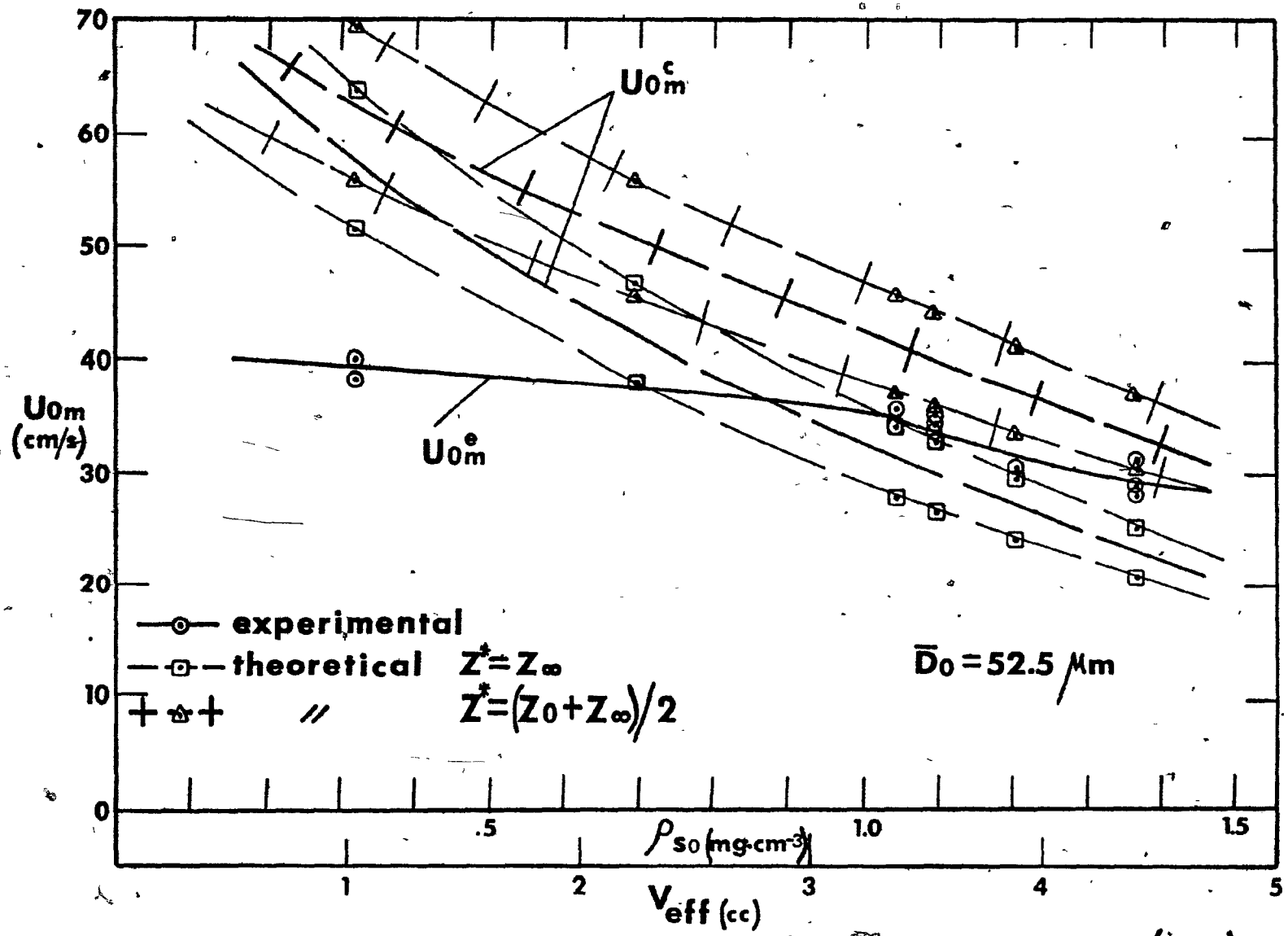

FIG. 31 VARIATION OF PEAK BURNING VELOCITY (U_{0m}) IN H_2S-AIR-H_2O MIXTURES WITH WATER SPRAY DENSITY (ρ_{s0}).

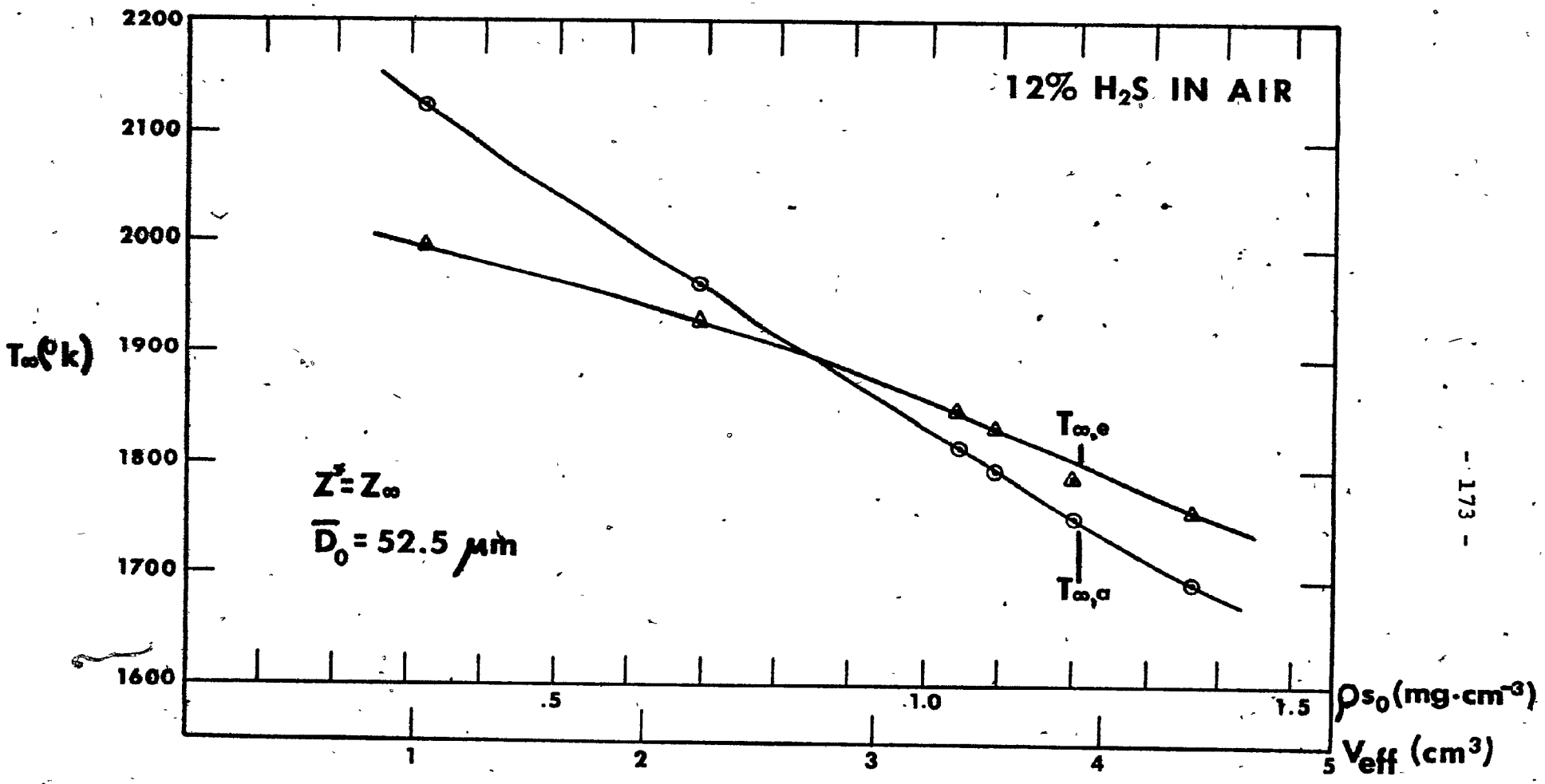

FIG. 32 VARIATION OF ADIABATIC FLAME TEMPERATURE (T_∞) WITH WATER SPRAY DENSITY (ρ_{s_0}).

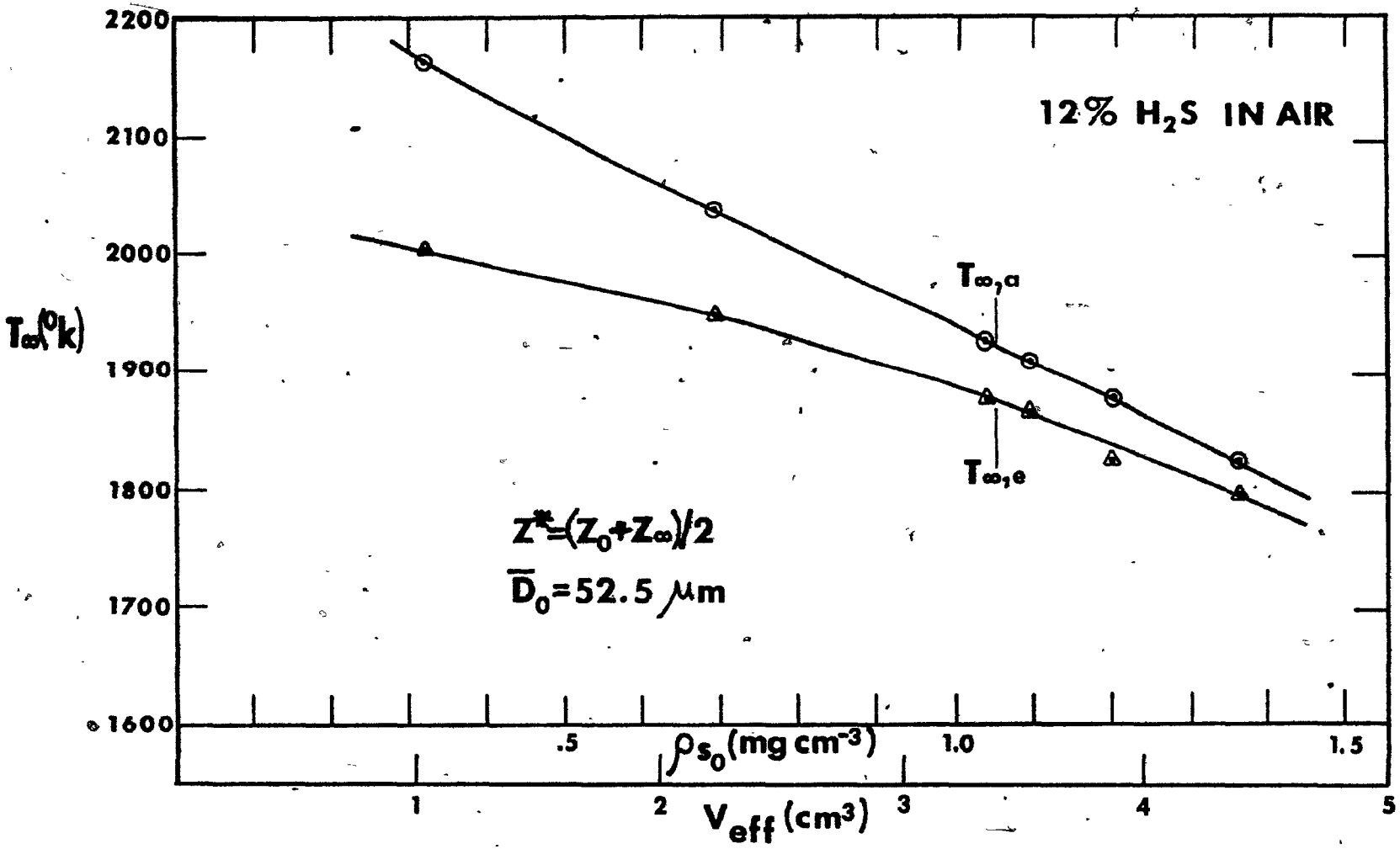

FIG. 33 VARIATION OF ADIABATIC FLAME TEMPERATURE, (T_∞) WITH WATER SPRAY DENSITY, (ρ_{s_0}).

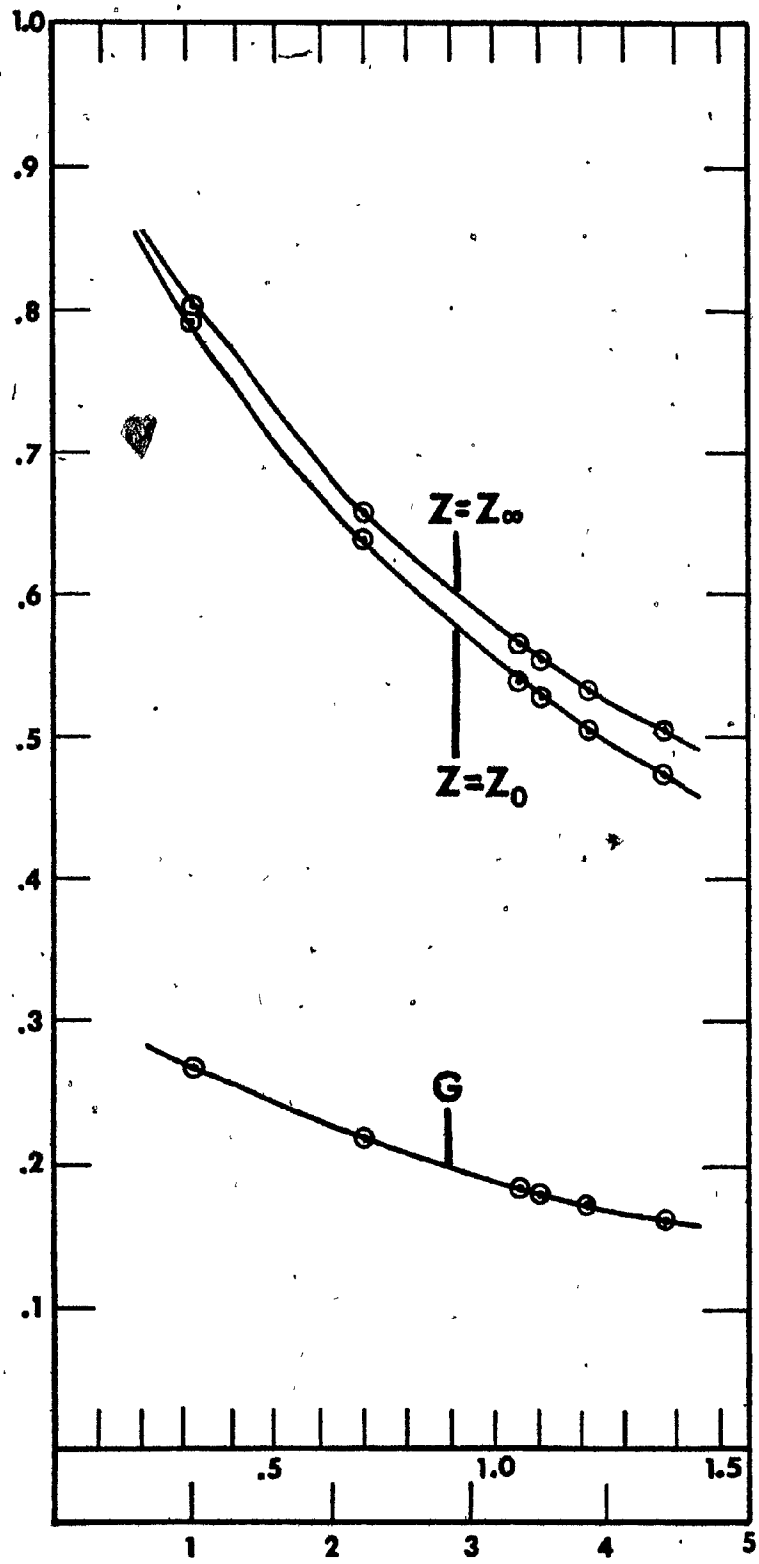

FIG. 34 VARIATION OF INITIAL AND FINAL GAS MASS FRACTION, (Z_0 and Z_∞) AND INITIAL REACTANT MASS FRACTION, (G) WITH WATER SPRAY DENSITY, (ρ_{s_0}).

APPENDIX I

DEFINITION AND INTERPRETATION OF PARAMETERS IN THE ANALYSIS OF LAMINAR FLAME PROPAGATION

The stoichiometric equation for the combustion process introduced in section 2.2 reads:

$$\sum_{K=1}^{r} \nu'_K M_K \underset{K_b}{\overset{K_f}{\rightleftharpoons}} \sum_{K=r+1}^{n} \nu''_K M_K \qquad (2\text{-}1)$$

Reference mass concentrations Y_K^* for the stoichiometric reaction (2-1) are defined as:

For the reactant species: $$Y_K^* = \frac{\nu'_K W_K}{\sum_{J=1}^{r} \nu'_J W_J} \quad K=1,\ldots,r. \qquad (I\text{-}1)$$

and

for the product species: $$Y_K^* = \frac{\nu''_K W_K}{\sum_{J=1}^{r} \nu'_J W_J} \quad K = r+1,\ldots,n$$

where W_K is the molecular weight of species K.

Each species in the flow has a mass fraction Y_K (or Y_I for inert species), a mass flux $\dot{m}_K$ (g/cm^2 sec) and a specific

enthalpy h_K (cal/g of species K).

If a_K and a_I are the coefficients (not necessarily stoichiometric) in the chemical equation of the reactant species prior to the reaction;

$$\sum_{K=1}^{r} a_K M_K + a_I M_I \underset{K_b}{\overset{K_f}{\rightleftharpoons}} \text{Products} + a_I M_I \qquad \text{(I-2)}$$

Then the following equalities hold:

$$\sum_{K=1}^{n} Y_K + Y_I \equiv \sum_{K=1}^{r} Y_K^* \equiv \sum_{K=r+1}^{n} Y_K^* \equiv \sum_{K=1}^{r} \frac{a_K W_K}{W_{total}} + \frac{a_I W_I}{W_{total}} \equiv 1 \qquad \text{(I-3)}$$

Where:

$$Y_K = \frac{\rho_K}{\rho} = \frac{W_K X_K}{\sum_{J=1}^{r} W_J X_J + W_I X_I} \qquad \text{(I-4)}$$

and

$$Y_I = \frac{\rho_I}{\rho} = \frac{W_I X_I}{\sum_{J=1}^{r} W_J X_J + W_I X_I}$$

with ρ_K, ρ_I, ρ, X_K and X_I representing respectively the species

K density, the total density of the inert species, the gas mixture overall density, the reactant species K mole fraction and the inert species mole fraction.

Now, if

$$a \equiv \min. \left(\frac{a_K}{\nu'_K} \right) \qquad K=1, \ldots, r \qquad \text{(I-5)}$$

then the mass fraction of consumable reactant species available for combustion initially is given by the "dilution", G, defined as:

$$G = a \sum_{K=1}^{r} \nu'_K W_K / W_{total} \qquad \text{(I-6)}$$

It follows that:

$$0 < G \leq 1 - \frac{a_I W_I}{W_{total}}$$

and equality on the right is equivalent to stoichiometry of the reacting gaseous mixture.

It can be shown [9] that all mass fractions are representable as linear expressions of a single function which will be called Y(X):

$$Y_K(X) = GY_K^*[Y(X)-1] + \frac{a_K W_K}{W_{total}} \qquad K=1, \ldots, r \qquad \text{(I-7a)}$$

$$Y_K(X) = GY_K^*[1-Y(X)] \qquad K=r+1, \ldots, n \qquad \text{(I-7b)}$$

$$Y_I = \frac{a_I W_I}{W_{total}} \qquad \text{(I-7c)}$$

From Eqn. (I-3) and the summation of Eqn. (I-7a), the definition of Y(X) is:

$$Y(X) = \frac{1}{G}\left[\sum_{K=1}^{r} Y_K + G - \left(1 - \frac{a_I W_I}{W_{total}}\right)\right] \qquad \text{(I-8)}$$

The definitions of Eqns. (I-1), (I-5) and (I-6) imply that

$$a_K W_K \geq G\, W_{total}\, Y_K^* \qquad K=1, \ldots, r \qquad \text{(I-9)}$$

with equality holding for at least one value of K.

If,

$$G = 1 - \frac{a_I W_I}{W_{total}} \qquad \text{(I-10)}$$

then the equality holds in (I-9) for all k; otherwise there is always at least one value of K for which the equality in (I-9) holds. For a physically sensible solution, it is required that $0 \leq Y_K \leq 1$ for all K; by Eqns. (I-7) and (I-9) this is equivalent to the requirement that,

$$0 \leq Y(X) \leq 1 \qquad X \geq 0 \qquad \text{(I-11)}$$

Equality on the left for any X is equivalent to complete combustion at that value of X. If G = 1, then $a_I = 0$ and it follows from Eqn. (I-8) that Y is simply the sum of all of the reactant mass fractions (Y was defined this way in Eqn. (2-10c) of [8]).

If G < 1, then for each of the reactant species, that portion of the species mass fraction which is available to be consumed in the forward reaction of (I-2) is Y_K*GY (K=1, ..., r). The total "consumable reactant mass fraction" at each point X in the flow is then:

$$\sum_{K=1}^{r} (Y_K * GY) = GY \qquad \text{(I-12)}$$

The addition of water sprays to the mixture is considered in this work to be equivalent to the addition of one inert species in the form of liquid droplets, converted partially or wholly by the propagating flame to vapor, hence to another inert species. From Eqn. (I-3) then:

$$\sum_{K=1}^{n} Y_K + Y_I + Y_v + Y_\ell = 1 \qquad \text{(I-13)}$$

Where Y_v and Y_ℓ are the vapor and liquid mass fractions respectively.

We define the mass fraction of the gaseous part in the overall mixture (gas plus liquid) by:

$$Z = \frac{\rho_g}{\rho} \qquad \text{(I-14)}$$

With ρ_g representing the gas density and ρ the overall mixture density including the spray density, ρ_s ($\rho = \rho_g + \rho_s$).

The definition of Z implies that the reaction species mass fraction, Y_K in the combustible mixture with water droplets (Eqn. (I-13)) is equal to Z times Y_K in the mixture without the addition of water droplets (Eqn. (I-3)). The same thing applies to G, the "dilution" factor defined in Eqn. (I-6) for the mixture without water droplets which is now equal to Z times that value, or

$$G_{\ell+g} = ZG_g = \text{constant} \qquad \text{(I-15)}$$

This stems from the fact that by adding more species to the existing mixture, the mass fractions of the species already in the mixture are reduced as can easily be seen from Eqn. (I-13).

The definition of Z also implies that,

$$Y = \frac{\rho_s}{\rho} = 1-Z \qquad \text{(I-16a)}$$

and

$$Y_v = \frac{\rho_v}{\rho} = Z-Z_0 \qquad \text{(I-16b)}$$

Initially, the gaseous mass fraction is Z_0 and the water mass fraction, $1-Z_0$. As the reaction progresses, Z is increased due to the evaporation of water droplets while the mass fraction of liquid, 1-Z, is reduced. For the case of total evaporation, $Z_\infty = 1$; this implies a completely gaseous mixture at the final equilibrium with no liquid water left.

APPENDIX II

CASTING OF THE GOVERNING DIFFERENTIAL EQUATION AND BOUNDARY CONDITIONS, INTO A FORM SUITABLE FOR THE NUMERICAL SOLUTION

The governing differential equation and boundary conditions were shown in section 2.2 to be:

$$\tilde{T}'(\zeta) - \tilde{T}''(\zeta) = \frac{\rho D \dot{w}}{\dot{Gm}^2} \qquad (2\text{-}26a)$$

$$\tilde{T}'(0) = 1 + \tilde{T}(0) \qquad (2\text{-}26b)$$

$$\tilde{T}(\infty) = 0 \qquad (2\text{-}26c)$$

The right-hand side term of Eqn. (2-26a) is highly non-linear. Therefore, it has to be brought to a form in which the eigenvalue is defined explicitly.

The particular form of $\dot{w}$, the chemical source function, which is derived from the law of mass action as applied to a one-step reversible reaction, is,

$$\dot{w} = \left(\sum_{K=1}^{r} W_K \nu'_K \right) \left[K_f(T) \prod_{K=1}^{r} \left(\frac{Y_K \rho}{W_K} \right)^{\gamma' K} - K_b(T) \prod_{K=r+1}^{n} \left(\frac{Y_K \rho}{W_K} \right)^{\gamma'' K} \right] \qquad (II\text{-}1)$$

where K_f and K_b, the specific forward and reverse reaction rate constants, are defined based on the Arrhenius law as expressions of the form (R is the gas constant 1.9867 (cal/mole °K))

$$K = BT^{\beta}\exp(-E/RT) \qquad \text{(II-2)}$$

The frequency factor B, molar activation energy E and temperature exponent β are constants which are generally different for the forward and reverse rates.

If Eqn. (2-1) describes an elementary reaction step, then the γ'_K and γ''_K exponents in Eqn. (II-1) are identical to ν'_K and ν''_K, respectively. However, it is more usually the case that Eqn. (II-1) represents an empirically observed rate law for the overall reaction, a so-called "global" approximation for a multi-step reaction. Then, γ'_K and γ''_K are regarded as non-negative, empirically determined constants. Thus the reaction is of the order γ'_K with respect to species K for K=1, ..., r and the overall order of the reaction for the forward and reverse reactions respectively, is r_f and r_b, defined as

$$r_f = \sum_{K=1}^{r} \gamma'_K \qquad r_b = \sum_{K=r+1}^{n} \gamma''_K \qquad \text{(II-3)}$$

It is possible by using Eqn. (II-1) to express the right-hand side of Eqn. (2-26a) as a function of $\tilde{T}$ only. For this purpose, Y_K and T are expressed as functions of $\tilde{T}$ through Eqns. (I-7), (2-20) and (2-23). Assuming that ρD is a function only of temperature, we may express it as [23, Chpt. XIX, Eqn. (18)],

$$\rho D = T^{\alpha}[(\rho D)_{\infty,a}/(T_{\infty,a})^{\alpha}] \qquad \text{(II-4)}$$

where $T_{\infty,a}$ is the adiabatic flame temperature and α is a number between 0.5 and 1 [23].

Since it is assumed that the entire mixture obeys the perfect gas law:

$$\rho = \frac{p\bar{W}}{RT} \qquad \text{(II-5)}$$

(R is the gas constant 82.057 atm-cm^3/mole °K) where the average molecular weight $\bar{W}$ is defined as:

$$\bar{W} = \left[\sum_{K=1}^{n} \frac{Y_K}{W_K} + \frac{Y_I}{W_I}\right]^{-1} = \bar{W}(\tilde{T}) \qquad \text{(II-6)}$$

Hence, ρ can be expressed also as a function of $\tilde{T}$ only.

The resulting expression for the right-hand side of Eqn. (2-26a) is:

$$\frac{\rho D\dot{w}}{G\dot{m}^2} = \frac{(\bar{K}p)^{r_f}}{u_0^2}\left[\mu_f(\tilde{T})\prod_{K=1}^{r}\left(\frac{a_K W_K}{GW_{total}Y_K^*} - 1 - \tilde{T}\right)^{\nu'_K}\right] \qquad \text{(II-7)}$$

where the back reaction is not included and the exponent γ'_K in Eqn. (II-1) will be considered to be identical to ν'_K. The overall order of the forward reaction then becomes:

$$r_f = \sum_{K=1}^{r} \nu'_K \qquad \text{(II-8)}$$

Eqn. (II-7) is in dimensionless form. The constant $\bar{K}$ and the dimensionless specific reaction rate function μ_f are defined in terms of previously introduced physical parameters as follows:

$$T^* = \frac{q}{c_p} \qquad \text{(II-9)}$$

$$\mu_f(\tilde{T}) = \left[\frac{\bar{W}(\tilde{T})}{\bar{W}(0)}\right]^{r_f}\left[\frac{T(\tilde{T})}{T^*}\right]^{\beta_f+\alpha-r_f}\exp[-E_f/RT(\tilde{T})] \qquad \text{(II-10)}$$

$$\bar{K} = \left[\frac{(\rho D)_{\infty,a}}{\rho_0}\left(\frac{T^*}{T_{\infty,a}}\right)^{\alpha} B_f(\tilde{T}^*)^{\beta_f}\left(\frac{\rho_0 G}{\sum_{K=1}^{r}\nu'_K W_K}\right)^{r_f-1}\prod_{K=1}^{r}(\nu'_K)^{\nu'_K}\right]^{1/r_f}\frac{\bar{W}(0)}{\rho_0 RT^*} \qquad \text{(II-11)}$$

Since Eqn. (I-9) shows that $a_K W_K \geq GW_{total} Y_K^*$ for K=1, ..., r with equality holding for some K in this range, we can have K=1, ..., s species for which $a_K W_K = GW_{total} Y_K^*$ where $1 \leq s \leq r$. If $s < r$ the fresh mixture is not in stoichiometric proportions and $a_K W_K > GW_{total} Y_K^*$ for K=s+1, ..., r. We then, define the number ν as the reaction order relative to the consumed species:

$$\nu = \sum_{K=1}^{s} \nu'_K \qquad \text{(II-12)}$$

Eqn. (2-26a), therefore may be written as,

$$\tilde{T}'(\zeta) - \tilde{T}''(\zeta) = \frac{(Kp)^{r_f}}{u_0^2} \mu(\tilde{T}) (-\tilde{T})^{\nu} \qquad \text{(2-27)}$$

where $\mu(T)$ is defined as:

$$\mu(T) = \mu_f(\tilde{T}) \prod_{K=s+1}^{r} \left(\frac{a_K W_K}{GW_{total} Y_K^*} - 1 - \tilde{T} \right)^{\nu'_K} \qquad \text{(2-28)}$$

With the expression on the right-hand side of Eqn. (2-27) being replaced by $\Lambda\Psi(\tilde{T})$, where $\Lambda = (\bar{K}p)^{r_f}/u_0^2$ is the eigenvalue defined in Eqn. (2-30) and $\Psi(\tilde{T})$ is the non-dimensional reaction

rate function, the boundary value problem in Eqns. (2-26) was shown to become:

$$\tilde{T}''(\zeta) - \tilde{T}'(\zeta) = -\Lambda\Psi(\tilde{T}) \qquad (2\text{-}31a)$$

$$\tilde{T}(0) = \tilde{T}_i \qquad (2\text{-}31b)$$

$$T'(0) = 1 + \tilde{T}_i \qquad (2\text{-}31c)$$

$$\tilde{T}(\infty) = 0 \qquad (2\text{-}31d)$$

where $\tilde{T}_i$ is the non-dimensional ignition temperature.

In order to formulate the eigenvalue solution, Eqns. (2-31) have to be reduced to a first-order boundary value problem using the following transformation:

$$u = \tilde{T}(\zeta) \qquad 0 \leq \zeta < \zeta_* \qquad (II\text{-}13)$$

$\zeta_* > 0$ and may be finite or infinite. The interval $0 \leq \zeta < \zeta_*$ is mapped onto the interval $\tilde{T}_i \leq u < 0$. Let

$$v(u) = \tilde{T}'(\zeta) \qquad (II\text{-}14)$$

It can be shown that $v(u) > 0$ if $\tilde{T}_i \leq u < 0$ and so

$$\frac{d\zeta}{du} = \frac{1}{v(u)} \qquad \text{if } \tilde{T}_i \leq u < 0$$

Hence,

$$\zeta = \int_{\tilde{T}_i}^{u} \frac{du}{v(u)} \qquad \tilde{T}_i \leq u < 0 \qquad \text{(II-15)}$$

It follows from Eqns. (2-31), (II-13), (II-14) and (II-15) that, $v(u)$ is a continuously differentiable function of u which satisfies the first-order boundary value problem:

$$v'(u) = 1 - \frac{\Lambda\Psi(u)}{v(u)} \qquad \text{(II-16a)}$$

$$v(\tilde{T}_i) = 1 + \tilde{T}_i \qquad \text{(II-16b)}$$

$$v(0-) = 0 \qquad \text{(II-16c)}$$

Upper and lower bounds for the eigenvalue Λ will now be derived. They provide a method for numerical computation of approximations to Λ along with bounds for the error. Eqn. (II-16a) can be written,

$$(v-u)' = -\frac{\Lambda\Psi}{v}$$

Multiplication by 2(v-u) yields,

$$[(v-u)^2]' = -2\Lambda\left(1 - \frac{u}{v}\right)\Psi$$

Integrating and using boundary conditions, Eqn.s (II-16b) and (II-16c), we obtain the relation,

$$2\Lambda\int_{\tilde{T}_i}^{0}\left[1 - \frac{u}{v(u)}\right]\Psi(u)du = 1 \qquad \text{(II-17)}$$

Multiplication of Eqn. (II-16a) by $2ve^{-2\int_{\tilde{T}_i}^{u}\frac{d\eta}{v(\eta)}}$ yields the equation,

$$\left[e^{-2\int_{\tilde{T}_i}^{u}\frac{d\eta}{v(\eta)}}v^2(u)\right]' = -2\Lambda e^{-2\int_{\tilde{T}_i}^{u}\frac{d\eta}{v(\eta)}}\Psi(u)$$

Integrating from $\tilde{T}_i$ to 0 and using boundary conditions, Eqns. (II-16b) and (II-16c), we obtain a second integral relation:

$$2\Lambda\int_{\tilde{T}_i}^{0} e^{-2\int_{\tilde{T}_i}^{u}\frac{d\eta}{v(\eta)}}\Psi(u)du = (1 + \tilde{T}_i)^2 \qquad \text{(II-18)}$$

Since $v(u) > 0$ and $\Psi(u) > 0$ for $\tilde{T}_i < u < 0$, the substitution of an upper bound for v in Eqn. (II-17) yields an upper bound for Λ, whereas the substitution of an upper bound for v in Eqn. (II-18) yields a lower bound for Λ.

Now according to Eqn. (II-16a), $v'(u) < 1$ if $\tilde{T}_i \leq u < 0$ and it follows with the use of Eqn. (II-16b) that,

$$v(u) < 1 + u \quad \text{if} \quad \tilde{T}_i < u < 0 \tag{II-19}$$

Hence $1 + u$ is an upper bound for $v(u)$ and can be substituted in Eqns. (II-17) and (II-18) to obtain the inequalities

$$\Lambda^- < \Lambda < \Lambda^+ \tag{2-33}$$

where

$$\Lambda^- = \left[2 \int_{\tilde{T}_i}^{0} \frac{\Psi(u)}{(1+u)^2} \, du \right]^{-1} \tag{2-34a}$$

$$\Lambda^+ = \left[2 \int_{\tilde{T}_i}^{0} \frac{\Psi(u)}{1+u} \, du \right]^{-1} \tag{2-34b}$$

are the lower and upper bounds respectively for the eigenvalue Λ.

A FORTRAN program was written for the integration of Eqns. (2-34) to solve for Λ^+ and Λ^- in various cases described

in Chapter V of this thesis. The numerical integration scheme used was the three-point Newton-Cotes formula better known as Simpson's method.

For the case of the laminar flame propagation in a combustible mixture with water droplets, the governing differential equation and boundary conditions were shown in section 2.4 to be:

$$\tilde{T}'(\zeta) - \tilde{T}''(\zeta) = \frac{Z\rho D\dot{w}}{J\dot{m}^2} \qquad (2\text{-}83a)$$

$$\tilde{T}'(0) = \frac{G}{J} + \tilde{T}(0) \qquad (2\text{-}83b)$$

$$\tilde{T}(\infty) = 0 \qquad (2\text{-}83c)$$

The above equations are similar in form to Eqns. (2-26) where the case of a mixture, purely gaseous with no water droplets, was considered. As a result, the procedure leading to the expressions for the higher and lower bounds of the eigenvalue (Eqns. (2-84), shown at the end of this appendix) is exactly the same again, except, for minor changes in some equations discussed previously in this appendix and those will now be shown.

The form of $\dot{w}$, the chemical source function, for a forward reaction only, was shown in Eqn. (II-1) to be:

$$\dot{w} = \left(\sum_{K=1}^{r} W_K \nu'_K \right) \left[K_f(T) \prod_{K=1}^{r} \left(\rho \frac{Y_K}{W_K} \right)^{\gamma'_K} \right]$$

Also, considering a stoichiometric composition, Eqn. (I-9) becomes:

$$a_K W_K = G W_{total} Y_K^*$$

Then, from Eqn. (I-7a) it follows that:

$$Y_K(X) = G Y_K^* Y(X) \qquad \text{(II-20)}$$

which is true only for the stoichiometric mixture. Whence,

$$\rho_K = \rho Y_K = (\rho_g + \rho_s) G Y_K^* Y \frac{\rho_g}{\rho_g} = \frac{\rho_g G Y}{Z} Y_K^* = \frac{\rho_g J(-\tilde{T})}{Z} Y_K^* \qquad \text{(II-21)}$$

where use has been made of the definitions for Z, Y_K and G, with the water droplets included, in Appendix I (Eqns. (I-14) and (I-15)) and the result, $Y^*(X) \triangleq \tilde{T}(X) = 0$ obtained in Eqn. (2-82). Substituting the expression for Y_K above (Eqn. II-21), in the equation for $\dot{w}$, we have:

$$\dot{w} = \left(\sum_{K=1}^{r} W_K \nu'_K \right) \left[K_f(\tilde{T}) \prod_{K=1}^{r} \left(\frac{Y_K^*}{W_K} \right)^{\gamma'_K} \right] \left[\frac{\rho_g J(-\tilde{T})}{Z} \right]^{r_f} \qquad \text{(II-22)}$$

Which in turn is then used on the right-hand side of the governing differential equation, Eqn. (2-83a).

The equation of state applies of course to the gaseous part of the mixture only and thus assumes the following form:

$$p = \rho_g RT/\bar{W} = Z\rho RT/\bar{W}$$

or,

$$\frac{Z\rho T}{\bar{W}} = \frac{p}{R} = \text{constant} \qquad \text{(II-23)}$$

Where the average molecular weight, $\bar{W}$, is now defined as:

$$\bar{W} = \left[\sum_{K=1}^{n} \frac{Y_K}{\bar{W}_K} + \frac{Y_I}{\bar{W}_I} + \frac{Y_v}{\bar{W}_v} \right]^{-1} = \bar{W}(\tilde{T}) \qquad \text{(II-24)}$$

Besides, in Eqn. (II-4) it is now $\rho_g D$ and not ρD which is used as a function of the temperature.

Similarly to Eqns. (II-16), the boundary value problem described by Eqns. (2-83) is transformed into the following 1st order governing differential equation and boundary conditions:

$$v'(u) = 1 - \frac{\Lambda\Psi(u)}{v(u)} \qquad \text{(II-25a)}$$

$$v(\tilde{T}_i) = a + \tilde{T}_i \qquad \text{(II-25b)}$$

$$v(0^-) = 0 \qquad \text{(II-25c)}$$

where

$$a = \frac{G}{J} . \qquad a \geq 1$$

Repeating the procedure in Eqns. (II-17) - (II-19) and realizing that now the upper bound for v(u) is a+u rather than 1+u by using the boundary condition in Eqn. (II-25b), we obtain the following expression for the lower and upper bounds of Λ:

$$\Lambda^- = \left[2 \int_{T_i}^{0} \frac{\Psi(u)}{(a+u)^2} \, du \right]^{-1} \qquad \text{(2-84a)}$$

$$\Lambda^+ = \left[2 \int_{T_i}^{0} \frac{\Psi(u)}{a+u} \, du \right]^{-1} \qquad \text{(2-84b)}$$

Eqns. (2-84) were integrated numerically within a modified numerical scheme which included the effect of water sprays (see section 2.4).

APPENDIX III

GENERAL SPRAY STATISTICS

The term "spray" is defined here to include all such systems in which there are so many particles that only a statistical description of their behavior is feasible.

A statistical description of the spray should be given by a distribution function

$$f(r,x,v,t)\,drdxdv$$

which is the probable number of particles in the radius range dr about r located in the spatial range dx about x with velocities in the range dv about v at time t. Here dx and dv are abbreviations for the three-dimensional elements of physical space and velocity space, respectively.

The droplets are assumed to be spherical, thus one parameter r is sufficient to determine the size of the droplet.

Integrating the function f over all the velocity space:

$$H = \int_0^\infty f dv \qquad \text{(III-1)}$$

we get the number of droplets per unit volume per unit range

of radius and integrating H over all the radius range:

$$n = \int_0^\infty Hdr = \int_0^\infty \int_0^\infty fdvdr \qquad \text{(III-2)}$$

results in the number of droplets of any size, r, per unit volume. Various functional forms for H were suggested and one which agrees well with observed size distributions for real sprays and simplifies many theoretical computations is the generalized Rosin-Rammler distribution, first proposed by Tanaswa [10, Chpt. 11; 63-65].

For formulations which have successfully yielded results, the statistical assumptions are highly restrictive and exclude effects such as droplet shattering, coalescence, nucleation, deformation, etc. [10, Chpt. 11; 31, 33, 60]. In this work consideration will be restricted to dilute sprays (i.e. the ratio of the volume occupied by the condensed phase to the volume occupied by the gas must be small), hence collisions between droplets do not exist. Furthermore, the droplets' velocity relative to the gas is small so that nucleation or particle break up are absent. This means the ratio of the dynamic force to the surface tension force which is given by the Weber number [10, Chpt. 11),

$$We = \frac{2r\rho_g |v-u|^2}{s} << 20 \qquad \text{(III-3)}$$

here, s is the surface tension of the liquid, ρ_g is the gas mixture density, v represents the droplet velocity and u is the velocity of the gas. When We << 20, droplets are nearly spherical as assumed in this work; as We increases, the droplets deform and eventually break up at We ≈ 20.

Essential to all of these treatments are explicit or implicit statistical hypotheses which permit the deduction of spray behavior from some known properties of single particles. In the present research the emphasis is on the steady state, spherically-symmetric evaporation of a single droplet in a quiescent atmosphere (see section 2.4), a phenomenon understood comparatively well [33] and encountered in heterogeneous burning investigations [10, Chpt. 11; 23, Chpt. XXII; 60].

APPENDIX IV

SAMPLE COMPUTER OUTPUTS

Sample program 1: For a flame in stoichiometric H_2S-air mixture without water spray. It calculates also the value for B_f which will give the experimental value of u_0 as an average between u_0^+ and u_0^-.

Sample program 2: For a flame in stoichiometric H_2S-air mixture with water spray, $\rho_{s_0} = 1.09$ mg/cm^3, $\bar{d}_0 = 52.5$ µm. It uses the value of B_f calculated in sample program 1.

```
*BATCH WATFIV ME55001 I07412864 Y. KINCLER                                    20:31 79/325
$WATFIV  .TIME=60,PAGES=100
C
C     ************************************************************
C     BURNING VELOCITIES CALCULATIONS OF H2S-AIR LAMINAR FLAMES
C     ************************************************************
C
C
C   THIS PROGRAM SOLVES THE EIGEN VALUE PROBLEM FOR THE BURNING VELOCITY
C   OF A LAMINAR H2S-AIR FLAME AT STOICHIOMETRIC COMPOSITION.
C   IT INTEGRATES THE BOUNDARY VALUE EQUATION PROCEEDING FROM THE COLD
C   BOUNDARY WHICH IS AT IGNITION TEMP. UP TO THE HOT BOUNDARY BEING AT
C   THE ADIABATIC FLAME TEMP..
C   THE INTEGRATION IS PERFORMED TWICE AND RESULTS IN UPPER AND LOWER
C   BOUNDS FOR THE EIGEN VALUE FROM WHICH THE CORRESPONDING BURNING
C   VELOCITIES ARE DETERMINED.
C   IT REPEATS THE INTEGRATION FOR FOUR DIFFERENT IGNITION TEMPS. IN AN
C     INCREASING ORDER.
C
C
C     SECTION 1:DATA INPUT INCLUDING THE TWO STUDY VARIABLES:DROPLET INITIAL
C     RADIUS,R0(CM) AND WATER SPRAY TOTAL VOLUME INPUT,VS(CC).
C     CALCULATION AND DEFINITION OF THE MIXTURE THERMOCHEMICAL PROPERTIES
C     FOLLOWS.
C     ************************************************************************
C
      IMPLICIT REAL*8(A-H,O-Z)
      DIMENSION VR(10),H(10),W(10),Y(10),WSPEC(10),HF(10)
      READ(5,1)(VR(I),H(I),W(I),I=1,4)
    1 FORMAT(3D10.3)
      WRITE(6,14)
      WRITE(6,15)
      DATA R,R1,CP,TC,TF,R0,P,TINIT/1.9864D0,82.057D0,.2805D0,2.693D-04,
     *2069.2D0,2.5D0,1.D0,298.D0/
      DATA WREAC,WPROD,A,B,AVMOR,AVMOP,VTR,VTP,SUMH,SUML/10*0./
C
C   CALCULATION OF THE COMBUSTION REACTANTS PROPERTIES.
C
      DO 21=1,2
      WSPEC(I)=VR(I)*W(I)
      HF(I)=H(I)/W(I)
      VTR=VTR+VR(I)
    2 WREAC=WREAC+WSPEC(I)
      REACM=1.D0
      DO 31=1,2
      Y(I)=WSPEC(I)/WREAC
      AVMOR=AVMOR+Y(I)/W(I)
      REACM=REACM*((Y(I)/W(I))**VR(I))
    3 A=A+Y(I)*HF(I)
C
C   CALCULATION OF THE COMBUSTION PRODUCTS PROPERTIES.
C
      DO 41=3,4
      WSPEC(I)=VR(I)*W(I)
      HF(I)=H(I)/W(I)
      WPROD=WPROD+WSPEC(I)
    4 VTP=VTP+VR(I)
      DO 51=3,4
      Y(I)=WSPEC(I)/WREAC
```

SAMPLE 1.

```
      AVMOP=AVMOP+Y(I)/W(I)
    5 B=B+Y(I)*HF(I)
C
C   TOTAL HEAT RELEASED PER GRAM OF COMBUSTION REACTANTS.
C
      Q=A-B
      G=1.D0-5.72D0*28.D0/(WREAC+5.72D0*28.D0)
      WINIT=(WREAC+5.72D0*28.D0)/(VTR+5.72D0)
      WFIN=(WPROD+5.72D0*28.D0)/(VTP+5.72D0)
      C1=G*Q/CP
      DENSE=(P*WINIT)/(R1*TINIT)
      S=(TC*WREAC*REACM*G**(RO-1.D0)/(DENSE*DENSE*CP*TF))**(1.D0/RO)*WFI
     *N/R1
C
CCCC  SECTION 2:NUMERICAL INTEGRATION OF THE EIGEN VALUE EQUATION AND
CCCC  CALCULATION OF UPPER AND LOWER BOUNDS FOR THE BURNING VELOCITY.
CCCC  ****************************************************************
C
      N=1
      E=26000.D0
      X=.01D0
      M=45
      Z=-.9D0
      DO 13J=1,4
      UI=Z
      DO 111I=1,M
      IF(N.EQ.1)GO TO 7
    6 N=2
      UI=Z+(2*I-1)*X
    7 WU=1./(G*UI*(AVMOP-AVMOR)+1./WFIN)
      T=C1*UI+TF
      RATE=DEXP(-E/(R*T))
      FUIH=(RATE*(-UI)**RO)/(1+UI)
      FUIL=(RATE*(-UI)**RO)/((1+UI)*(1+UI))
      GO TO(8,9,10),N
    8 SUMH=SUMH+FUIH
      SUML=SUML+FUIL
      GO TO 6
    9 SUMH=SUMH+4*FUIH
      SUML=SUML+4*FUIL
      IF(I.EQ.M)GO TO 12
      UI=Z+2*I*X
      N=3
      GO TO 7
   10 SUMH=SUMH+2*FUIH
      SUML=SUML+2*FUIL
   11 CONTINUE
   12 EIGENH=1.D0/(2.D0*X/3.D0*SUMH)
      EIGENL=1.D0/(2.D0*X/3.D0*SUML)
      IF(J.NE.1)GO TO 20
      BH=DSQRT((S*P)**RO/EIGENH)
      BL=DSQRT((S*P)**RO/EIGENL)
      F=(84.D0/(BH+BL))**2
      SCALE=S*F**(1.D0/RO)
   20 BH=DSQRT((SCALE*P)**RO/EIGENH)
      BL=DSQRT((SCALE*P)**RO/EIGENL)
      T=C1*Z+TF
      WRITE(6,16)TF,T,EIGENH,BH,EIGENL,BL
```

```
C
C     TRYING THE NEXT IGNITION TEMP. AND REINITIALIZING THE PROPER VALUES.
C
      Z=Z+.1D0
      M=M-5
      N=1
      SUMH=0.D0
      SUML=0.D0
   13 CONTINUE
      WRITE(6,17)
   14 FORMAT('1',41X,'THE BURNING RATE OF STOICHIOMETRIC H2S-AIR FLAMES'
     *)
   15 FORMAT(///,4X,'FINAL TEMP.(K)',6X,'IGNITION TEMP.(K)',7X,'UPPER BO
     *UND', 9X,'BURNING RATE(CM/S)',7X,'LOWER BOUND', 8X,'BURNING RATE(C
     *M/S)')
   16 FORMAT(//5X,D12.5,1X,5D22.10)
   17 FORMAT('1')
      STOP
      END

$DATA
```

THE BURNING RATE OF STOICHIOMETRIC H2S-AIR FLAMES

FINAL TEMP.(K)	IGNITION TEMP.(K)	UPPER BOUND	BURNING RATE(CM/S)	LOWER BOUND	BURNING RATE(CM/S)
0.20692D 04	0.28926195 30D 03	0.1650821098D 06	0.38214639 76D 02	0.1150044432D 06	0.4578516024D 02
0.20692D 04	0.48703284 71D 03	0.1650821129D 06	0.38214839 41D 02	0.1150044510D 06	0.4578515869D 02
0.20692D 04	0.68480374 12D 03	0.1650889690D 06	0.38214045 88D 02	0.1150162252D 06	0.4578281433D 02
0.20692D 04	0.88257463 53D 03	0.1655199164D 06	0.38164266 43D 02	0.1155792778D 06	0.4567116185D 02

```
                *BATCH WATFIV Z906999 107412864 Y. KINCLER
                ********************************************************************************  09:49 80/092
$WATFIV  ,TIME=60,PAGES=100
C
C     ***********************************************************
C     BURNING VELOCITIES CALCULATIONS OF H2S-AIR LAMINAR FLAMES
C     ***********************************************************
C
C    THIS PROGRAM SOLVES THE EIGEN VALUE PROBLEM FOR THE BURNING VELOCITY
C    OF A LAMINAR H2S-AIR FLAME AT STOICHIOMETRIC COMPOSITION.
C    IT INTEGRATES THE BOUNDARY VALUE EQUATION PROCEEDING FROM THE COLD
C    BOUNDARY WHICH IS AT IGNITION TEMP. UP TO THE HOT BOUNDARY BEING AT
C    THE ADIABATIC FLAME TEMP..
C    THE INTEGRATION IS PERFORMED TWICE AND RESULTS IN UPPER AND LOWER
C    BOUNDS FOR THE EIGEN VALUE FROM WHICH THE CORRESPONDING BURNING
C    VELOCITIES ARE DETERMINED.
C    IT REPEATS THE INTEGRATION FOR FOUR DIFFERENT IGNITION TEMPS. IN AN
C      INCREASING ORDER.
C
C      SECTION 1:DATA INPUT INCLUDING THE TWO STUDY VARIABLES:DROPLET INITIAL
C      RADIUS,R0(CM) AND WATER SPRAY TOTAL VOLUME INPUT,VS(CC).
C      CALCULATION AND DEFINITION OF THE MIXTURE THERMOCHEMICAL PROPERTIES
C      FOLLOWS.
C      ***************************************************************************
C
  1         IMPLICIT REAL*8(A-H,O-Z)
  2         DIMENSION VR(10),H(10),W(10),Y(10),WSPEC(10),HF(10)
  3         READ(5,1)(VR(I),H(I),W(I),I=1,4)
  4       1 FORMAT(3D10.3)
  5         WRITE(6,14)
  6         WRITE(6,15)
  7         DATA R,PI,P,TINIT,CPV,CPL,HFG,RO/1.9864D0,82.057D0,1.D0,296.D0,
           *.59D0,1.D0,539.D0,2.5D0/
  8         DATA VOLTOT,VOLEFF,VLAMDA,ROWAT,ROSAT,ROGAS,TADB,TIME/4586.6D0,
           *3264.5D0,2.75D-04,1.D0,.972D0,1.188D-03,2069.2D0,2.5D-04/
  9         CP=.2805D0
 10         TC=5.592D-04
 11         RO=2.625D-03
 12         VS=6.D0
 13         DATA WREAC,WPROD,A,B,VTR,VTF,SUMH,SUML/ 8*0.D0/
C
C    CALCULATION OF THE COMBUSTION REACTANTS PROPERTIES.
C
 14         DO 2I=1,2
 15         WSPEC(I)=VR(I)*W(I)
 16         HF(I)=H(I)/W(I)
 17         VTR=VTR+VR(I)
 18       2 WREAC=WREAC+WSPEC(I)
 19         REACM=1.
 20         DO 3I=1,2
 21         Y(I)=WSPEC(I)/WREAC
 22         REACM=REACM*((Y(I)/W(I))**VR(I))
 23       3 A=A+Y(I)*HF(I)
C
C    CALCULATION OF THE COMBUSTION PRODUCTS PROPERTIES.
C
 24         DO 4I=3,4
 25         WSPEC(I)=VR(I)*W(I)
```

SAMPLE 2

```
      HF(I)=H(I)/W(I)
      WPROD=WPROD+WSPEC(I)
    4 VTP=VTP+VR(I)
      DO 5 I=3,4
      Y(I)=WSPEC(I)/WREAC
    5 B=B+Y(I)*HF(I)
C
C     TOTAL HEAT RELEASED PER GRAM OF COMBUSTION REACTANTS.
C
      Q=A-B
C
C     ****************************************************************************
C
C     SECTION 2:CALCULATION OF WATER SPRAY EVAPORATION PARAMETERS INCLUDING THE
C     INITIAL AND FINAL GASEOUS MASS FRACTION(Z0 AND ZF RESPECTIVELY).
C     ALSO CALCULATED IS THE INFLUENCE OF THE EVAPORATION ON THE PHYSICAL
C     PROPERTIES OF THE MIXTURE.
C     ****************************************************************************
C
      XI=VLAMDA*DLOG(1.D0+(TADB-373.D0)*CPV/HFG)/(CPV*ROSAT)
      RF=DSQRT(R0*R0-2*XI*TIME)
      FRAVAP=1.D0-(RF/R0)**3
      VOLSPR=VOLEFF/VOLTOT*VS
      WVAP=FRAVAP*VOLSPR*ROWAT
      ROSPR=ROWAT*VOLSPR/VOLEFF
      WINIT=(WREAC+5.72D0*28.D0)/(VTR+5.72D0)
      ROGAS=(P*WINIT)/(R1*TINIT)
      ROTOT=ROGAS+ROSPR
      Z0=RUGAS/ROTOT
      ZF=Z0+WVAP/(ROTOT*VOLEFF)
      YI0=5.72D0*28.D0/(WREAC+5.72D0*28.D0)
      G=Z0*(1.D0-YI0)
      WTOTAL=WREAC/G
      VAPMOL=WTOTAL*(ZF-Z0)/18.D0
      WFIN=(WPROD+5.72D0*28.D0+VAPMOL*18.D0)/(VTP+5.72D0+VAPMOL)
      ENTLOS=(ZF-Z0)*HFG+(1.D0-Z0)*CPL*(373.D0-TINIT)
      CPF=Z0*CP+(ZF-Z0)*CPV
      DLOSS=(1.D0-Z0)*CPL*(373.D0-TINIT)+(ZF-Z0)*(HFG-CPV*373.D0)-CP*TIN
     *IT*Z0
      TF=(G*Q-DLOSS)/CPF
      C1=(G*Q-ENTLOS)/CPF
C
C     ****************************************************************************
C     SECTION 3:NUMERICAL INTEGRATION OF THE EIGEN VALUE EQUATION AND
C     CALCULATION OF UPPER AND LOWER BOUNDS FOR THE BURNING VELOCITY.
C     ****************************************************************************
C
      F=2.8625388339957554D13
      N=1
      E=26000.D0
      X=.01D0
      M=45
      Z=-.9D0
      BJ=G-ENTLOS/G
      A1=G/BJ
      S=(TC*WREAC*REACM/(ROTOT*ROTOT*CPF*TF*BJ))**(1.D0/RO)
     **WFIN*BJ/(R1*ZF)
      SCALE=S*F**(1.D0/RO)
      DO 13 J=1,4
```

```
      UI=Z
      DO 11 I=1,M
      IF(N.EQ.1)GO TO 7
    6 N=2
      UI=Z+(2*I-1)*X
    7 T=C1*UI+TF
      RATE=DEXP(-E/(R*T))
      FUIH=(RATE*(-UI)**RO)/(A1+UI)
      FUIL=(RATE*(-UI)**RO)/((A1+UI)*(A1+UI))
      GO TO(8,9,10),N
    8 SUMH=SUMH+FUIH
      SUML=SUML+FUIL
      GO TO 6
    9 SUMH=SUMH+4*FUIH
      SUML=SUML+4*FUIL
      IF(I.EQ.M)GO TO 12
      UI=Z+2*I*X
      N=3
      GO TO 7
   10 SUMH=SUMH+2*FUIH
      SUML=SUML+2*FUIL
   11 CONTINUE
   12 EIGENH=1.D0/(2.D0*X/3.D0*SUMH)
      EIGENL=1.D0/(2.D0*X/3.D0*SUML)
      BH=DSQRT((SCALE*P)**RO/EIGENH)
      BL=DSQRT((SCALE*P)**RO/EIGENL)
      T=C1*Z+TF
      WRITE(6,16)TF,T,EIGENH,BH,EIGENL,BL
C
C   TRYING THE NEXT IGNITION TEMP. AND REINITIALIZING THE PROPER VALUES.
C
      Z=Z+.1D0
      M=M-5
      N=1
      SUMH=0.D0
      SUML=0.D0
   13 CONTINUE
      WRITE(6,18)
      WRITE(6,17)
      PRINT,ZF,Z0,G,ROTCT,ROSPR,FRAVAP,SCALE,VOLSPR,VAPNUL
   14 FORMAT('1',41X,'THE BURNING RATE OF STOICHIOMETRIC H2S-AIR FLAMES'
     *)
   15 FORMAT(///,4X,'FINAL TEMP.(K)',6X,'IGNITION TEMP.(K)',7X,'UPPER BO
     $UND',8X,'BURNING RATE(CM/S)',7X,'LOWER BOUND',8X,'BURNING RATE(C
     *M/S)')
   16 FORMAT(//5X,D12.5,1X,5D22.10)
   17 FORMAT('1')
   18 FORMAT(///)
      STOP
      END

$DATA
```

THE BURNING RATE OF STOICHIOMETRIC H2S-AIR FLAMES

FINAL TEMP.(K)	IGNITION TEMP.(K)	UPPER BOUND	BURNING RATE(CM/S)	LOWER BOUND	BURNING RATE(CM/S)
0.17929D 04	0.45380415640 03	0.36446384900 06	0.26055063510 02	0.24379227390 06	0.31857331580 02
0.17929D 04	0.60258744080 03	0.36446935110 06	0.26054865420 02	0.24380602740 06	0.31856433000 02
0.17929D 04	0.75137072520 03	0.36477400080 06	0.26043584400 02	0.24430817460 06	0.31823677560 02
0.17929D 04	0.90015400960 03	0.36873313280 06	0.25903788360 02	0.24922345980 06	0.31508295110 02